POLITECNICO
MILANO 1863

Effect of temperature and viscosity on size-selected polyynes production and investigation of nanocomposites of polyynes embedded in electrospun polymeric nanofibers

Author: **Alessandro Paniz**

Student ID: 991740
Supervisor: Prof. Carlo S. Casari
Co-supervisor: Simone Melesi
Academic Year: 2022-23

Alla mia famiglia.

Abstract

Carbynes are a carbon allotrope that appears as one-dimensional linear chains composed solely of *sp*-hybridized carbon atoms. They may come in the form of cumulenes or polyynes, depending on the bond joining the various atoms. Specifically, polyynes consist of atoms with sp hybridization alternated by single and triple bonds. To exploit these materials for future applications, one needs good concentrations and stability. The purposes of this thesis can be divided into two macro-categories: the first concerns the study of strategies and process parameters, *i.e.,* temperature and viscosity, aimed at improving the production yield and length of polyynes by physical synthesis, i.e., Pulsed Laser Ablation in Liquid (PLAL); the second study concerns the investigation and analysis of the morphologies of composite nano-materials for the optimization of stability over time. For the first case, the ablations were conducted at 0°C. Uv-Vis spectroscopy and High-Performance Liquid Chromatography (HPLC) were mainly used to perform polyynes detection and analysis. This strategy proved to be effective in increasing the production yield of the longer chains. Different compounds have been considered to perform ablations in solutions with increased viscosity. Among the most effective results are the use of glycerol in aqueous solutions and the addition of a polymer in an acetonitrile solution. The synergistic action of viscosity and Silver Nanoparticles (AgNP) to maximize the production yield was also investigated, obtaining, in this case, the best increase of about 450%. The production of nano-composites made of polyynes embedded inside electrospun nanoifbers was also investigated. Polyynes were embedded starting both from PLAL poly-dispersed mixtures and HPLC size-selected solutions. To date, the polyynes produced via PLAL are found to have low concentrations and, for this reason, their detection and characterization are done by exploiting the interaction with AgNP to display signals given by Surface Enhanced Raman Scattering (SERS). Among the analyses performed, electrospun membranes produced starting from different solutions have been produced. The role of different electrospinning parameters on the morphologies, and the effect that different diameters can have on the stability in time of the embedded polyynes have been investigated. The various dimensional studies were carried out with the help of images obtained by Scanning Electron Microscope (SEM) and a Matlab program written

specifically for dimensional analysis.

Keywords: carbynes, polyynes, viscosity, electrospinning, silver nanoparticles, HPLC, SERS, SEM

Abstract in lingua italiana

Le carbine sono un allotropo del carbonio che si presenta come catene lineari mono-dimensionali composte esclusivamente da atomi di carbonio ibridizzati *sp*. Possono presentarsi sotto forma di cumuleni o di poliine, a seconda del legame che unisce i vari atomi. In particolare, le poliine sono costituite da atomi con ibridazione sp alternati da legami singoli e tripli. Per sfruttare questi materiali per applicazioni future, è necessario avere buone concentrazioni e stabilità. Gli scopi di questa tesi possono essere suddivisi in due macro-categorie: la prima riguarda lo studio di strategie e parametri di processo, *i.e.,* temperatura e viscosità, finalizzati a migliorare la resa produttiva e la lunghezza delle poliine prodotte mediante sintesi fisica, *i.e.,* l'ablazione laser pulsata in liquido (PLAL); il secondo studio riguarda l'indagine e l'analisi delle morfologie dei nano-materiali compositi per l'ottimizzazione della stabilità nel tempo. Per il primo caso, le ablazioni sono state condotte a 0°C. La spettroscopia Uv-Vis e la cromatografia liquida ad alte prestazioni (HPLC) sono state utilizzate principalmente per effettuare il rilevamento e l'analisi delle poliine. Questa strategia si è dimostrata efficace nell'aumentare la resa produttiva delle catene più lunghe. Sono stati presi in considerazione diversi composti per effettuare le ablazioni in soluzioni con viscosità aumentata. Tra i risultati più efficaci vi sono l'uso di glicerolo in soluzioni acquose e l'aggiunta di un polimero in una soluzione di acetonitrile. L'azione sinergica della viscosità e delle nanoparticelle d'argento (AgNP) per massimizzare la resa produttiva, ha permesso di ottenere, in questo caso, il miglior incremento di circa il 450%. È stata studiata la produzione di nano-compositi costituiti da poliine incorporati all'interno di nanofibre elettrofilate. Le poliine sono state inglobate partendo sia da miscele polidisperse ottenute tramite PLAL, sia da soluzioni selezionate per dimensioni tramite HPLC. Ad oggi, le poliine prodotte tramite PLAL risultano avere basse concentrazioni e, per questo motivo, il loro rilevamento e la loro caratterizzazione avvengono sfruttando l'interazione con AgNP per visualizzare i segnali dati dal Surface Enhanced Raman Scattering (SERS). Tra le analisi effettuate, sono state prodotte membrane elettrofilate a partire da diverse soluzioni. È stato studiato il ruolo di diversi parametri di elettrofilatura sulle morfologie e l'effetto che diversi diametri possono avere sulla stabilità nel tempo delle poliine incorporate. I vari studi dimensionali sono stati effettuati con

l'aiuto di immagini ottenute al microscopio elettronico a scansione (SEM) e di un programma Matlab scritto appositamente per l'analisi dimensionale.

Parole chiave: carbine, poliine, viscosità, elettrofilatura, nanoparticelle di argento, HPLC, SERS, SEM

Contents

Introduction

In recent decades, the research and use of carbon-based nanomaterials has increased more and more. Graphene, fullerenes, and carbon nanotubes are among the allotropes of carbon that are being most investigated, due to their versatile uses ranging from energy to biomedical applications. Carbon Atomic Wires (CAWs) are sp-carbon compounds and, because of their theoretically excellent properties, have recently been gaining increasing attention. However, the stability of these compounds is still one of the main problems, for which their use in devices or applications is so far limited. It is precisely this high instability that, to date, does not allow the fabrication of solid sp-carbon structures. The properties can be described using infinite chains as a model, however, for real chains, and therefore with finite length, it is necessary to take into account the effects of the end groups, which can vary considerably from the theoretical results. In accordance with this model, there are two possible configurations: cumulenes, characterized by altering double bonds, and polyynes, with alternating single and triple bonds. Because of structure type issues, polyynes are more stable, although the effect of end groups plays a key role in stabilizing the cumulenic form. Chemical synthesis was first used to produce CAWs, but nowadays studies focus more on production through physical syntheses. These appear to be less expensive and with the ability to scale up. Pulsed Laser Ablation in Liquid (PLAL) is one of the techniques exploited and was chosen in this thesis work. Briefly, this exploits an interaction between a laser beam, a graphite target, and a solvent to form sp carbon chains. By changing the type of solvent, chains with different terminations can be obtained, although those terminated with hydrogen turn out to be the most abundant. Techniques to increase the stability of these compounds include the synthesis of composite nanomaterials that incorporate polyynes within them. Among these possible techniques, in this work electrospinning was used to produce nanoifbers embedding polyynes. This technique is versatile and takes advantage of a large potential difference applied between a syringe containing the solution to be electrospun, and a collector, where the nanofibers are deposited. Besides stability, the use of fibers is fascinating because it would allow the use of these materials in a variety of fields, such as biomedical to the textile industry. The objectives of this thesis are to increase the production yield of polyynes and their

stability by exploiting their embedding in electrospun polymeric nanofibers. The thesis is divided as follows:

Chapter 1 provides an overview of the types of carbon hybridization, and then delves further into Carbon Atomic Wires (CAWs) by describing theoretical models, properties, synthesis and characterization techniques, and problems and strategies for CAW stability.

Chapter 2 describes nanocomposites by providing an in-depth look at electrospinning, describing the process and what parameters and how they affect the process. The goals of this thesis work are then presented.

Chapter 3 illustrates the materials, experimental methods, equipment, and their parameters, used for the production and characterization of polyynes via PLAL and electrospun polymeric nanofibers.

Chapter 4 shows and discusses experimental results regarding the increase in the production yield of polyynes by PLAL.

Chapter 5 describes the various experiments regarding the analyses conducted on electrospun polymer nanofibers containing polyynes.

1 —— Carbon Atomic Wires (CAWs)

1.1.   An Overview on Carbon Allotropes

Carbon, the sixth element in the periodic table, is a major actor in the evolutionary scheme of the universe. Due to its ability to form complex species, its abundance and to bond with other elements, it is fundamental for life and many technological applications. The resulting structural diversity of the Carbon-based compounds is related to the possibility of the formation of up to four different bonds that can be explained by the hybridization theory and by its peculiar electronic configuration, $i.e.$, $1s^2 2s^2 2p^2$, in which four electrons are in the outer electronic shell. In particular, due to the linear combination of the atomic orbitals, there is the possibility of the formation of new hybrid orbitals. Due to the similarity of their energy, the $2s$ and $2p$ are the atomic orbitals of carbon involved in the hybridization process, and with their superposition, the new hybrid orbitals are generated, $i.e.$, sp, sp^2, sp^3 [1, 2]. These three hybrid orbitals arise from the different possibilities of combination between atomic orbitals; if the $2s$ orbital combines with three $2p$ orbitals there will be the sp^3 hybrid orbital, when the $2s$ orbital combines with two $2p$ orbitals there will be sp^2 hybrid orbital, if instead $2s$ orbital combines with just one $2p$ orbital, there will be sp hybrid orbital. Depending on the kind of orbitals involved and by considering the Linear Combination of Atomic Orbitals (LCAO) theory, it is possible to determine the structure and geometry of the generating molecules. In the sp and sp^2 configurations, there are respectively two and one $2p$ orbitals which remain non-hybridized and that, when interacting with other carbon atoms, may recombine generating a new type of orbital, the so-called π molecular orbital. The latter is of fundamental importance due to the fact that determines the delocalization of electrons, which guarantees peculiar electronic properties of the called π-electron conjugated molecules. The hybridization occurs and it is favored since the energy of the hybrid orbitals is lower than the ones non-hybridized [3, 4].

Among the many possible carbon structures, in nature it is mostly present as two al-

lotropes, diamond and graphite, an extended network of sp^3- and sp^2- hybridized carbon atoms, respectively. In 1797 Tennant demonstrated that these two carbon structures, even if they are characterized by different properties, are constituted by the same building block, *i.e.*, only carbon atoms [2, 5]. The completely different properties arise from the two different hybridizations, which lead to two different atom arrangements in space. In fact, in graphite, the carbon atoms are organized in a planar layer with a hexagonal pattern, and each atom forms a covalent bond to other three. The fourth one is a Van der Waals bond, *i.e.*, the interplanar one, and it is much weaker and keeps the bonding between layers. On the other hand, in diamond each carbon atom is covalently bonded to other four atoms, assuming a tetrahedral disposition. Indeed, the former is characterized by a peculiar softness, while the latter has a distinctive hardness. The diversity between bonds causes the properties of the two materials to be different and, in addition, in the case of graphite they turn out to be anisotropic [6, 7].

In recent decades, one of the most investigated carbon nanostructures is graphene, carbon-based sp^2 system. It is a single layer of graphite and, with it, shares the same honeycomb structure, with the important difference that the structure is no more a 3D crystal, but it is a 2D hexagonal lattice. This means that hybridization could also be found at the nanoscale and at such a level of scale the kind of hybridization as a key role in both geometry and properties [8]. More recently discovered, there are also carbon nanotubes (CNTs), carbon fibers, fullerenes, which are characterized by an intermediate hybridization $sp^2 - sp^3$, or graphynes and yne-diamond, which possess intermediate hybridization $sp^1 - sp^2$ and $sp^1 - sp^3$ respectively. [5, 7, 9, 10]. Figure 1.1 shows a ternary diagram of various carbon nanostructures.
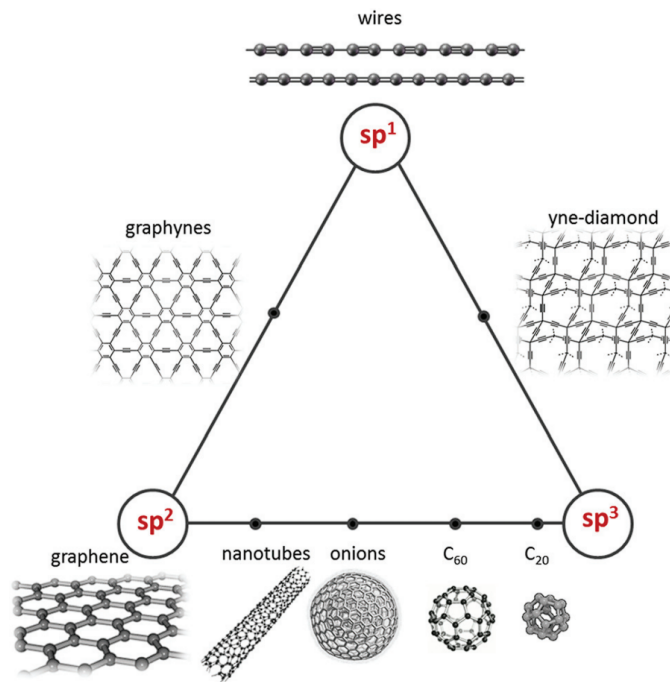
Figure 1.1: Nanocarbon structures divided according to their carbon hybridization [5].

1.2.   The Third Carbon Allotrope

Following the history of carbon, initially, the possibility of the existence of allotropes with *sp* hybridization was not considered. It was not until the late nineteenth century that the first experiments aimed at the synthesis of the first linear carbon systems began. In 1870, Glaser [11] attempted to create linear *sp*-carbon chains, while a few years later in 1885 Baeyer [12] also attempted the fabrication of linear *sp*-carbon chains, but without successful outcomes. In fact, he stipulated that the creation of such allotropes was not possible because of their high instability. Research aimed at the study and discovery of finite chains of carbon *sp* came to a halt until a number of natural compounds derived from minerals, plants, and fungi were discovered [13, 14].

In particular, compounds formed entirely of carbon with alternating single and triple bonds, called polyynes, were found [13]. Thanks to these discoveries, the desire and a new impetus toward the search for these compounds was reborn, and around 1960 Kudryavtsev *et al.* succeeded in chemically synthesizing *sp* chains of carbon. They also christened their discovery by registering the name "carbyne" as the third allotrope of carbon [15].

Optimism renewed, and further discoveries on new synthetic allotropes of carbon, such as fullerenes [16] and nanotubes [17], followed. All these new structures differ from the type

of hybridization of carbon orbitals, and the combination of these structures, if possible, has opened up possibilities for new structures [5, 9].

Nowadays, when we use the term *carbyne*, we refer to an ideal model consisting of an infinite chain of carbon atoms with *sp* hybridization and no longer to finite-length systems as Kudryavtsev did. Indeed, to refer to finite chains of carbon with *sp* hybridization, we use *carbon-atom wires* (CAWs). This means that one of the main differences between the two terms is that, in the case of CAWs, we consider the effect on properties contributed by the end groups [5]. This will be discussed more thoroughly in the next chapters.

1.2.1.   Carbyne Physical Properties and Models

One cannot fail to mention the peculiar mechanical properties, which can be computed from the ideal carbyne model. Carbynes show incredible performance with Young's modulus of more than 32 TPa and, when subjected to tension, reach values up to specific strength 7.5×10^7 Nm/kg resulting by far the stiffest material [18].

In a first approximation, CAWs can be considered as an ideal one-dimensional infinite chain made only of *sp*-hybridized carbon atoms. Their properties can be studied by exploiting an approach derived from solid-state physics.

If *sp*-hybridization is deemed, only two different geometric configurations exist: one that possesses alternating single and triple bonds, called polyyne, and one that possesses all double bonds, called cumulene. Both structures can be considered as a one-dimensional crystal lattice having as unit cells, respectively, two and one atoms (Figure 1.2) [5].

Figure 1.2: Sketch of a cumulene on the left and on the right of a polyyne. Adapted from [5].

Cumulenes, being characterized by all equal bonds, possess two $2p$ orbitals containing one electron each. As preempted in Section 1.1 with LCAO theory, these orbitals are allowed to interact with each other, forming a delocalized π-molecular orbital. As a consequence, the property of electron delocalization along the cumulene chain and the corresponding π-conjugation of CAWs turn out to be maximized [19]. Precisely, because of the formation of the latter orbital, cumulenes are characterized by metallic behavior because their conduction band is half-filled. Figure 1.3 shows the band structure of CAWs. On the left, the characteristic metal structure of cumulenes is displayed, while on the right the characteristic band of polyynes is observed. In contrast of cumulenes,

polyynes exhibit semiconductive properties because they hold single bonds, and because their unit cell consists of two atoms, thus filling the conduction band [5]. In the latter, the conduction band is completely full and is separated by a bandgap formed at the edges of the Brillouin zone. The opening of this bandgap accounts for the semiconductive behavior [5, 19].
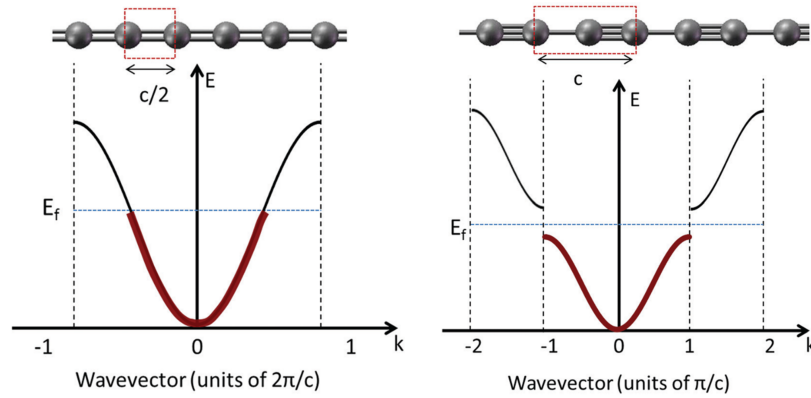

Figure 1.3: Band Structure of cumulenes on the left and of polyynes on the rigth [5].

One parameter that is fundamental to describing and characterizing CAWs properties is the *Bond Length Alternation* (BLA), which defines the difference in length between two adjacent bonds. BLA is affected by the degree of conjugation of the structure: the more a molecule is conjugated, the more BLA is decreased [20]. Theoretically, the value of this parameter is equal to zero for an infinite linear chain formed by all equally double bonds, which corresponds to cumulenes [21].

Figure 1.4 shows the change in the energy gap between the valence and conduction bands as a function of the BLA; as the BLA increases, the energy gap also increases. This means that the higher the BLA, the more the transition from cumulene-like metallic behavior to the semiconductor-like behavior of polyynes. The correlation between the conjugation and the energy gap can also be highlighted above. Indeed, the BLA changes as the conjugation varies and, as the BLA switches, the energy gap changes. Therefore, the smaller the conjugation, the larger the energy gap [5, 21].
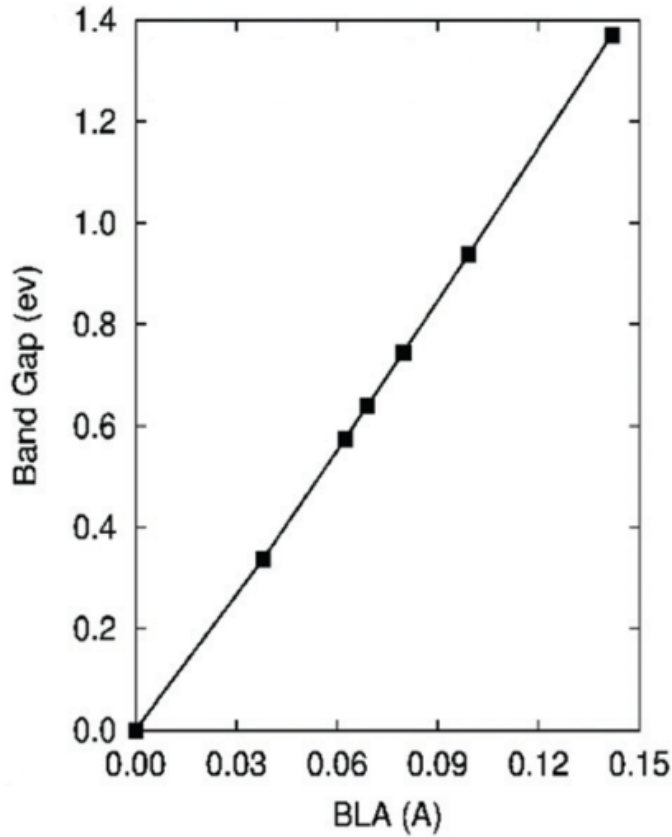
Figure 1.4: Representation of value of energy band gap as a function of BLA [5].

The probability of formation of cumulenes and polyynes is uneven, and the reason lies in the different stability of the two structures. The polyynes origin arises from the interaction between the delocalized electrons of the π-molecular orbital of the cumulenic structure, with the longitudinal phonons, *i.e.*, Peierls distortion. Figure 1.5 shows the trend of potential energy as a function of BLA through a quantum chemical approach [5]. These periodic lattice deformations result in a dimerization leading to atoms in the unit cell going from one to two and lead the system into an energetically favored situation. These important results were demonstrated and obtained through *density functional theory* (DFT), which for a fixed value of BLA, evaluates the vibrational dynamics of the chain [21–24].
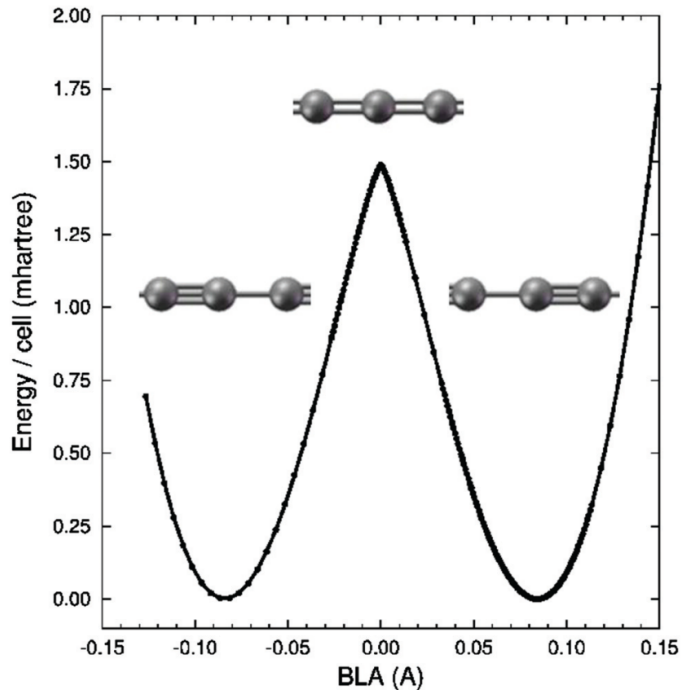
Figure 1.5: Potential energy surface of an infinite linear carbon chain as a function of BLA. It shows the Peierls distortions and the two equivalent possible stabilized structures holding alternating bonds [5].

Discussion has been held so far about an ideal carbyne model. Nevertheless, as previously mentioned, in order to have a more faithful description of a real system, one must take into account the effects that the end groups bring to the chains and the number of *sp*-carbon atoms in the chain. As a matter of fact, the finite length of CAWs and the presence of the end groups are what give the characteristic structural, electronic, and vibrational properties. By being able to control the different terminations and lengths of polyynes, one is able to modify and tune the optical and electronic properties. Hence, this dependence between properties and terminal groups is what is of interest, as it could allow the realization of new functionalized materials [25].

Considering CAWs of finite length, it is worth investigating the correlation between BLA and Peierls distortions. The latter is of fundamental importance in carbyne theory. Indeed, for very long chains, they are responsible for the formation of polyynes chains. However, for shorter chains, it turns out to be the terminal groups that are the ones responsible for the structure of the wire. Yang *et al.* showed experimentally that in the case of chains possessing more than 52 carbon atoms, the most stable configuration is the alternating bond configuration, attributing the reason to Peierls' distortions [26]. Another evidence proved by Chou *et al.* demonstrates that for very long chains, regardless

of the type of end-capping, Peierls distortions in the center of the wire induce a cumulenic structure, while the terminal parts of the chain turn out to be strongly influenced by the type of termination [27]. The aforementioned results confirm how the termination type is of relevant importance for chains of finite length and whether it is appropriate to consider Peierls distortion only for infinite chains. To investigate more about this concept, two distinct situations of two finite chains can be considered: one that has hydrogen as terminations and the other that has CH_2. In the first case, a single bond will be established between the hydrogen and the carbon of the chain forcing, to comply with the octet rule, the formation of a triple bond between the two adjacent carbons. Conversely, in the second case, a double bond will be promoted, thus promoting a cumulene-like structure along the entire chain. Therefore, these differences are reflected throughout the structure, and as a result, the value of the BLA will also vary. It will tend to be closer to zero the more the terminal groups promote a cumulenic structure (Figure 1.6) [5, 25].
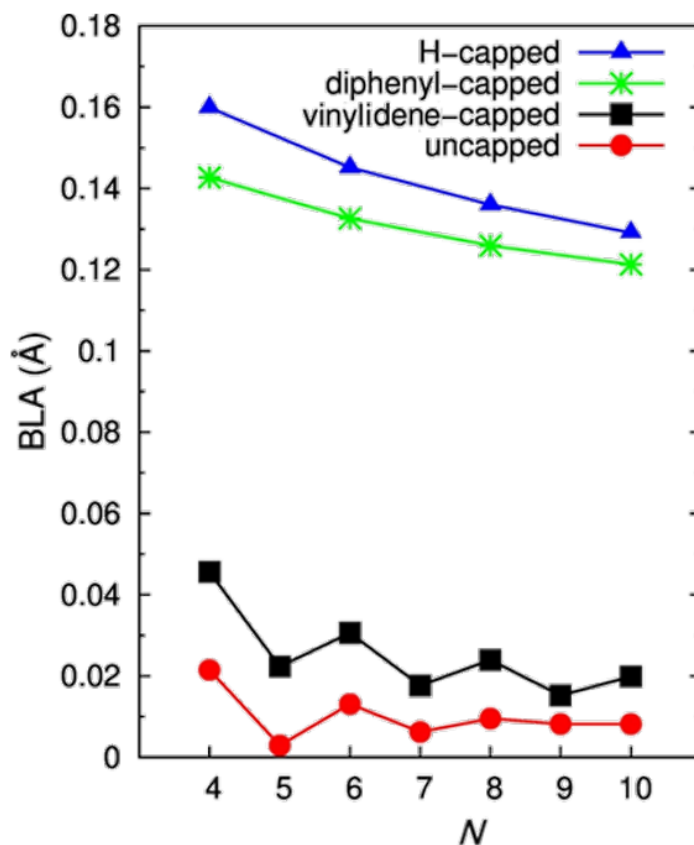

Figure 1.6: BLA as a function of the number of carbon atoms within the chain having different terminations [25].

Figure 1.6 additionally shows how BLA changes as the length of the finite chains varies,

a key feature because it influences the oscillation frequency, a topic that will be discussed in more detail in Section 1.4.1 [25]. It can be seen that at the same chain length, those vinylidene-capped chains compared to hydrogen-capped chains have a more cumulene-like structure. This highlights how geometry is strongly influenced by end effects. Therefore, depending on the type of end groups, it is possible to change the chain structure, greatly reducing the BLA, thus forming structures that are practically considered as cumulenes [25].

1.3.   Synthesis of Carbon Atomic Wires

Carbon-atom wires can be synthesized in several ways, however, the bottom-up approach is generally more widespread. The main methods to produce CAWs are divided into chemical synthesis and synthesis by physical processes.

Chemical Synthesis
As anticipated in Section 1.2, the first chemical synthesis can be attributed to Kudryavtsev [15]. The strategy used here exploits the polymerization of precursors such as acetylene, while other studies show how polycondensation reactions can be exploited using precursors such as acetylide. These syntheses are generally conducted in solution and production is efficient with the advantage that CAWs are produced in a single step. However, due to the nature of production, the products tend to have fairly high polydispersity [15, 28, 29]. Another method proposed by Glaser aims to provide reactions such that products with defined lengths and terminal groups are obtained. The reaction in question is a dimerization of ethynyl groups. In this way, CAWs with consistent lengths and terminal groups can be obtained, allowing for more targeted studies based on length type [30, 31].
The chemical synthesis of polyynes, however, is by no means simple, mainly because of their highly conjugated structure, which therefore requires the use of highly reactive and therefore unstable precursors [32]. For reactions such as those aforementioned, the yield rates are good, but they are functions of the length of the products themselves, *i.e.*, the yield for the production of longer polyynes is lower [33]. Currently, to improve reaction yields, studies are proposing reactions that incorporate sterically demanding end groups in order to "protect" the polyynes structure [32, 34].

Physical Synthesis
Synthesis methods through a physical process are generally based on the formation of a carbon vapor or plasma that is rapidly quenched in a way that promotes the production of carbon structures in non-equilibrium conditions [35]. There are several ways to realize

carbon vapor such as laser ablation or arc discharge, and inert gases or liquids can be used for cooling [36, 37]. Figure 1.7 schematically illustrates different techniques that can be used to produce carbon-atom wires. The techniques of Submerged Arc Discharge (SADL) and Pulsed Laser Ablation in Liquid (PLAL), allow the formation of carbon sp structures in a liquid solution, while pulsed microplasma cluster source and pulsed laser deposition require the presence of a substrate on which the sp-carbon structures can grow [38, 39]. In comparison with chemical syntheses that usually proceed in solutions, physical procedures are more versatile and avoid the use of unstable and harmful precursors. In addition, the first two techniques, *i.e.,* SADL and PLAL, allow one to decide the type of termination by changing the type of solvent that is used to cool the carbon vapor and are more scalable for possible mass-scale production [40]. However, physical syntheses have several drawbacks such as the production of numerous by-products, low reaction yields, and difficult control over the length of chains to be produced [37, 40, 41].
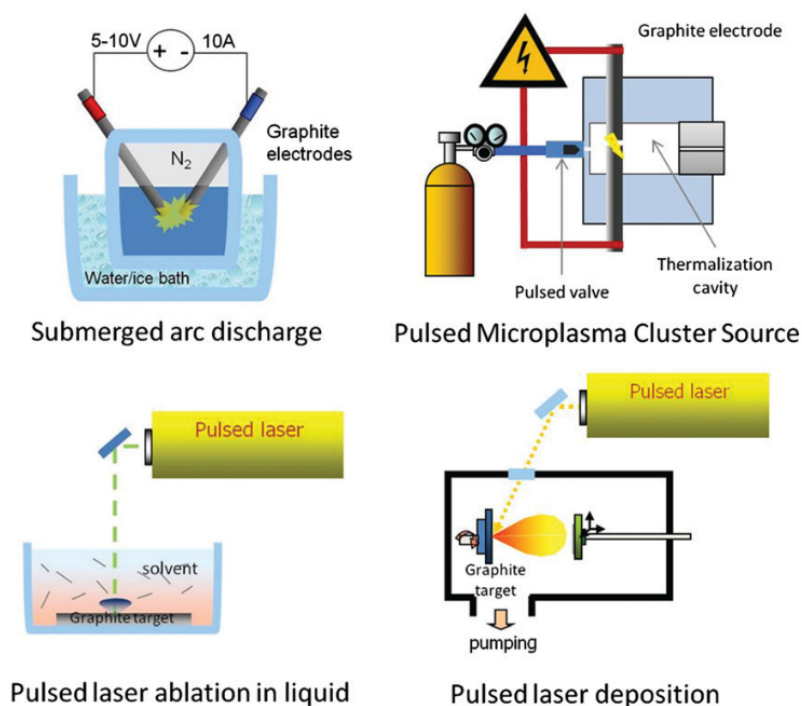

Figure 1.7: Schematic representation of four methods that are used for the fabrication of carbon-atom wires [5].

Because techniques that produce sp-carbon chains in liquid (*i.e.,* SADL and PLAL) seem to be the most promising for industrial production, they will be discussed in more detail. SADL is a technique that exploits the formation of an electric arc in a liquid generated through the application of a voltage between two graphite electrodes. Since the two

electrodes are immersed in liquid, a large electric field must be generated and the position of the electrodes must be carefully controlled. At the beginning of the process, the two electrodes are brought into contact and then slowly separated to maintain the formation of the electric arc. When they come into contact, due to the Joule effect, the temperature rises sharply and steam is generated around the electrodes. Therefore, the electric arc develops inside the vapor, causing the formation of radicals, which are essential for the formation of the structures in our interest. At the same time, carbon vapor is supplied from the electrodes. The liquid therefore functions both to cool the electrodes and to provide the necessary environment for the nucleation of polyynes. This results in the simultaneous formation of chains with different lengths [37, 41, 42].

In this work, polyynes have been produced using pulsed laser ablation in liquid. A detailed discussion of this technique is provided in the following Section 1.3.1.

1.3.1. CAWs Synthesis by Pulsed Laser Ablation in Liquid

Pulsed Laser Ablation in Liquid (PLAL) is a physical synthesis technique where plasma resulting from the interaction between the laser beam and a graphite target is used to produce polyynes. This technique, similar to the submerged arc discharge seen in the previous section, also requires the presence of a liquid solvent where actual nucleation of the *sp* chains takes place [43].

The parameters governing this technique can be divided into two main categories: the so-called material parameters, *i.e.,* the type of target material used for ablation (graphite), the type of solvent, temperature, and pressure of the system, and laser parameters, *i.e.,* wavelength, energy, frequency, number of pulses, and spot area on the target [44, 45].

The formation mechanism of polyynes through PLAL can be explained by following the temporal evolution of physico-chemical phenomena [45]. The first stage is determined when the laser pulse penetrates the liquid (Figure 1.8 (a)). The laser shot, in order to reach the target, must pass through liquid. Moreover, for the entire laser energy to be transmitted only to the target, it is important to avoid liquid breakdown. At this stage, one must also select a solvent that is transparent to the laser wavelength, otherwise, some of the energy will be absorbed by the solvent itself. The second stage is identified when laser pulse absorption occurs (Figure 1.8 (b)). This happens when the laser hits the target, and given the short duration of the laser pulses (nanoseconds) and pulse fluence, linear and nonlinear optical phenomena are generated, causing instantaneous localized photo-induced ionization. At the same time, thermal phenomena also occur such as thermionic emission, boiling, melting, and vaporization. Subsequently, detachment of the ablated material occurs (Figure 1.8 (c)). Indeed, all the phenomena of the previous stage

promote the detachment of material from the target. The temperature locally reaches very high values compared to the parts not irradiated by the laser, and at the juncture, when the material detaches, three different thermal processes can occur that would justify the detachment. Specifically, vaporization, normal boiling, and "explosive boiling". The latter would seem to be the main phenomenon driving the process and occurs when the target is heated rapidly to a critical temperature, leading to its decomposition into vapor. [45–47]. Due to the very high temperature and photo-ionization, the ablated material contains ionized species and is regarded as a non-equilibrium "plasma plume". Afterward, the expansion and quenching of the plasma plume occurs (Figure 1.8 (d)). Owing to the presence of the liquid, the plasma plume is confined near the ablation zone. This confinement of the expansion, causes the cooling rate to be slowed down and a larger portion of the target to receive the energy. Therefore, the material target receives energy from both the laser pulse and the plasma plume [45, 48]. Thereafter, some of the energy is transferred to the solvent and so it, as well, heats up considerably. In this phase, ionization, pyrolysis of its molecules and degradation occur. At this very stage, mixing occurs between the species of the target and those of the solvent. Following the time course of the process, the expansion and collapse of cavitation bubbles occurs (Figure 1.8 (e)). Plasma plume after a short time is extinguished, and due to the energy released to the solvent, cavitation bubbles arise [47]. Then, the bubbles collapse and a shockwave is emitted. The latter is crucial because of the increase of both temperature and pressure at its collapse point. Thus, the condition can be compared to the one of the plasma and new phase transitions are promoted. Lastly, the slow growth and agglomeration of nanomaterials occur (Figure 1.8 (f)). Indeed, subsequently the cavitation bubbles and their collapse and generation of shockwaves, a steady state condition is reached. In this stage, the nanomaterials will be modified due to the condensation of ablated atoms and molecular clusters [45, 49].
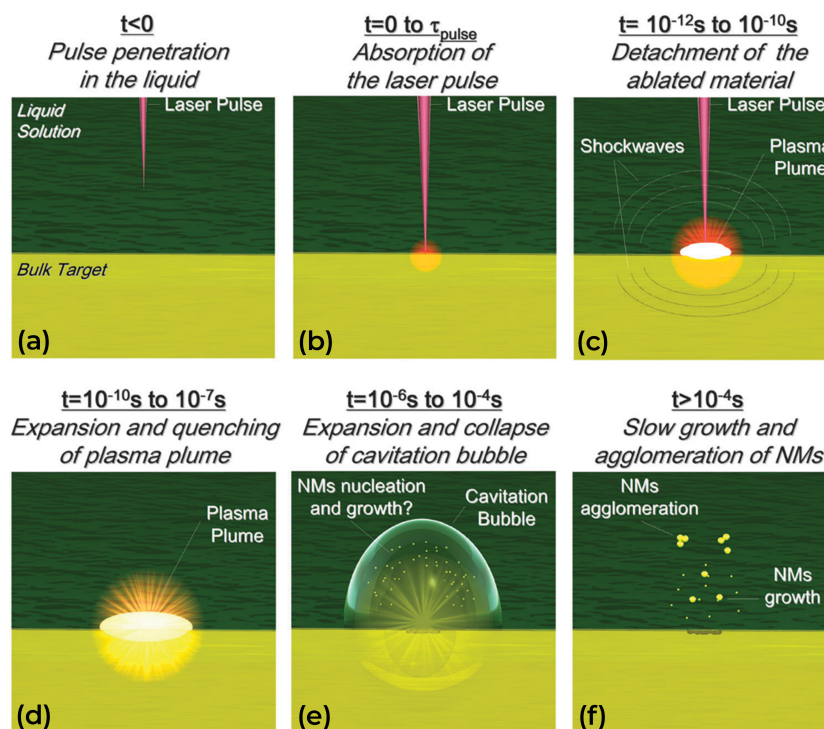
Figure 1.8: Sketch of formation of nanomaterials with nanosecond pulses laser ablation [45].

As mentioned in Section 1.3, physical techniques have advantages over chemical methods. In this work, PLAL was chosen because the degree of purity of the final solution is better and the operational cost is lower. Particularly, with PLAL the volume of solvent used is much less, and also the quantity of byproducts generated during the production of polyynes is lower [50]. In addition, one of the ultimate purposes is to expand mass-scale production, and PLAL lends itself to scaling [40, 51]. Therefore, because one of the aims of this thesis is to seek to increase the production of polyynes while maintaining a higher degree of solution purity, the use of PLAL as a physical synthesis method is preferable.

1.4. Characterization Methods of Polyynes

Several techniques exist to be able to characterize polyynes. In the next Sections, a Raman-based techniques (*i.e.,* Surface Enhanced Raman Spectroscopy (SERS)), UV-Vis spectroscopy, and High-Performance Liquid Chromatography (HPLC) will be explored as these are the techniques that were adopted in this thesis work.

1.4.1.   Raman and Surface Enhanced Raman Spectroscopy (SERS)

Raman spectroscopy is a technique exploiting light-matter interaction; specifically, monochromatic radiation is incident on a sample, and inelastic scattering occurs, *i.e.*, the Raman scattering. Indeed, when a sample is irradiated by monochromatic light, the electrons in the sample are promoted from the ground state to a higher energy virtual state, *i.e.*, the excitation process (Figure 1.9). Afterward, relaxation occurs with a radiative process either at the same energy level or in a different one. If the decay occurs with the emission of a photon having the same energy as that of the incident photon that caused the excitation, the scattered radiation will have the same frequency as the source, and this phenomenon is called elastic scattering or Rayleigh scattering (Figure 1.9). If, on the other hand, the decay occurs with the emission of a photon with energy greater or less than that of the incident radiation, it is called anti-Stokes and Stokes scattering, respectively (Figure 1.9). The latter two possibilities are inelastically scattered radiation and generally occur much less frequently than in the elastic case [52].
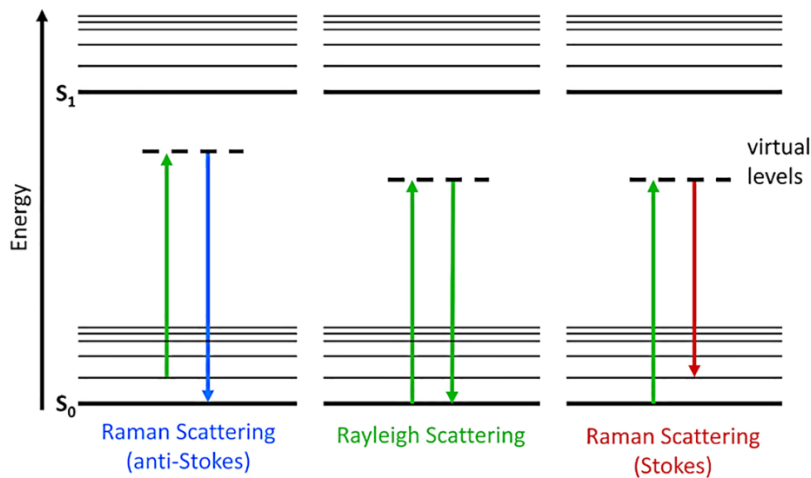

Figure 1.9: Jablonski diagram showing Rayleigh and Raman scattering [53]

The energy variations possible during inelastic scattering events rely on the vibrational levels of the sample, which, in turn, are dependent on the nature of the sample itself [54]. Therefore, through quantum correlations, it is possible to associate the variation in energy of the emitted photons with respect to the incident photons. Because of this modulation on the frequency that is specific to the molecular vibrational states of the sample, it is possible to analyze the composition of the material through the information of the Raman spectrum. Precisely, it is the analysis of the frequency shift, *i.e.*, Raman shift, that provides information about the sample. A Raman spectrum is hence obtained

by showing the intensity of inelastically scattered light as a function of the Raman shift generally expressed in cm^{-1} [52].

Among the many applications of Raman spectroscopy, Raman is of particular importance for the characterization of carbon nanostructures. This is mainly because of the unique fingerprint that sp-carbon structures have in the Raman spectrum. Indeed, Raman signals of carbon structures are of considerable importance because they enable the detection of the different hybridizations of the various allotropes. As shown in Figure 1.10, depending on their hybridization, carbon nanostructures present Raman-peaks in different spectral regions. In particular, carbon-atom wires have signals located in the region between 1800-2300 cm^{-1}, sp^2 structures between 1300-1600 cm^{-1}, and sp^3 structures around 1300 cm^{-1} [25].
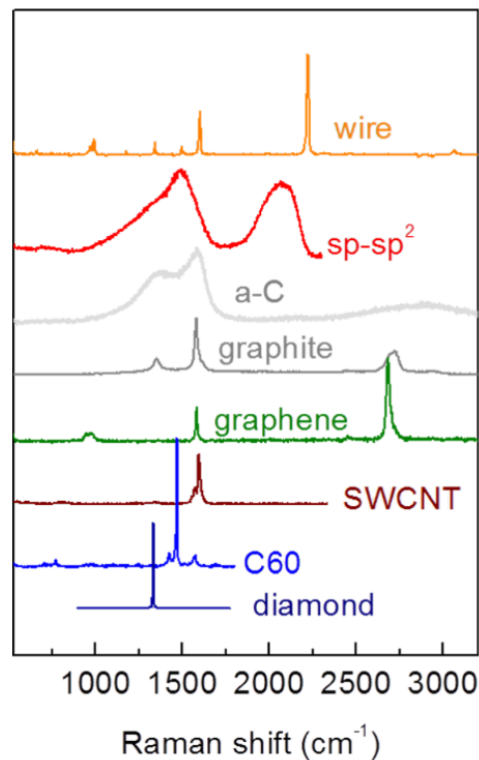

Figure 1.10: Raman spectra of different carbon structures [25]

Delving into sp-carbon wires, their Raman spectra are characterized by an intense peak called "*ECC mode*" (Effective Conjugation Coordinate model) or "α *line*" that corresponds to the in-plane oscillations of BLA with the simultaneous collective stretching of CC triple bonds and contraction of CC single bonds [25]. The second signal peculiar to sp wires is called the "β *line*". This is less intense than the ECC signal, is observed for shorter wavelengths, and corresponds to the out-of-phase stretching of CC triple bonds.

The latter appears only when the length and termination of real finite CAWs are taken into account [25, 40, 55–57]. Tabata *et al.* showed how these signals vary in the case of hydrogen-capped polyynes, and it is observed that as the length of the chains increases, the position of the α line signal varies toward smaller values of wavelength, while the β line signal changes erratically and its intensity decreases [58]. More precisely, as the length of the chain increases, the ECC signal becomes intense enough to cover the secondary peak making the latter appear as if there is a decrease in intensity in the beta peak itself. The increase in intensity is explained by the fact that strong electron-phonon coupling is generated. Whereas the redshift in the frequency of the alpha signal can be explained by the fact that an increase in the length of the chain increases the conjugation [56].

The problem of characterizing CAWs by Raman spectroscopy is the sensitivity limit of this technique. As shown in Section 1.3, physical synthesis techniques have low yields of production. The concentrations of polyynes produced with PLAL are in the range of 10^{-5}-10^{-6} mol/l [56]. However, through the Raman technique, a signal cannot be obtained unless the concentration is at least 10^{-3} mol/l [59]. Therefore, a technique that is more sensitive is needed. One of the objectives of this thesis is to try to observe this phenomenon through Surface-Enhanced Raman Scattering (SERS) for size-selected polyynes embedded in electrospun polymeric nanofibers. As mentioned above, the so-called Surface Enhanced Raman Spectroscopy (SERS) can be used. SERS allows increasing the sensitivity of Raman Spectroscopy because it exploits the interaction between the analyte and appropriate metal nanosurfaces [56]. By introducing metal nanoparticles, usually of noble metals (Silver in the case of this thesis work) the sensitivity of Raman signals can be increased by a factor of 10^6 [56, 60]. The physical mechanism that describes SERS is the near-field enhancement of the Raman laser probe by resonance with surface plasmons formed in the metal nanoparticles. The enhancement is greater the closer the excitation wavelength of the laser is to the plasmonic resonance frequency of the nanoparticles. Moreover, for polyynes, an additional contribution defined as chemical enhancement occurs [60]. The latter results when the analyte, the solution containing polyynes in this case, generates complexes with the nanoparticles. This promotes charge transfer and the Raman signal is thus further enhanced [60–62]. As shown in Figure 1.11, the SERS spectra of polyynes turn out to be different from the Raman spectra. New signals arise around frequencies of 2000 cm^{-1}, and the α line peaks are also observed to widen and shift to lower frequencies [25].
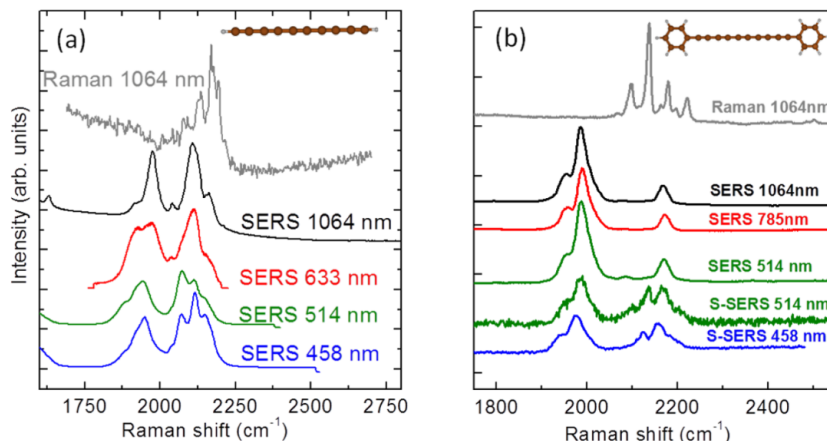
Figure 1.11: Comparison between Raman and SERS signal of H-capped (a) and phenyl-capped (b) polyynes at various laser wavelengths [25].

The reason for the formation of the new signal is still not entirely clear, although studies attribute the cause to the interaction of Silver Nanoparticles (AgNPs) and polyynes [61]. For example, complexes could form between polyynes and nanoparticles, or low-frequency modes could be generated with the interaction between AgNPs and polyynes edges, or the hydrogen terminations of polyynes are replaced with silver atoms [56, 61]. These are some of the possible explanations for the formation of the peak around 2000 cm^{-1}, however, the presence of this intense peak is what makes SERS a popular technique for the detection of polyynes [58, 60].

1.4.2. UV-Vis Spectroscopy

UV-Vis spectroscopy is a widely used technique to investigate electronic and optical properties that exploits light-matter interaction. A light beam, whose wavelength is in the visible to ultraviolet range, interacts with the sample. Then, the sample interacts with the incident light, and if the energy of the photon perfectly matches a transition between two energy states of the sample, some electrons of the sample are promoted to a higher energy state. Specifically, the energy must be equal to the difference between the two electronic energy states. Hence, as long as the energy of the photon is matched by this difference, there will be an interaction (*i.e.,* the photons are absorbed), otherwise, the light beam will pass through the sample (*i.e.,* the photons are transmitted). With this instrument it is then possible to estimate a ratio between the number of incident photons and photons that are absorbed or transmitted through the sample. An absorbance ($A = \epsilon c l$, which will be descrbed later) or transmittance ($T = I/I_0$, *i.e.,* ratio of transmitted radiant flux intensity to incident radiant flux intensity) can be determined from these values.

Through UV-Vis spectroscopy measurements, quantitative measurements of product concentration can also be obtained. The Lambert-Beer law linearly correlates absorbance with the molar concentration of the analyte: $A = \epsilon c l$. A is the absorbance, ϵ is the molar extinction coefficient (cm^2/mol), c is the concentration (mol/cm^3) and l is the optical path in the sample (cm) [63].

The absorption spectrum of polyynes exhibits peaks in the ultraviolet region [40, 64]. These peaks are caused by the transition between the HOMO (Highest Occupied Molecular Orbital) and LUMO (Lowest Unoccupied Molecular Orbital) band, *i.e.*, the energy gap [26]. As discussed in Section 1.2.1 as the length changes, the conjugation and consequently the energy gap will change. The longer the polyynes are, the more the value of the energy gap decreases, therefore the absorption peak will also move in agreement, as shown in Figure 1.12 (a).
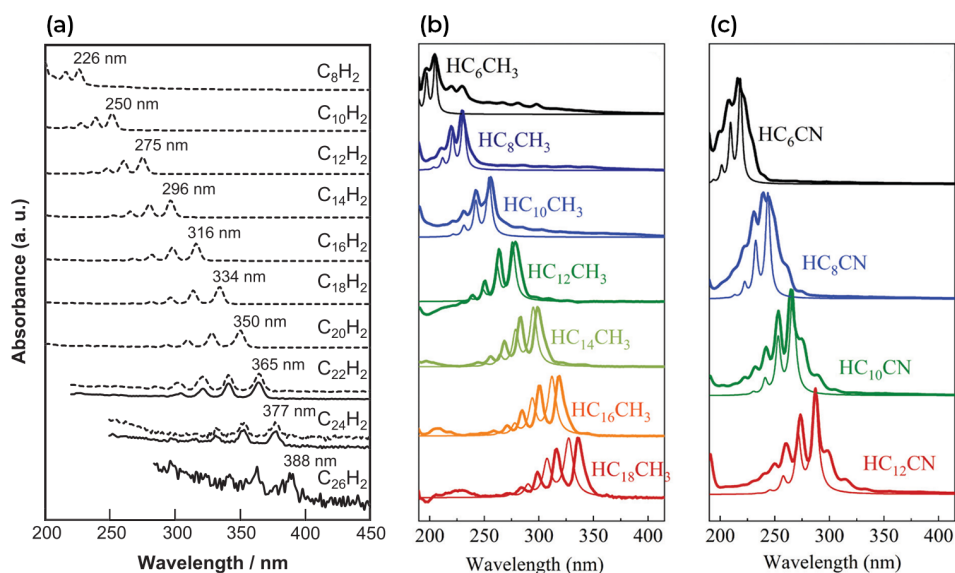
Figure 1.12: UV-Vis spectra of different length H-capped polyynes obtained by PLAL in decalin (a), UV-Vis spectra of different length methyl-capped polyynes obtained by PLAL in acetonitrile (b), UV-Vis spectra of different length cyano-capped polyynes obtained by PLAL in acetonitrile (c) [40, 65]

Furthermore, Figure 1.12 (b) and (c) show the effect of terminal groups, which influence vibrational properties and change the position of absorption peaks. Thus, through UV-Vis spectroscopy it is possible to both determine the lengths of the polyynes, their termination type, and their concentration [40].

1.4.3. High-Performance Liquid Chromatography (HPLC)

The second technique, High-Performance Liquid Chromatography (HPLC), is used to separate polyynes according to their length and termination. The process takes advantage of two different phases, a mobile and a stationary phase. The latter is a column whose interior is composed of a solid particles functionalized in order for it to interact with the molecules passing through its inside. Specifically, interactions based on polarity are exploited. The column is the key element of HPLC; indeed, the retention time of the molecules inside the column depends on their structure. The more similar the structure is to that of the stationary phase, the longer it will take for the molecules to pass through the entire column. Moreover, one must consider the steric hindrance, namely that the longer or larger a molecule is, the more it will struggle to overcome the particles in the column. Our specimen is diluted in the mobile phase and then injected into the stationary phase. Through a pumping system, the mobile phase is constantly pushed through the column, and simultaneously a detector records a time-dependent chromatogram. Moreover, HPLC holds a UV-Vis spectrophotometer, which, as described above, allows the polyynes to be identified according to their length and termination. This provides a real-time spectrum of what is flowing into the column, which is essential to be able to separate polyynes. For polyynes, the stationary phase is generally composed of micrometer-sized particles of silica, and the mobile phase is a mixture of solvents, usually water and acetonitrile. Through interaction with functionalized silica, polyynes with longer lengths tend to have longer retention times. This happens, as explained just above, because of the different chemical interactions and the steric hindrance of long chains. By observing the characteristic UV-Vis spectrum, it is possible to determine and separate the different polyynes as a function of time and to obtain mono-dispersed solutions [37, 40]. This is important because through physical techniques such as PLAL or SADL solutions containing polyynes of different lengths, with different terminations and with the presence of by-products are obtained. After the HPLC process, pure samples containing only polyynes with a given length and termination are achieved [40].

1.5. Stability and Degradation

The main problem faced by CAWs is stability. To date, two main causes of the degradation of CAWs are attributed, *i.e.*, crosslinking and oxidation reactions [25, 66–69]. Crosslinking reactions occur spontaneously due to interactions between the chains themselves. This happens because the structures tend to form more stable sp^2 compounds, and physical factors such as high temperatures, light exposure, high concentrations, and basic

solvents accelerate these processes [69]. They are subject to degradation and the more severe the longer they are. Furthermore, the environment in which they are situated may greatly accelerate their degradation. The type of termination influences the rate at which degradation occurs. This is because different terminal groups have electro-attractive or electro-donative functions. Hence, not only the environment in which they are located but also the nature of the polyynes themselves plays a crucial role [70]. Several strategies have been proposed over the years to improve the stability of polyynes. A first possibility to try to reduce chain interactions, and thus the possibility of crosslinking, is to produce polyynes having sterically bulky end groups [71, 72]. This succeeded in producing chains over 40 carbon atoms long that are stable under normal conditions [73]. Another strategy is to encapsulate CAWs inside nanotubes [33]. The idea is to use nanotubes as a protection for the *sp*-chain and has allowed the realization and achievement of the longest CAW ever observed, exceeding 6000 carbon atoms in length [33]. Finally, a last strategy is to incorporate CAWs into composite solid systems. Studies aim to incorporate polyynes into polymeric matrices, obtaining signals of polyynes stability for more than six months [74, 75], thanks to the synergistic action of solid-matrix systems and use of silver nanoparticles (see Section 1.4.1) [76]. The use of polymer and the formation of composite materials with a polymer matrix allowed for increased stability of the polyynes, as it reduces the mobility of the chains thus reducing the possibility of crosslinking. Furthermore, the combined action with metal nanoparticles as discussed in Section 1.4.1, besides allowing the SERS signal, promotes the formation of complexes with the polyynes themselves and would appear to have stabilizing functions [76]. Increasing the stability of polyynes is crucial for developing applications, and understanding how the parameters for nanocomposite formation affect stability has not yet been explored. Hence, this is one of the goals of this thesis work and will be further explored in Section 5.

2 — Polymeric Wires Nanocomposites

As the name suggest, composites can be defined as a combination of two or more different materials. They are composed by a matrix, the most plentiful material, and by reinforcements, the minor components. The former could be made by different classes of materials, but polymeric ones are identified among the most studied [77]. In general, the reinforcements are embedded inside the matrices with the aim of producing composites with increased properties (*e.g.*, mechanical, electrical, etc.). Nanocomposites are defined as if one or more components have dimensions less than 100nm [78]. Nowadays, nanocomposites have interested many studies due to the high enhancement of properties that they can provide, even with small amount of reinforcement [78]. Indeed, despite the nanometer size of the reinforcement, effects occur on the macroscopic properties of the final composite [79]. Among the properties for which nanocomposites stand out, one of the most noticeable effects, given the presence of the filler, is the greatly improved load transfer between the matrix and the reinforcement, due to the high area/volume value of the nanoscale filler. Improvements outside the mechanical domain also occur; for example, by using carbon-based reinforcements, the conductivity of the polymer is improved. Therefore, depending on the type of reinforcement used, it is possible to improve different specific properties [78–80].

There are several studies related to polymer nanocomposites using CAWs as the reinforcing element [79]. However, the main difference that distinguishes Carbon-Atom Wires from other reinforcements is that the incorporation into polymer matrices is mainly to improve the stability of the wires themselves. As discussed in Section 1.5, there are several advantages and improvements related to the stability of CAWs using nanocomposites. Those can be explained considering that the incorporation of polyynes within polymer matrices stabilizes the polyynes themselves by reducing the possibility of crosslinking and the formation of sp^2 structures [74].

2.1.   Electrospinning

Among the many possible techniques that can be used to produce polymeric nanocomposites, in this thesis, we explored the use of electrospinning. Specifically, the aim is to produce polymeric nanometer-sized fibers embedding polyynes. With the correct choice of polymer type, discussed in Section 3.1.2, it is also possible to embed silver nanoparticles within the composite, which are essential to achieve SERS and the detection of polyynes produced with PLAL, as discussed in Sections 1.3.1 and 3.2.1.

Electrospinning produces nanofibers whose diameter reaches only hundreds of nanometers. The working mechanism is well known and exploits a large potential difference that is applied between the solution to be electrospinned and a conductive surface, *i.e.,* the collector. To facilitate the process, the solution is placed inside a syringe, with which it is possible to control the pump rate and, consequently, the amount of solution emitted from the needle at each instant, and a small amount of the solution is electrified and stretched until it forms a fiber. The latter is deposited on the conductive surface or on top of a substrate. The solution should be liquid and generally contain a dissolved polymer within it [81–83]. A typical electrospinning apparatus (Figure 2.1) consists of a polymer solution that is placed inside a syringe and is pumped through a thin nozzle having a diameter of about 100 μm. To ensure that the flow is uniform and controllable, a mechanical system is used to manage the thrust pressure outside the syringe. The nozzle, in addition to handling the amount of solvent, is simultaneously employed as an electrode. An High-Voltage power supply is used to apply the voltage (in the order of tens of kV) between the nozzle and the metal collector. The counter electrode is a metallic plate placed at 10-25 cm to the nozzle. On this, typically, the electrospun fibers are collected on a substrate that is placed on this plate and put in electrical contact with it in order to ensure proper deposition. [83].
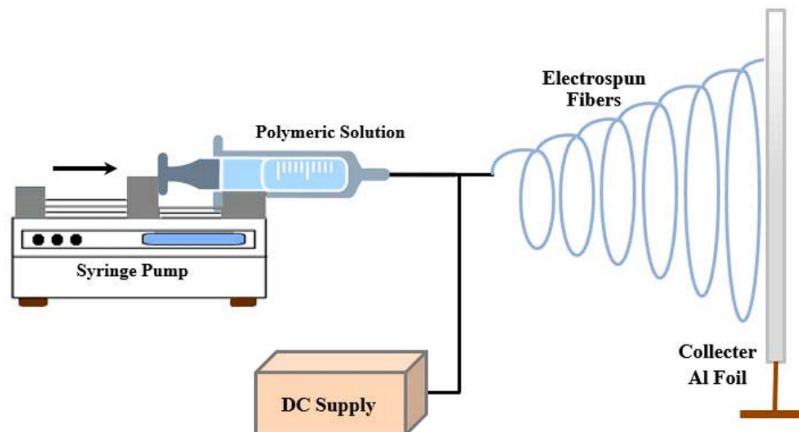
Figure 2.1: Sketch of a typical electrospinning apparatus [84].

Fibers with different characteristics can be obtained using different types of counter electrodes (also called collectors). With static collectors, fiber deposition is a chaotic process, and the final membrane will be composed of fibers randomly distributed. On the other hand, to obtain a material composed of fibers whose orientation is well-controlled, dynamic collectors must be used, like rotating cylinder or rotating disk [83].

The physical process of electrospinning can be described as follows. The polymer solution inside the syringe and at the tip of the nozzle is kept on it by surface tension. Applying the potential difference, a charge is generated on the surface of the liquid, and the repulsion of the charges themselves generates a force in the direction opposite to that of the surface tension. As the electric field strength increases, the shape of the liquid droplet at the end of the nozzle changes from a hemispherical to a conical shape, *i.e.*, the Taylor cone [85, 86]. Once a critical value is reached, the electrostatic repulsive force overcomes the surface tension and the charged solution is ejected from the nozzle. During this phase, the solvent in the polymer solution evaporates, and a charged polymer fiber is then generated. On the way to the collector, the fiber is stretched and its diameter is reduced. Finally, the fiber is collected directly on the collector or the substrate placed on it. The single jet can split into several jets due to the electrical charges that are generated. This would account, along with the elongation due to the acceleration of the jet itself, for the very small size of the fiber diameter. This process, called splaying, is not yet fully understood [86, 87] and it is regarded as a phenomenon of process instability. There are other instabilities: those caused by fiber whipping instability, which causes jet bending, or, if electrospinning parameters are not properly chosen, asymmetrical instabilities, known as Rayleigh instabilities, can occur, leading to the formation of so-called pearl-necklace arrangements (Figure 2.2) [83, 86].
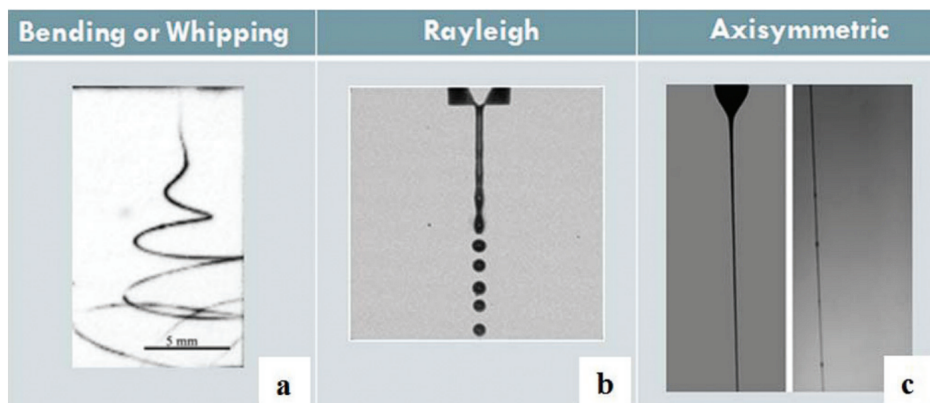
Figure 2.2: Different types of jet instabilities: Bending or whipping instability (a), Rayleigh instability (b) and axisymmetric instability (c) [88].

Modifying the electrospinning parameters it is possible to control the fiber morphology reducing the presence of defects and controlling the fiber diameters. Those parameters can be divided into machine parameters (Section 2.1.1), solution parameters (Section 2.1.2), and setting parameters (Section 2.1.3).

Many polymers can be processed with electrospinning and they can be subdivided into natural or synthetic [77]. Examples of synthetic polymers are polystyrene (PS) [89], polyethylene terephthalate (PET) [90], polyvinyl alcohol (PVA) [91], polyethylene oxide (PEO) [92], and many others; while natural polymers are for example proteins, polysaccharides, terpenes, and lipids [93]. In this thesis work, a synthetic polymer was used, *i.e.,* PVA, and regarding solvents, the most commonly used are organic solvents since they provide, depending on the polymer, good solubility. However, for insoluble polymers in organic solvents, water can be used, although due to its high dielectric constant, it is not among the best solvents for electrospinning [94].

2.1.1. Process Parameters

Process parameters refer to the value of the applied potential, the distance between the two electrodes, the flow rate, and the type of collector.

Voltage

As discussed in the Section 2.1, the potential difference that has to be applied must be sufficient to overcome the force resulting from the surface tension of the solution and initiate the electrospinning process [83]. To date, the role and effect that the potential value has on the final diameter of nanofibers is not yet entirely clear and partly controversial

[95–98]. Studies suggest that using large voltages promotes the formation of fibers with larger diameters (Figure 2.3 on left) [95]; conversely, other studies associate increased voltage with an increase in jet repulsive forces thus favoring thinner fibers [96]. Other studies, on the other hand, do not attribute a change in diameter to changes in voltage, but using higher voltages decreases the probability of fiber breakage and results in more homogeneous fibers (Figure 2.3 on right) [97]. However, even for this last consideration, there are divergent views. Namely, studies associate high voltages with decreasing Taylor cone, causing inhomogeneity in the jet [98]. Thus, despite the controversy, the role of voltage is important and varies depending on the type of solution and the other several parameters.
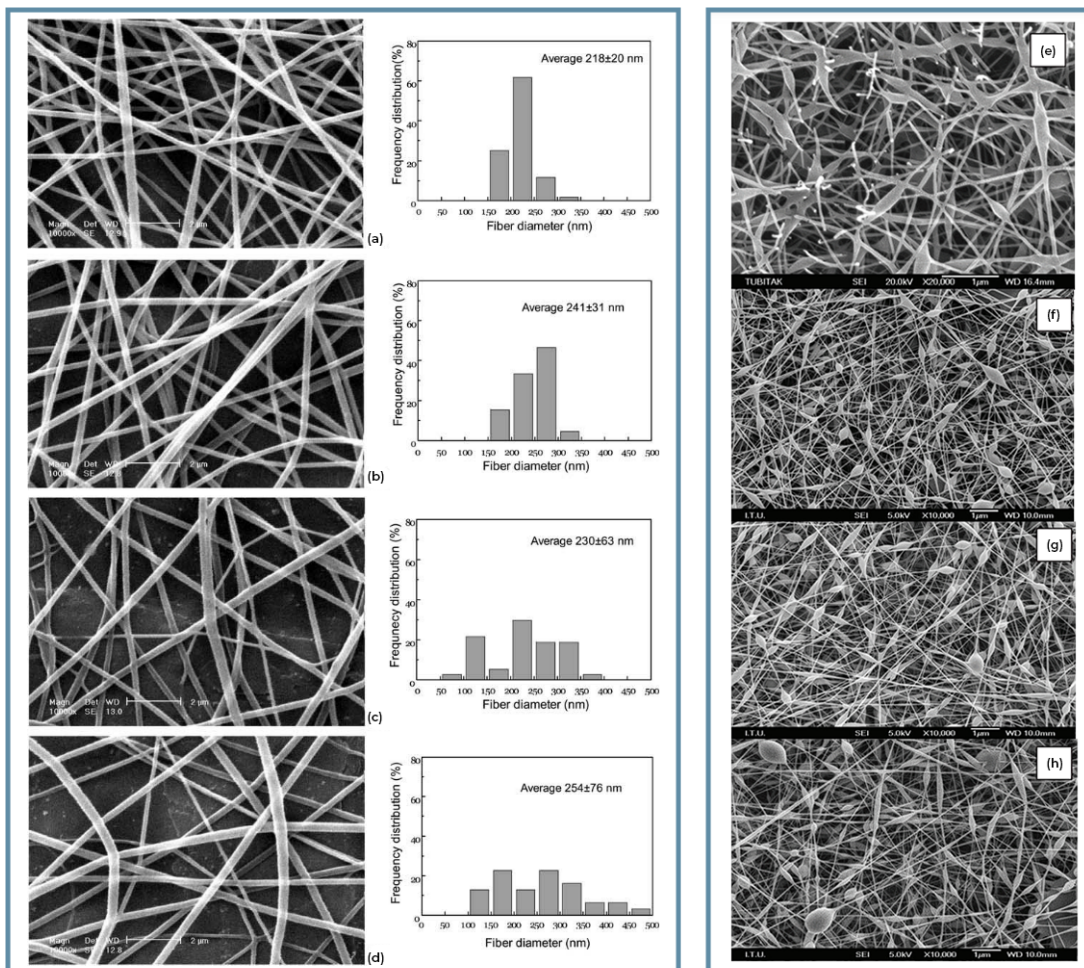
Figure 2.3: On the left, effect of voltage on fiber diameter of a PVA/water solution. Voltage: 5kV (a); 8kV (b); 10kV (c); 13kV (d). On the right, effect of voltage on fiber beads of a PVA/sodium alginate solutions. Voltage: 28 kV (e); 35 kV (f); 40 kV (g); 45 kV (h) [95, 97].

Distance

The distance between the tip and the collector should be in the range of 10 to 25 cm [83]. The reason for this is that a minimum distance must be ensured for the solvent to evaporate during fiber stretching. Proper evaporation of the solvent is necessary to prevent the formation of beads inside the fibers. Indeed, the process of nanofiber formation is governed by the simultaneous evaporation and elongation of the solidifying fiber [99]. While the greater the distance, the more the fibers will be stretched and, therefore, the lower the diameter. However, as explained just above because of the simultaneous effect between evaporation and fiber stretching, the distance may not be excessively large, otherwise, the deposition of the fibers themselves will not occur [83, 98].

Flow rate

The role of the flow rate is similar to the distance between the tip and collector. Namely, the value of the flow rate should not be too high, otherwise, the solvent will not totally evaporate. In this case, defects, uneven deposition, droplets, and beads may occur. Conversely, low flow rate values allow proper evaporation, enhancing electrospinning overall. However, for too low values of flow rate, solvent may evaporate at the end of the syringe, risking clogging the nozzle [98, 100].

Collectors

As described in Section 2.1, the main role of the collector is to be a conductive surface to act as an electrode, and, if fibers are deposited above a substrate placed on the collector, an electrical connection should be ensured. Among the many possible collector configurations, the simplest one is a static collector, thereby obtaining membranes with randomly distributed fibers. Then, more complex systems exist, such as those shown in Figure 2.4, to achieve membranes made of aligned fibers. The latter include possibilities for rotating and dynamic collectors with particular shapes [101, 102].
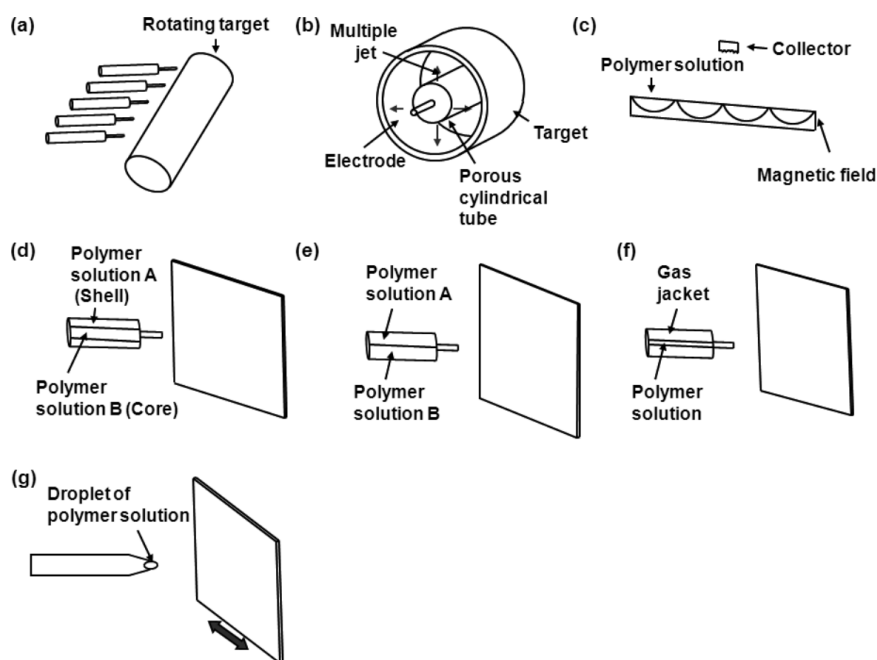
Figure 2.4: Sketch of various electrospinning nozzle: multiple nozzles (a); porous tube with multiple jets (b); multiple electrodes using a normal magnetic field (c); coaxial nozzle (d); bicomponent nozzle (e); gas jacket nozzle (f); scanning tip electrospinning (g) [102].

2.1.2. Solution Parameters

Solution parameters include polymer concentration, molecular weight of the polymer, viscosity of the solution, type of solvent, surface tension, and conductivity.

Concentration

Polymer concentration is a critically important parameter, and depending on the value, different situations can be identified. If the concentration is very low, the result is not a proper electrospinning, but more of an electrospray. This is because polymeric micro and nano-particles will be obtained on the substrate instead of fibers. The reason is that a too low concentration of the polymer does not guarantee the correct viscosity and surface tension of the solution [103]. Furthermore, a minimum concentration is required to allow entanglement of the molecular chains and for electrospinning to proceed [94]. When the concentration increases, the viscosity of the solution increases and a more continuous and homogeneous polymer jet begins to occur. Gradually increasing the concentration, it transitions from a phase where the fibers have numerous defects until a proper balance between the forces involved is achieved, resulting in fibers free of beads and defects. Afterward, a range of concentrations results in homogeneous fibers [104]. Lastly, when the

concentration is excessively high, the fibers begin to be discontinuous due to the excessive viscosity of the solution and, as the concentration increase, the diameters go from nanometer to micrometer scale [98] (Figure 2.5).
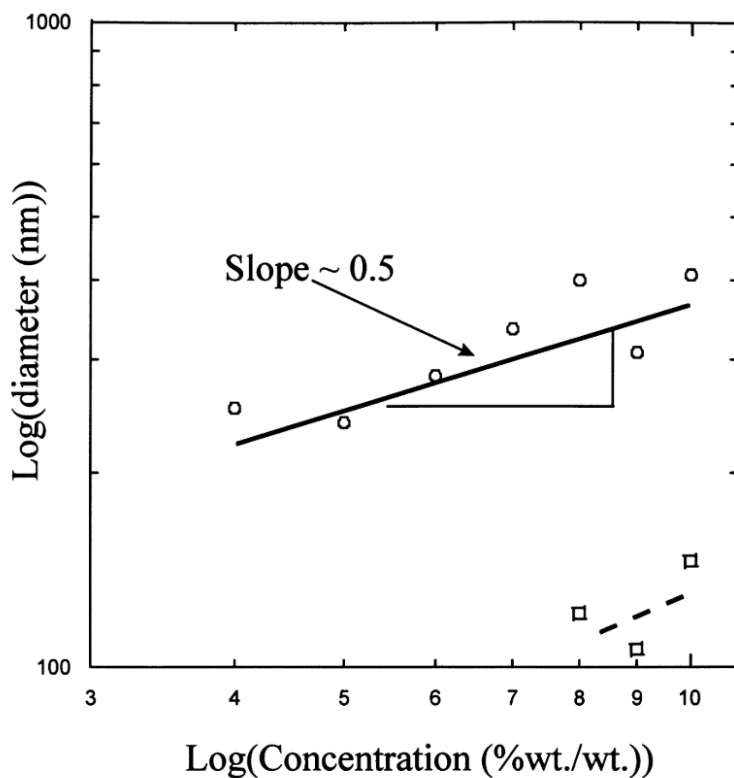
Figure 2.5: Diagram of the average fiber diameter as a function of PEO solution concentration. Circles are the primary distribution, squares are secondary distribution [103].

Molecular Weight (MW)

The effect of molecular weight is relevant because it affects fiber morphology. Similarly to concentration, it is possible to identify an optimal range for fiber production. Namely, keeping constant the concentration and changing the molecular weight of the polymer, there is a variation in the fiber morphology and happened that for low values, the fibers will tend to form beads. Increasing this parameter, there is a range in which fibers are homogeneous and defects-free. A further increase leads to fibers with excessively large diameters and a higher defectiveness (Figure 2.6). These phenomena can be justified by the fact that the molecular weight is directly related to the entanglements of the polymer in the solution. Hence, as the molecular weight increases, the viscosity increases as well and the role of viscosity will be discussed in the following section. [91].
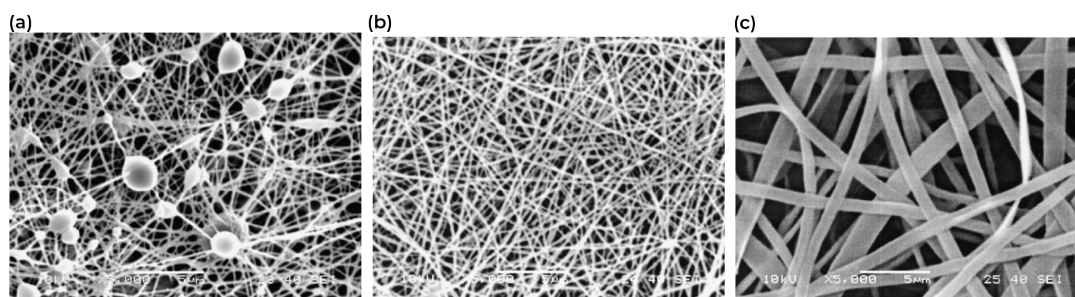
Figure 2.6: Effect of the molecular weight on electrospun fibers diameter. Molecular weight: 9000–10,000 g/mol (a); 13,000–23,000 g/mol (b); 31,000–50,000 g/mol (c). The concentration was 25 wt.% [91].

Viscosity

The viscosity of the solution is crucial to obtaining good fibers. As previously shown, it changes as the other parameters of the solution change, and to perform electrospinning, a suitable value is necessary. Indeed, when the viscosity is too low, surface tension will be dominant during the process and the fibers produced will contain beads. The formation of nanofibers containing beads is due to the relationship of solution viscosity with the net charge density carried by the jet during the process and the value of surface tension. These parameters change the morphology of the fibers, in particular higher viscosity and net charge density reduce the presence of beads. While the effect of surface tension is opposite, *i.e.,* a low value improves fiber homogeneity [94]. Conversely, when the viscosity is too high, the flow through the nozzle may become obstructed and the spinning process may be discontinuous [105]. Lastly, it is also important to consider how environmental parameters can affect the viscosity; a detailed discussion will be given in Section 2.1.3 [106].

Solvent and Surface Tension

In the electrospinning process, it is important to select the proper solvent since it can affect the surface tension. Moreover, depending on the type of polymer, a compatible solvent must be selected. As explained earlier, surface tension balances the forces involved, and values that are not high allow for beadless fibers. One way is keeping the concentration fixed, and varying the type of solvent to reduce the surface tension and improving the production of homogeneous fibers (Figure 2.7) [107].
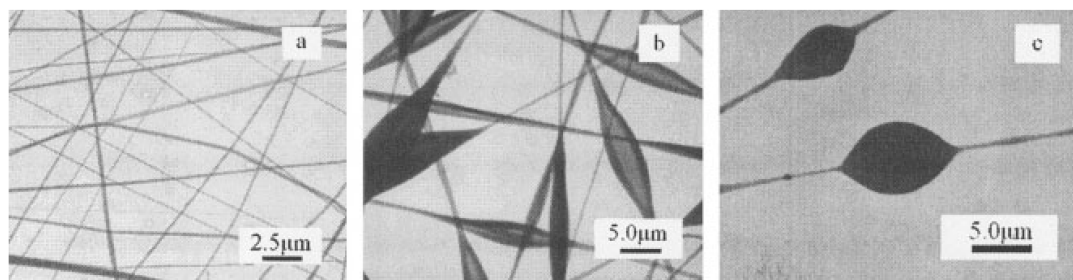
Figure 2.7: Effect of solvent on morphology of electrospun fibers of 4 wt.% poly(vinyl pyrrolidone) solution. Solvent: ethanol (a); dichloromethane (b); N,N-dimethylformamide (c) [107].

Conductivity

Conductivity depends on many factors, such as the type of solvent, the polymer, and the presence of salts or other compounds [108]. Studies show how a higher conductivity of the solution, promotes the formation of thinner fibers (Figure 2.8) [108]. This happens because a high charge increases the elongation of the jet due to electrical forces [108]. For instance, the use of salts such as NaCl has resulted in nanofibers with a small diameter [108, 109]. One of the goals of this thesis work discussed in Section 5.1 is to observe how the presence of silver nanoparticles (AgNP) in the solution, influences the diameter of the fibers. Among the possible reasons, there is precisely a change in the conductivity of the solution.
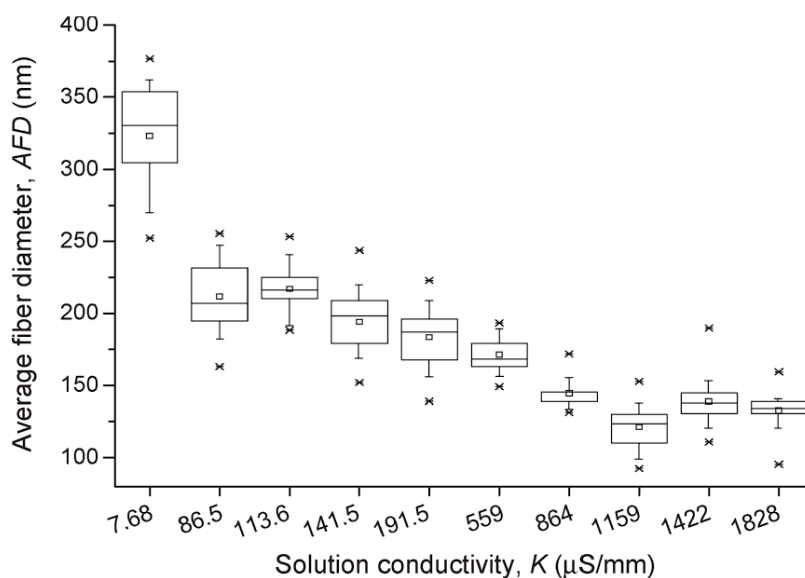
Figure 2.8: Average fiber diameter as a function of the conductivity of the solution [108].

2.1.3.   Setting Parameters

Setting parameters refers to the environmental parameters that affect fiber morphology, namely, temperature and relative humidity. As discussed in Section 2.1.2, temperature affects the viscosity of the solution, and in particular, given the inverse relationship between temperature and viscosity, it is found that higher temperatures favor the formation of thinner fibers [106].

The humidity of the environment affects the evaporation of the solvent. In dry environments, the rate of evaporation will be faster; conversely, in humid environments, evaporation will be slower and promote the formation of thicker fibers. However, the effect of humidity may be controversial and strongly depend on the nature of the polymer in the solution [110].

2.2.   Thesis Goals

The objectives of this experimental thesis work can be divided into two categories: the first concerns the increase of polyynes production yield by PLAL by acting on the temperature and viscosity of the solution to be ablated; the second concerns a study of how the morphology of electrospun polymer nanofibers containing polyynes, can affect their stability, and how the addition of plasticizers, *i.e.,* glycerol, can improve it. Furthermore, a study was conducted on the stability of size- and termination- selected polyynes embedded within polymer nanofibers.

3 — Materials and Experimental Methods

This chapter describes the materials used and the synthesis and characterization techniques of polyynes, silver nanoparticles (AgNPs), and nanocomposites.

Solutions containing polyyne mixtures were produced by Pulsed Laser Ablation in Liquid (PLAL) using different solvents. The main characterization techniques of the latter are UV-Vis absorption spectroscopy and High-Performance Liquid Chromatography (HPLC). Silver nanoparticles were produced both in water, following the Lee-Meisel approach [111], and in glycerol, following the approach described in Section 3.1.3 [112]. UV-Vis spectroscopy and Scanning Electron Microscopy (SEM) were used to verify their concentration and their distribution of diameters.

Nanocomposites were made by electrospinning using poly(vinyl alcohol) (PVA) as the polymer, embedding both AgNPs and polyynes. The techniques used for characterization are Surface-Enhanced Raman Spectroscopy (SERS) and Scanning Electron Microscopy (SEM).

3.1. Materials

3.1.1. Solvents and Targets

The solvents that have been used for this thesis work were mainly for the polyynes production by PLAL, for the purification of the solutions to be processed by HPLC, and for the preparation of the solutions to be electrospinned. The organic solvents used were acetonitrile (MeCN), cyclohexane, isopropyl-alcohol (IPA), and glycerol (GLY). The first three were purchased from Sigma Aldrich and characterized by a purity $\geq 99.9\%$. The only non-organic solvent that has been used is water. This is Milli-Q deionized water having a conductance of 0.055 μS. Other materials, namely isinglass (ISIN) and Carboxymethylcellulose (E466), were employed in this work, and both can be obtained from retailers.

The targets have been employed during PLAL processes to produce the polyynes mixtures. In this work, we used graphite targets since their use is crucial because they are the main source of carbon for the formation of the *sp*-chains [40]. Moreover, this avoids the use of highly polluting and toxic compounds, increases process efficiency, and allows polyynes to be produced in inexpensive solvents, *i.e.*, water [40, 50]. Regarding the latter, due to the eco-friendly nature of this process and the low cost of production, one of this thesis goal is to increase the production and length of polyynes produced in water. It also offers excellent compatibility with AgNPs needed to do SERS.

3.1.2. Polymers

Polyvinyl alcohol (PVA) was selected for the production of the nanocomposites. The choice stems from the fact that creating nanocomposites containing polyynes, as discussed in Section 1.5, is an excellent strategy for stabilizing *sp*-chains. Moreover, to characterize polyynes, SERS measurements are exploited, which therefore require the presence of metal nanoparticles, as explained in Section 1.4.1. Water colloidal solutions of silver nanoparticles (AgNPs) were used, and therefore the polymer needed to be soluble in water to include them. A further reason for choosing PVA is because Raman signal of PVA does not hinder the signal of polyynes. Namely, PVA's most intense peaks are found between 2800-3000 cm^{-1} caused by the stretching of CH bonds [113] and is far from the characteristic region of *sp* structures, *i.e.,* the ECC region between 1800-2300 cm^{-1}. Other polymers used are poly(methyl methacrylate) (PMMA) and polyethylene glycol (PEO). These were used for experiments to understand the reason for nanocomposite degradation, discussed in Section 5. PMMA is insoluble in water, while PEO is soluble. Therefore, because of the two different behaviors and two different structures, the aim was to investigate whether somehow these parameters had influences on stability. Similar to PVA, for these two polymers their characteristic Raman peaks do not overlap with those of polyynes. Figure 3.1 shows the different repetitive units of the three polymers, and all were bought from Sigma Aldrich having respective Molecular Weights (MW) of 130000 (PVA), 350000 (PMMA), and 1000 (PEO).
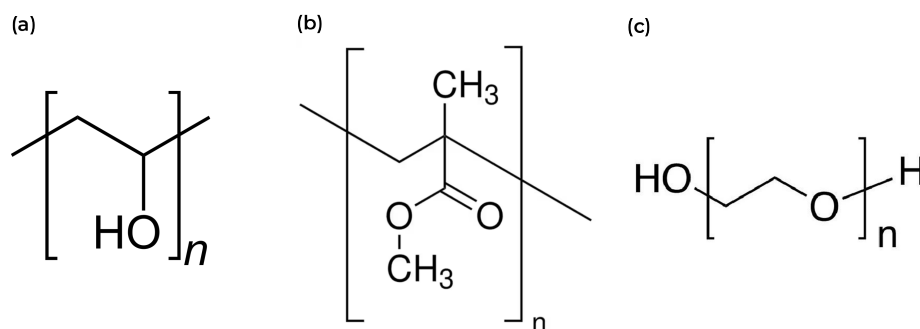
Figure 3.1: Chemical structure of PVA (a), PMMA (b), and PEO (c).

3.1.3. Silver Nanoparticles (AgNP)

Silver nanoparticles (AgNPs), as described in Section 1.4.1, were used in this work to obtain the SERS and as stabilizers of polyynes. Two methods have been used for production; the first commonly called the Lee-Meisel method allows the synthesis of AgNPs in water [111], while the second method uses glycerol as a solvent [112]. Colloidal aqueous solutions were mainly used within the nanocomposites, while the others in glycerol were used to understand their effect on the polyynes production during PLAL.

Lee-Meisel's method involves using silver precursors, specifically silver nitrate ($AgNO_3$), in an aqueous solution, and then, due to the effect of a reducing agent, sodium citrate, silver ions reduce to form metallic silver in the form of nanoparticles. Sodium citrate has a dual role; indeed, it is the surfactant agent that prevents the precipitation of AgNPs as well. It is precisely this latter aspect that is one of the reasons why this method was chosen: the very simplicity of the synthesis method, given the few compounds used, and the thin capping layer that stabilizes the AgNPs makes SERS intense [111, 114]. Figure 3.2 shows the typical setup used, and to achieve an optimal result, it is important to carefully monitor the temperature throughout the synthesis process.
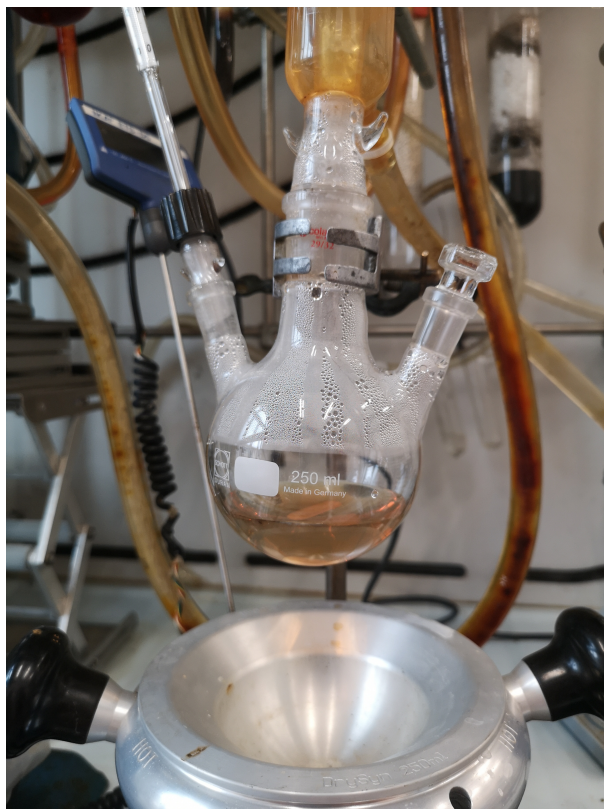
Figure 3.2: Setup used for the production of AgNPs by Lee-Meisel methods.

For the preparation of the nanocomposites, AgNPs were concentrated. This is because the initial concentration of the nanoparticles is not very high, and to further increase the SERS signal enhancement, it is good to have more concentrated solutions. A laboratory centrifuge (EBA 21 Hettich Zentrifugen) was used and the AgNPs were treated for 20 minutes at 9000 rpm. They were concentrated so that the final concentration in the solutions to be electrospun was about 40 times the initial value.

The second preparation method followed the procedure proposed by Sarkar *et al.* [112]. In this case, AgNPs were synthesized in glycerol, but the process is similar to that of Lee-Meisel. Namely, AgNO$_3$ was also used as the precursor in this case, and potassium hydroxide and Sodium Dodecyl Sulfate (SDS) were used as the reducing agent and surfactant, respectively. Compared with the proposed procedure [112], the compounds used were varied slightly. Specifically, potassium hydroxide was used instead of sodium hydroxide. In comparison with synthesis in an aqueous solution, glycerol is much more viscous and it is good to make sure the proper mixing between the various reagents. A deposition was produced with these AgNPs and through SEM the size was observed (Figure 3.3). In Appendix A is shown the result obtained through the program written specifically for this thesis work , which allows automatic detection and calculation of the size of objects

contained in an image. In this case, the average diameter turns out to be about 5 ± 2 nm and these AgNPs were used to prepare solutions to be employed for PLAL.
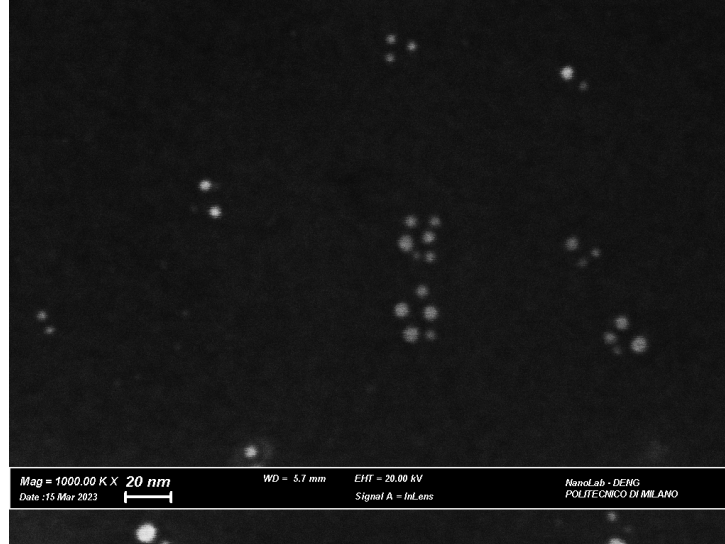
Figure 3.3: SEM image of AgNPs on silicon substrate

3.2. Experimental Techniques

3.2.1. Pulsed Laser Ablation in Liquid

The polyynes used in this work were all produced by Pulsed Laser Ablation in Liquid (PLAL). Figure 3.4 shows the setup used. It consists of a Nd:YAG pulsed laser (Quantel Q-Smart 850), and a handling system. The laser operates with a repetition rate of 10 Hz and the duration of each pulse is 6 ns, while the handling system consists of a stage controlled through a computer program.
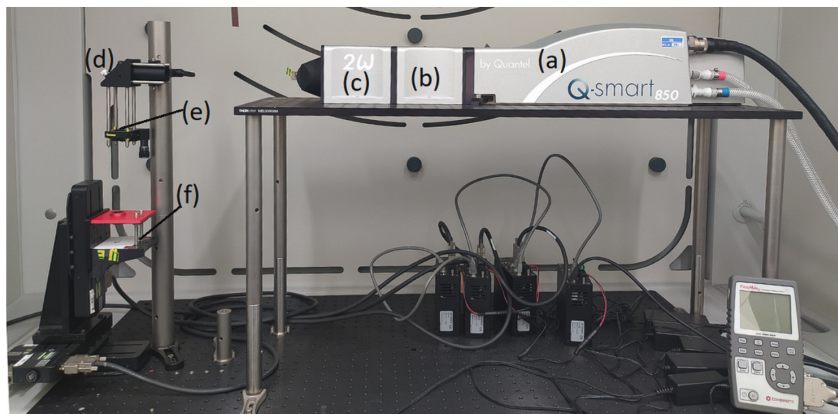
Figure 3.4: Set up of PLAL apparatus; the laser head (a), the beam attenuator (b), the second harmonic generation module (532 nm) (c), the 45° mirror (d), the focusing lens (e) and the stage (f) [115].

The laser head, mounted on a bread board, emits a beam that is reflected at 45° and, through the focal lenses, reaches the vial, containing the graphite target and the chosen solvent, located on the handling system. The latter is used to ensure proper and homogeneous erosion of the target itself. All ablations were conducted using the 1064 nm fundamental harmonic of the solid-state laser and the energy per pulse was set at 50 mJ. Another parameter taken into account was the refractive index of the liquid, which was changed according to the type of solvent. Regarding the fluence, it was set at 2.72 J/cm^2 by fixing the spot size of the laser on the target at diameter of 0.766 mm. These values have been optimized in previous works and were found to be the most effective [40]. Through PLAL, polyynes are obtained as a mixture in the solvent chosen for ablation. This means that polyynes of different lengths and with different terminations are present in the same solution. Therefore, for the studies and characterizations that required selection on the type of polyyne, HPLC, described in Section 3.2.5, was utilized.

3.2.2.   Electrospinning

Nanocomposites, particularly nanofibers, which are discussed in this thesis work (Section 5), were obtained by electrospinning. PVA was chosen as the polymer for all nanocomposites. Figure 3.5 shows the horizontal setup used. Specifically, polymer solutions were placed inside a Hamilton Gastight syringe with a volume of 5 ml, and the feed rate was managed by a KD Scientific infusion pump (model series 200). The voltage between the syringe and the collector was managed by Spellman SL30P300, a high-voltage power supply.
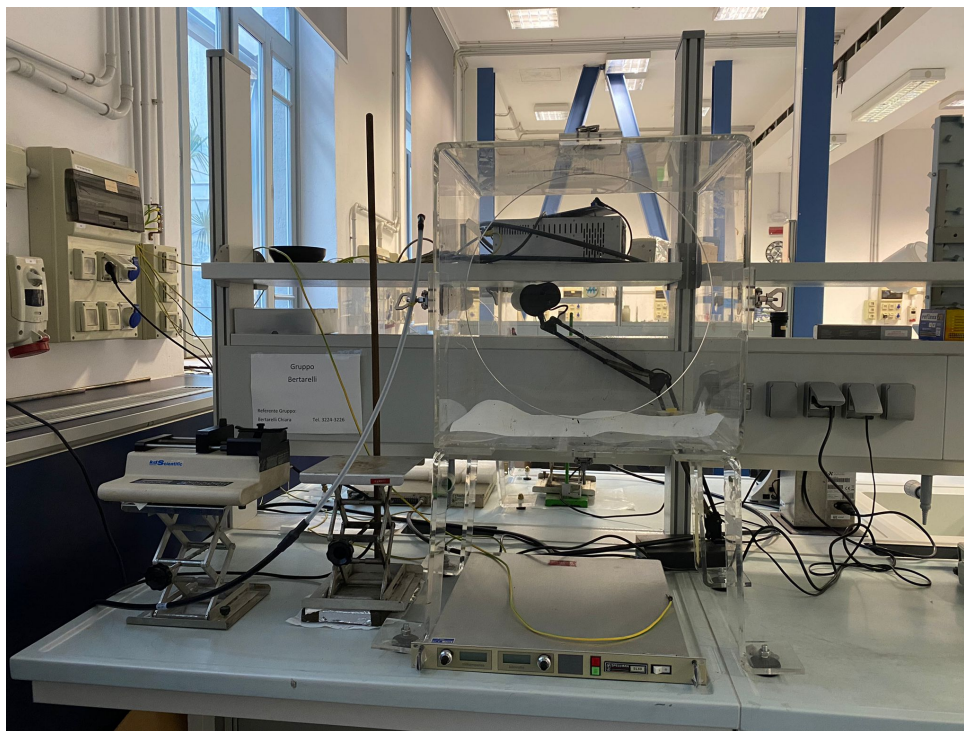
Figure 3.5: Horizontal electrospinning setup used in this thesis work.

Depending on the type of experiment, the applied potential value varied between 13-17 kV, the flow rate between 0.1-0.3 ml/h, and the distance between the nozzle and collector was set to 20 cm. The temperature and relative humidity of the environment were monitored and recorded in the various experiments, however, due to the non-isolated configuration of this setup, accurate control could not be performed during spinning. On each sample, preliminary tests were performed on glass substrates and then observed under an optical microscope to check for inhomogeneities and macroscopic defects.

3.2.3. SERS Analysis

Raman spectroscopy and more specifically Surface-Enhanced Raman Scattering (SERS), is the most widely used technique in this work for studying the stability over time of nanocomposites (Section 5). AgNPs in aqueous solution described in Section 3.1.3 were used to obtain the SERS signal.

The measurements have been performed with a Renishaw in Via Raman microscope equipped with diode-pumped solid-state lasers having two available wavelengths: 532 nm and the other 660 nm. The specimen is placed on a stage that allows the movement along the three axes. The laser beam, passing through filters and mirrored correctly, is focused through a microscope on the sample. After the interaction, the scattered radia-

tion is filtered and reaches a grating system that separates its frequencies. There are two options at 1800 that 600 lines/mm and the first option has always been used. Thus, the scattered inelastic photons can be detected and acquired by the charge-coupled device detector. The intensity of the signals is plotted toward the Raman shift and the Raman spectrum is obtained. In this thesis work, all the spectra were acquired using the 532 nm laser, a 50x microscope lens, and the choice of using the extended method detection is because, in this way, the SERS signal of the polyynes and AgNPs and that of the polymer can be simultaneously obtained. The choice of laser is justified by the fact that this frequency is closer to the plasmonic resonance frequency of AgNPs, compared with the 660 nm laser, and therefore a better SERS signal is obtained. With a few exceptions that will be mentioned later, all spectra were obtained by setting a laser power of 0.553 mW, an acquisition time of 10 s, and 3 signal accumulations.

3.2.4. UV-Vis Analysis

In this thesis work, Uv-Vis spectroscopy has been extensively used to study the increased production and length of polyynes (Section 4). The spectrophotometer used to obtain absorption spectra is the Shimadzu UV-1800. This machine has two different lamps as light sources that can cover the spectral range from 190 to 1100 nm. However, as discussed in Section 1.4.2, the wavelengths of interest for polyynes detection are in the ultraviolet range. For this reason, spectra were acquired in this range (between 190 and 330 nm), discarding the large wavelengths. Two quartz cuvettes are placed inside the apparatus, one containing the reference solution and the other containing the solution to investigate. The light beam is filtered, passed through a monochromator, and then split in two such that it can reach both cuvettes. The spectrum obtained is the absorbance at different wavelengths. The final data is subtracted from the reference solution data, resulting in a spectrum that provides information only about the products contained in the solvent. Often, to avoid signal saturation, solutions have been diluted.

3.2.5. HPLC Analysis

Reverse-Phase High-Performance Liquid Chromatography (RP-HPLC) was used to study concentrations and to be able to separate polyynes according to their length and terminations. In this thesis work, HPLC was used for two reasons: the first is to perform more accurate analysis in those experiments where a single analysis by UV-Vis spectra was insufficient; the second reason is to separate polyynes by termination and length. As discussed in Section 1.4.3, the columns inside the machinery are very sensitive and susceptible to impurities. Furthermore, the final solution coming out of the machinery

is diluted. For these reasons, depending on the type of experiment, filtrations, purifications, and concentrations of the solutions to be investigated were performed. Specifically, for some experiments, the mixture of polyynes obtained by PLAL was purified by cyclohexane, made a phase transfer in acetonitrile, and finally concentrated by rotavapor. Through the purification process, the aim is to remove all impurities in the solution, *i.e.*, by-products as well as reagents that are no longer desired. Theoretically, this process, in addition to avoiding possible snags in the HPLC column, should also increase the stability of the polyynes, as by-products that could promote the formation of sp^2 and crosslinking structures are being removed. The phase transfer is necessary in case there is no proper compatibility between the solution to be injected and the chromatographic column. Furthermore, through proper choice of solvent, depending on the type of experiment, phase transfer can also be used to completely remove un-reacted reagents. Finally, rotavapor was used to concentrate the purified solutions. The concentration of the solution, before injection into HPLC, was done when polyynes separated by termination and length were to be obtained. This was to ensure a good concentration after the process so that the polyynes could be analyzed by SERS. This was performed to detect the SERS signal even for very long chains, as the high dilution produced during the HPLC process might otherwise hinder its identification.

Purification by cyclohexane was performed using a separating funnel. The starting solution was stirred with cyclohexane, and then by placing the funnel vertically, separation of the two phases was performed. Then carefully the two solutions were removed and these steps were repeated several times. The amount of cyclohexane used was about 2-3 times the volume of the solution to be purified. Finally, the purified solution was placed with acetonitrile in a round-bottomed flask and concentrated with rotavapor. The amount of acetonitrile used was about equal to that of cyclohexane. To avoid thermal degradation of the polyyens, rotavapor was done by setting a bath temperature of 25°C and rotation between 180-220 rpm. As the process proceeded, all the cyclohexane evaporated leaving only the acetonitrile. Finally, the acetonitrile was kept evaporating as well to concentrate the polyynes.

Figure 3.6 shows the apparatus used in this work, Shimadzu High-Performance Liquid Chromatography (HPLC).
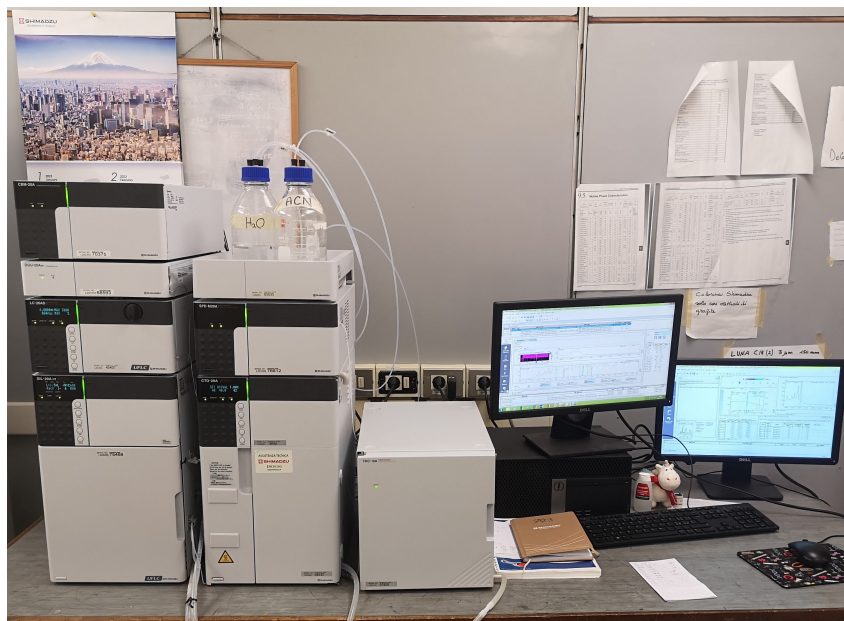
Figure 3.6: HPLC setup.

A Phenomenex Luna C18 column (150 mm x 4.6 mm) was used as a stationary phase. It contains silica particles of 5 μm size functionalized with alkyl chains of 18 carbon atoms. The mobile phase used for all experiments is a solution of water and acetonitrile. A constant-flow elution of 0.8 ml/h was used, and the composition of the mobile phase changes over time: for the first 4 minutes it consists of a mixture 35% water by volume and 65% acetonitrile by volume; then from 4 to 22 minutes the concentration changes linearly over time until it reaches 5% water by volume and 95% acetonitrile by volume; finally the composition was kept constant until the end of the process, which lasted 45 minutes. The injection volume was changed between 5-80 μL depending on the experiment. All the solution before the injection were filtered to eliminate any significant contaminants using Phenomenex Phenex RC-membrane syringe filters with 0.45 μm pore sizes. For the collection of polyynes separated by length and termination, the UV-Vis absorption spectrum of the analyte was observed through a photodiode array (DAD) UV-Vis spectrometer, equipped in the HPLC, as a function of time and at a fixed wavelength. Hence, when the characteristic peaks of polyynes began to be noticed, the polyynes could be collected due to an FRC-10A fraction collector.

3.2.6. Scanning Electron Microscopy

Through Scanning Electron Microscopy (SEM), studies regarding the size of the nanofibers were performed (Section 5). The machinery used is Zeiss Supra 40 Field Emission Scan-

ning Electron Microscope. To obtain sharp images to distinctly identify diameters, avoiding overlapping of multiple fibers, few fibers and not membranes were deposited, as opposed to when the intent is to do SERS. To observe the nanofibers, these were deposited on silicon substrates. The latter were placed on a holder by carbon tape to ensure conductivity. Several images were made for each sample and they were analyzed using the Matlab program specifically created for dimensional analysis (Appendix A) to evaluate the diameters of the fibers. Thus many values were obtained and a study of the average size distribution could be made. Depending on the type of sample, two different secondary electron detectors were used. The InLens detector was exploited to obtain high-contrast images, a key parameter to best optimize the functionality of the program in Appendix A. The second detector SE2, on the other hand, provided images with greater depth, where the architecture of the nanofibers could be appreciated.

4 — Process Optimization for Polyynes Production

This Section discusses the experiments related to improving the yield production and length of polyynes mixtures by PLAL. Specifically, the first part analyzes the effect of temperature during the ablation process, and the second part the effect of solution viscosity. In these Sections, the main investigative techniques used are UV-Vis spectroscopy and HPLC.

4.1.   Effect of Temperature during PLAL

In this first experiment, ablations were conducted while maintaining the solvent temperature at 0°C. This was accomplished by performing an ice bath during the PLAL process. In the work of Tabata *et al.,* a 5-h long ablation is performed in cyclohexane while maintaining the temperature around 0°C [58]. By doing this they were able to obtain a normal Raman signal, namely without the use of SERS. As discussed in Section 1.4.1, to obtain a visible Raman signal, high concentrations are required, in the case of Tabata*et al.*'s work on the order of 10^{-4} mol/l [58]. However, usually with PLAL processes, the order of magnitude is 10^{-6} mol/l, and thus far values to visualize a normal Raman signal. Hence, the idea was to try to conduct ice bath ablations to maintain a constant and low temperature during the PLAL process. This will limit solvent evaporation during the process and the preliminary parameters set for ablation should remain more stable over time, *i.e.*, the height of the solvent in the vial affecting the laser focus and the spot area of the laser beam [58].

To carry out the experiment, a container was designed and printed via a 3D printer. For the printing, a thickness of 0.4 mm was selected for each layer, the highest resolution available. Afterwards, a cylindrical container was made. By operating in this way, it was possible to have accurate control over the final thickness of the container itself of 1.2 mm. This is important because it changes the length of the path the laser has to travel to the graphite target, and knowing exactly the distance is good to set the parameters correctly.

Figure 4.1 on the left shows the schematic used for the setup, and on the right an actual photo of the apparatus.
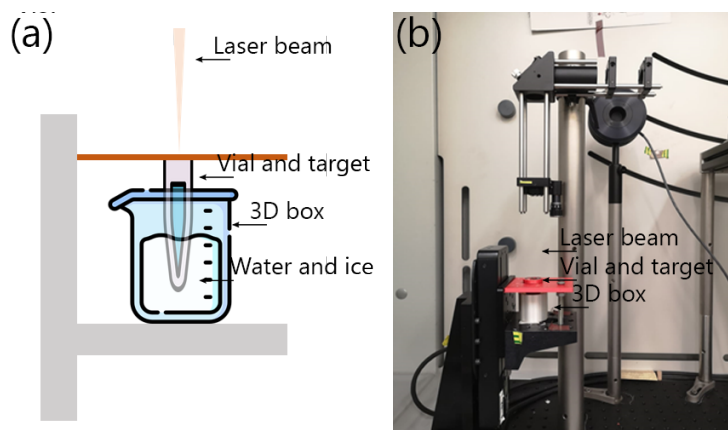
Figure 4.1: (a) sketch of the setup used for ice bath with labels indicating the various components used. (b) Actual picture of the setup used with labels of the various components so that a comparison can be made with diagram (a).

The container was filled with water and ice and placed on the PLAL handling stand. Then the vial, via another upper support, was held in place inside the ice bath. To be sure that the temperature was constant and equal to 0°C throughout the process, the vials, before ablations, were stored in the refrigerator at 4-5°C to preliminarily lower the temperature of the solvent. They were then placed in the ice bath, and at the end of each ablation, it was checked that there was residual ice in the container. Furthermore, water was added inside the container in addition to ice to maximize the contact area between the vial and the ice bath itself, thereby maximizing heat transfer. Operating in this way sought to have the most precise control of the solvent temperature.

Ablations with this setup were conducted in vials containing 2 ml acetonitrile (MeCN) and a graphite target. Each ablation lasted 15 min. The other laser parameters used are described in Section 3.2.1. UV-Vis spectra were made as soon as the ablations were finished, and the data from this setup were compared with those from the setup without an ice bath. Figure 4.2 shows the UV-Vis absorption spectrum of polyynes mixtures in MeCN. To avoid signal saturation, both solutions were diluted 10 times.
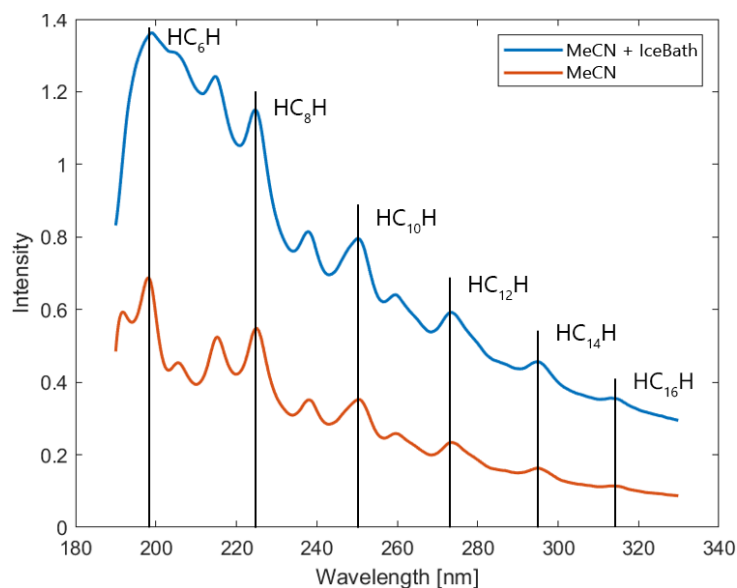
Figure 4.2: UV-Vis spectra of polyynes mixtures. Black lines show the absorption peaks of individual polyynes.

Figure 4.2 shows the comparison between the two situations, and the signal obtained under ice bath conditions is more intense. Specifically, in the region between 190-210 nm, the signal is saturated despite dilution, and the peaks visible between 210-330 nm are of greater magnitude. Because the area subtended below the peaks can be attributed to the concentration of polyynes as explained in Section 1.4.2, it would seem that conducting PLAL with an ice bath would produce a solution of more concentrated polyynes mixture, but it should be ruled out that such signals are not caused by by-products. Specifically, the background trend is being discussed. The background information comes from the superposition of the polyynes peaks and the absorption of the by-products. Because the background, in the case of the ice bath solution, grows more rapidly for lower wavelength values, compared with the setup without ice bath, it is good to investigate whether the intense peak signal for low wavelength values can be attributed to increased production of polyynes or by-products. In contrast, for larger wavelength values, the two backgrounds appear to be nearly similar, and thus the signals are probably more intense due to the presence of polyynes. To further investigate this study, a measurement was made by HPLC, and the concentrations of polyynes were evaluated according to their length. The amount of polyynes mixture injected into the HPLC was 30 μl. The study focused on H-capped polyynes and in this way, UV-Vis absorption spectra of HC_8H, $HC_{10}H$, $HC_{12}H$, $HC_{14}H$, and $HC_{16}H$ were obtained. Figure 4.3 shows examples of the UV-Vis spectra obtained, and Table 4.1 shows the relative concentration and percentage changes.
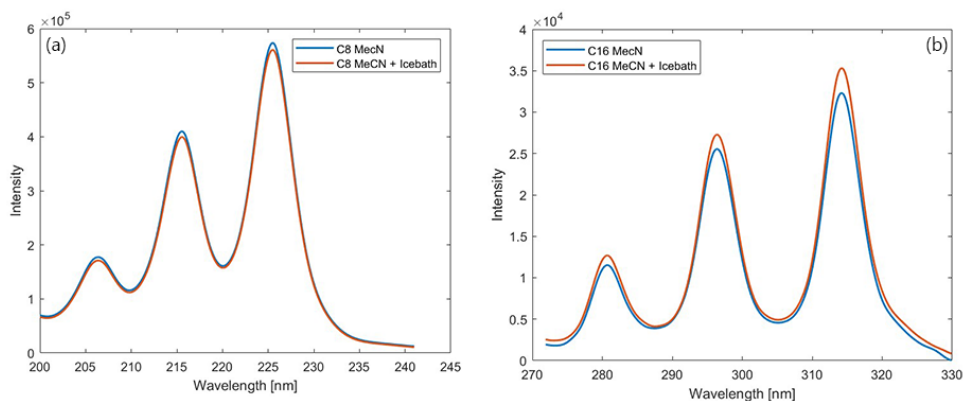
Figure 4.3: (a) UV-Vis spectra of HC_8H from MeCN and MeCN with ice bath configuration; (b) UV-Vis specta of $HC_{16}H$ from MeCN and MeCN with ice bath configuration.

Polyynes	Concentration [mol/l]	Concentration (IB) [mol/l]	Change %
HC_8H	2.01e-05	1.88e-05	- 6,58%
$HC_{10}H$	1.05e-05	9.72e-06	- 7,70%
$HC_{12}H$	4.52e-06	4.47e-06	- 1,28%
$HC_{14}H$	2.33e-06	2.47e-06	+ 6,16%
$HC_{16}H$	9.43e-07	1.03e-06	+ 9,64%

Table 4.1: Value of concentrations and percentage change for separated polyynes without and with Ice Bath (IB).

The results from the HPLC analysis show that only for the longer polyynes there was an increase in production, while for the shorter polyynes, there was a decrease. Consequently, this means that the intensity of the peaks in the UV-Vis spectra in Figure 4.2 positioned for short wavelengths, is derived from by-products. This type of testing has been performed several times and the results have always been comparable. Therefore, the use of ice baths during PLAL increases the concentration of long polyynes, but provides a mixture containing many by-products. A possible justification for this behavior might lie in how temperature affects the PLAL process, especially relative to plasma formation. Indeed, because of the lower solution temperature, the viscosity of the solution could be changed so that the appearance of the plasma plume during ablation also changes. The latter could be associated with a different temperature gradient. For these reasons, the radicals formed after expansion and cavitation bubbles tend to interact more to increase the chains rather than take over the termination process. However, the excess of these radicals that fail to form the longer chains turn into byproducts.

4.2. Impact of Viscosity on Polyynes Length and Production

This section discusses the various experiments aimed at increasing the viscosity of the solution to be ablated. Indeed, in addition to the effect seen in the previous section that could attributed to a change in viscosity, the effect of viscosity on the yield of polyynes production was explored and analyzed. Studies state that the length of polyynes depends on both the density of C_2 radicals and the number of hydrogen atoms contained in the solvent molecule used to ablate, *i.e.*, the number of hydrogen atoms per carbon atom. The amount of C_2 radicals, due to suppression of diffusion, could be higher in solvents with high density [116, 117]. While the role of hydrogens in polyynes terminations is still not entirely clear, studies justify via roaming theory the formation of radicals [118]. For these reasons, the idea of increasing solvent viscosity has been considered.

The first experiment was conducted by ablating solutions of water and isinglass. The latter is commonly used for the production of gelatins and is easily soluble in water. The idea was to use a small amount to avoid the gelling process, but such an amount was sufficient to increase the viscosity of the water. The procedure for activating the compound to make the solution more viscous is the following: the water is heated through a hotplate until just before it reaches the boiling point. At the desired temperature, stirring the solution, isinglass is added, and then the solution is allowed to stand and then placed in the refrigerator. After numerous attempts to find the correct dosage such that the viscosity of the solution was increased but avoiding gelation, a mass ratio of 1:10000 was the most satisfactory. As can be seen, the amount of isinglass added is small, but this is justified by the great ability of this compound to tend to gel the solution.

Ablations were done in vials containing 1 ml of previously described solution, and the graphite target, for the duration of 30 min. Immediately after the ablations, UV-Vis spectra were performed, shown in Figure 4.4, diluting the solution 2, 5, and 10 times. These spectra are compared with a 2-fold diluted spectrum, of an ablated solution of water only and graphite target in a 1 mL vial, for 30 minutes.
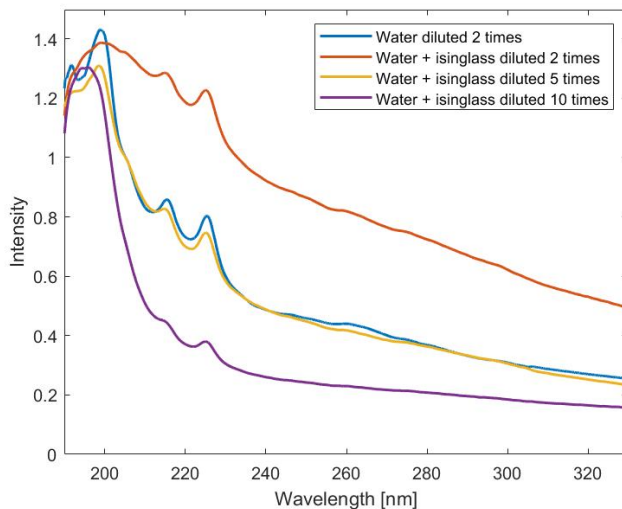
Figure 4.4: UV-Vis spectra of solutions containing polyyne mixtures derived from water, and water and isinglass (1:10000 mass ratio) in different dilutions.

As can be seen, the spectrum of the solution with isinglass, obtained with the same dilution as the solution with water alone, has a saturated signal in the area between 190-220 nm. To obtain a spectrum comparable to that of water, it is necessary to dilute the solution by as much as 5 times. In this case, the two spectra appear to overlap, and given the different dilutions, one might think of increased production of the short chains. Moreover, the signal around 225 nm, related to HC_8H, is also visible well after a 10-fold dilution. To get confirmation that there was an actual increase in polyynes production and not by-products as discussed before, a cyclohexane purification was performed. Purification occurs due to the better compatibility of polyynes in cyclohexane, given the apolar nature of both compounds. Specifically, ablation of a volume of 5 ml of water, isinglass, and graphite target was done for 30 min, after which through a separatory funnel, the polyynes were transferred into 15 ml of cyclohexane. The same procedure was done for a solution containing water and graphite target, with same process parameters, so that the data could be compared. Figure 4.5 shows the spectra of the polyynes mixtures of the two different cases, and given the 15-times dilution of the starting solution, it was not necessary to dilute the samples to obtain the UV-Vis spectra.
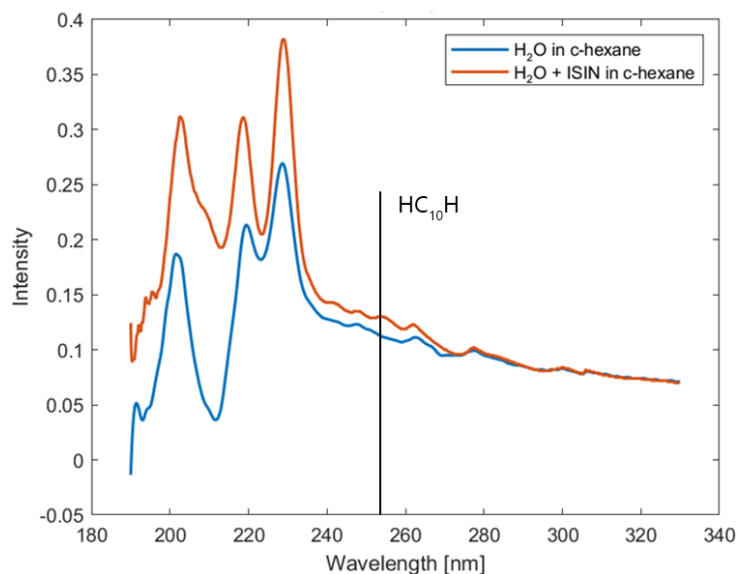
Figure 4.5: UV-Vis spectra of mixure of polyynes derived from water, and water and isinglass (ISIN) (1:10000 mass ratio) purified in cyclohexane. Black line highlight peak associated to $HC_{10}H$.

In this case, due to purification, the peak related to $HC_{10}H$ around 251 nm is also more visible. Noticeable is the increase in the signals related to the shorter chains compared with the water-only case, while the increase in the longer chains is not as pronounced. For this experiment, it was chosen not to perform an analysis by HPLC, because not knowing precisely the constituent molecules of isinglass, there was a risk of clogging the chromatographic column. Therefore, it was not possible to accurately evaluate the concentration values of the separated polyynes. However, observing Figure 4.5, it can be said that with this solution there is about a 150-200% increase in the production of short chains, while the production of long chains remains almost constant. These values were estimated by evaluating the intensity and area values of the various peaks, eliminating the contribution made by the backgorund. Isinglass is a compound of animal origin, but the precise chemical formulation is not known. To further investigate the reason for this production improvement and to understand the constituent elements, a normal Raman spectrum, shown on the left in Figure 4.6, of the water and isinglass solution was performed.
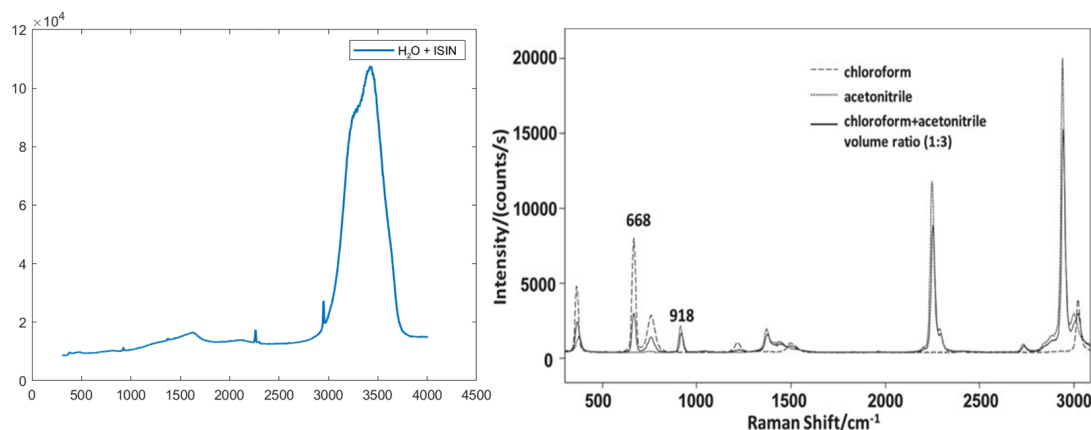
Figure 4.6: On the left the Raman spectrum of water and isinglass solution (1:10000 mass ratio) obtained with 532 nm laser at power of 70 mW; On the right superimposed Raman spectra of chloroform, acetonitrile and chloroform and acetonitrile solution (1:3 volume ratio) [119].

Comparing the two images in Figure 4.6, except for the large band above 3000 cm^{-1} caused by the presence of water, similarities can be seen in the position of some peaks between the solution of water and isinglass and the spectra of chloroform and acetonitrile. This preliminary analysis may indicate the possible presence of chlorine and nitrogen within the isinglass. The possible presence of these chemicals could account for the reason why there is increased production of short chains. Furthermore, since isinglass is animal-derived, it is most likely to contain carbon atoms. This further promotes the formation of polyynes, since in addition to the graphite target, the solvent itself may be a source of carbon for the nucleation of polyynes.

The main problem with the solution containing isinglass was that after PLAL, the solution no longer showed the starting viscosity. Probably the high plasma temperatures degraded the organic molecules of isinglass, denaturing the final solution. However, due to purification, as shown in Figure 4.5, no by-products are observed.

To try to overcome the degradation, isinglass was replaced with carboxymethyl cellulose (E466). The latter is also an additive used in the formation of jellies, but unlike isinglass, it is not of animal origin. Indeed, it is a chemical compound derived from cellulose. The idea is to see if increasing the viscosity of water, but with a different compound, results in increased production and if degradation of the solution after the ablation process can be avoided. E466 similarly to isinglass is a compound that should be added to hot water, and then the solution should be allowed to stand in the refrigerator, thus promoting the setting of the molecules and promoting the gelation process. Again, an amount was added that would not cause the solution to gel, but only increase its viscosity. One of the

main differences between these two gelling agents is the amount needed to be added to observe visible effects on viscosity change. Indeed, a solution was prepared with the same mass ratio as isinglass, namely 1:10000. In this case, however, no substantial increase in viscosity was noticed. Therefore, another solution was then made with a mass ratio of 1:1000. In the latter case, the desired effect was obtained. Shown in Figure 4.7 are the UV-Vis spectra of these two solutions ablated for 30 min in a volume of 1 ml and then compared with the spectrum of a solution containing only water subjected to the same conditions. All three spectra were diluted twice to avoid peak saturation.
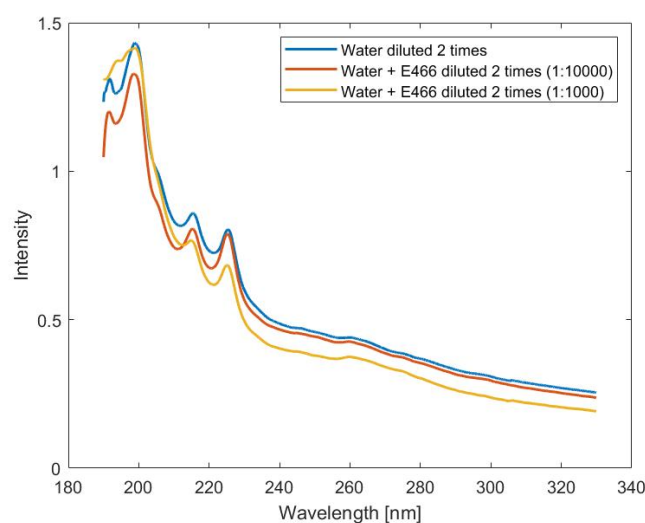
Figure 4.7: UV-Vis spectra of a mixture of polyynes produced with ablation in water, water and E466 (1:10000 mass ratio), and water and E466 (1:1000 mass ratio).

As can be seen, the solution with the lower E466 content made practically no substantial changes from the reference spectrum of the water solution. In contrast, the more concentrated E466 solution would appear to have suffered a deterioration in polyynes production, given the lower peak intensity and area. One possible reason for this behavior is that an amount of 1:1000 by mass is sufficient to change even some solution parameters, *i.e.,* refractive index, thus worsening the ablation process. However, due to the lower gelling capacity of E466, less concentrated solutions could not be used to equally achieve an increase in viscosity. Another possible solution could lie in the nature of the compound itself, which unlike, isinglass, not being of animal origin, contain different elements within it. Thus, it could also be a possible cause for the absence of increased production. Finally, a final cause could lie in the greater stability of this compound compared to isinglass and thus less prone to the formation of radicals useful for the polyynes formation process. Since the UV-Vis spectra did not show the expected result, no further analysis was done,

but alternatives were sought and different and new combinations were tried again to try to improve the production and length of the chains. Specifically, using the same two compounds, but changing the solvent in which they were dissolved. With both isinglass and E466, solutions were made with acetonitrile and acetone. These solvents were chosen because of their better yield of polyynes production, compared to water. However, in all cases, compatibility between these substances and these solvents have never been obtained. Indeed, either the compounds could not be dissolved, or they precipitated to the bottom creating an inhomogeneous solution. An initial solution was also tried to be formed with water and isinglass or E466, and then it was added to acetonitrile or acetone. In each case, there was no compatibility between these compounds and the two new solvents.

Because of all these reasons, I try other approaches. Glycerol and water were used to change viscosity avoiding gelling agents. This change meant that the amounts needed to be added to the water were greater than in the case of gelling agents, and therefore it is important to know the parameters of the final solution well to perform the ablations correctly. An initial solution of water and glycerol 10% by volume was made and 1 ml was ablated for 30 minutes. UV-Vis spectra are shown in Figure 4.8 and are compared with an ablated solution under the same conditions with only water.
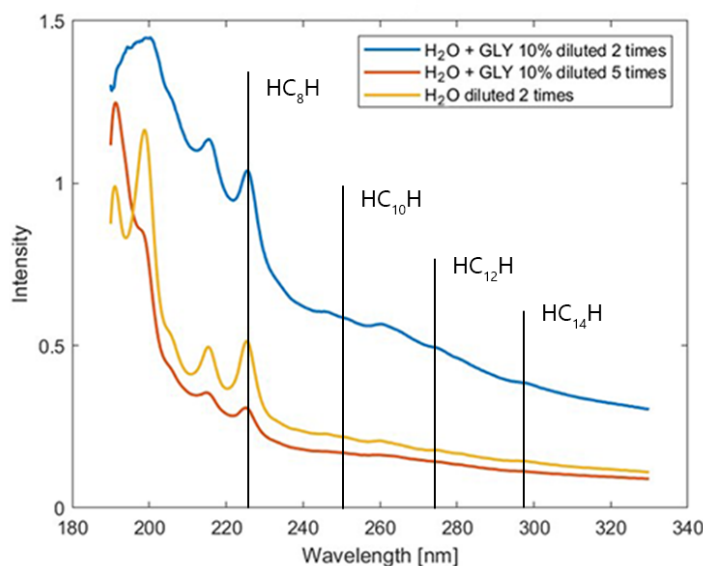
Figure 4.8: UV-Vis spectra of mixture of polyynes produced with ablation in water, and water and glycerol (GLY) (10% volume ratio) with different dilution. The black arrow highligths the signal associated to $HC_{14}H$.

As can be seen, the signal of the solution with glycerol, at the same dilution, is much

more intense than that of water and, as done previously, the nature of this increased intensity needs to be investigated, which could result from either by-products or polyynes. Indeed, between 190-205 nm the signal saturates and the other peaks are significantly more intense. Diluting the solution by 5 times, the signals are still visible. Unlike the case seen previously with isinglass, where the increase was more for short chains, in the solution with glycerol, the peaks associated with longer chains are also of greater magnitude. Notably, they are appreciable up to the signal around 300 nm associated with $HC_{14}H$ (see black arrow in Figure 4.8). Given the increased availability of literature regarding parameters, such as refractive index as composition changes [120], to understand what the optimal amount of glycerol was to maximize production yield, a study was done on varying concentrations. Four different solutions were prepared at 5%, 10%, 15%, and 20% by volume of water and glycerol, respectively. 1 ml of each solution was ablated for 30 min, appropriately changing the refractive index values as the composition changed. At the end of each ablation, a UV-Vis spectrum of the obtained polyynes mixtures, all diluted 2 times, was made. Figure 4.9 shows and compares these UV-Vis spectra, and it can be seen that for concentrations greater than or equal to 10%, the signals are all of similar magnitude.
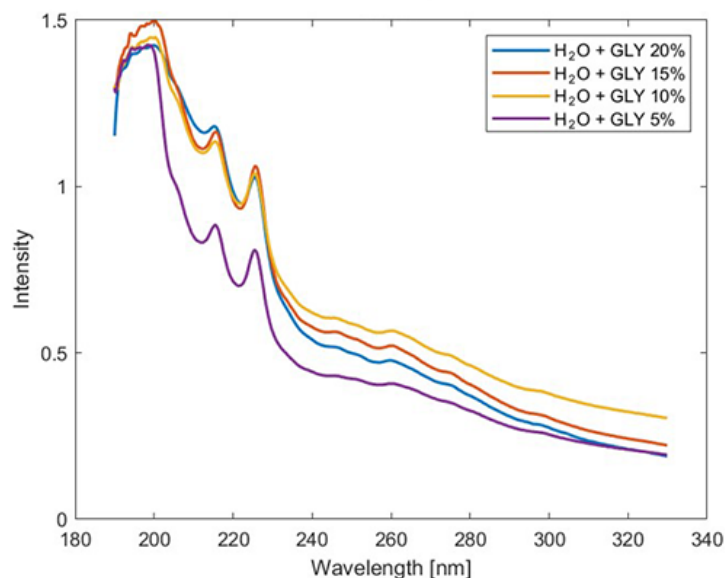
Figure 4.9: UV-Vis spectra of mixture of polyynes derived from water and glycerol (GLY) at different volume concentration.

Analyzing the spectra, there is a limiting value around 10% by volume of glycerol, so beyond that, there is no more improvement in production. This could be justified by the fact that to optimize polyynes production there is an optimal range of viscosity. If the

viscosity is too low, the radicals and active species formed after plasma can quickly move away from the zone where nucleation and growth of polyynes occur. If the viscosity is too high, the same radicals and active species formed with the plasma remain confined, as well as the polyynes that are generated. Thus, on the next pass of the laser at the same location, these can be hit and be degraded. These two processes distancing and confinement, coexist and this justifies the existence of a threshold value in the volume of glycerol for improving the production yield.

For these reasons, the decision was made to use the 10% by volume solution for further study. A purification in cyclohexane was done, then a phase transfer in acetonitrile, and finally HPLC was conducted to quantify the increase in production. Specifically, 5 ml of the solution was ablated for 30 min, and then through a separatory funnel, the polyynes mixture was purified in 10 ml of cyclohexane. The exact same procedure was performed with water only to compare the two results. Figure 4.10 shows the two UV-Vis spectra compared. Following the purification, the presence of $HC_{14}H$ in the solution with glycerol is even more appreciable, and in general larger peaks are observed.
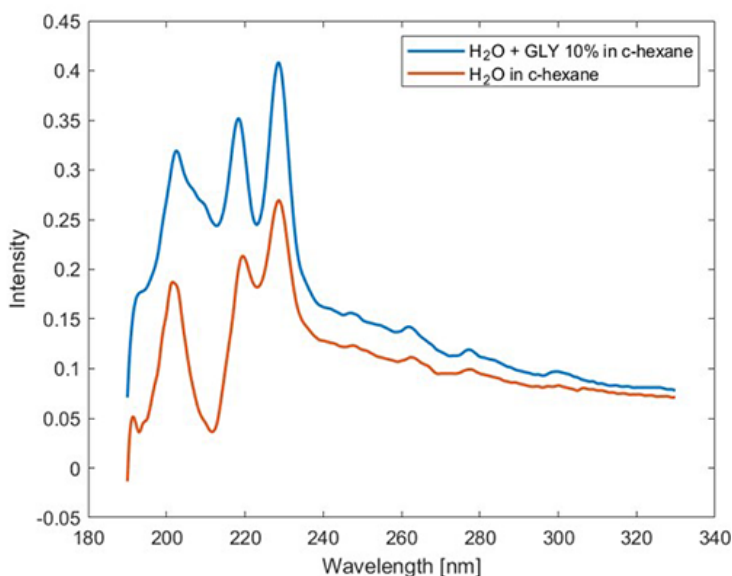
Figure 4.10: UV-Vis spectra of polyynes mixtures purified in ciclohexane (c-hexane), deriving from water, and water and glycerol (GLY) (10% by volume) solutions.

After that, 20 ml of acetonitrile is added to each solution, and a phase transfer and concentration to a volume of 5 ml is performed for both solutions by rotavapor. Figure 4.11 shows the comparison between the purified mixture in cyclohexane and the purified, phase-transferred, and the concentrated mixture in acetonitrile deriving from the glycerol solution.
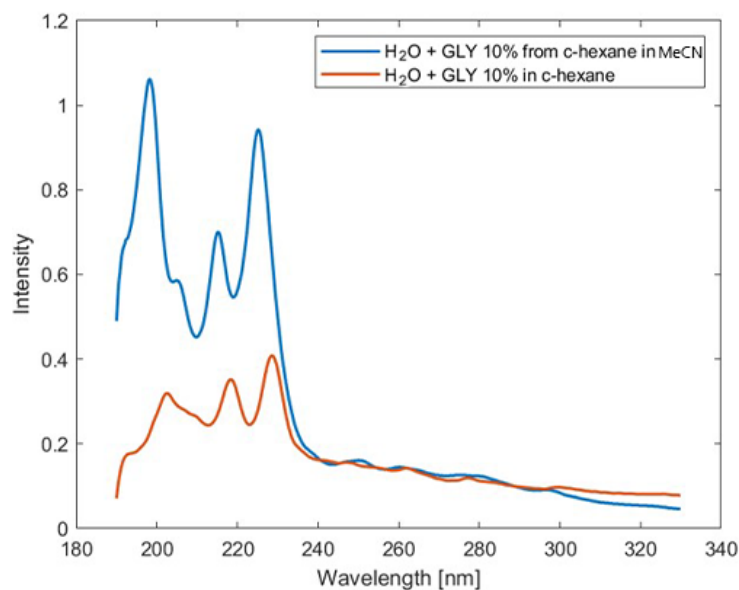
Figure 4.11: UV-Vis spectra of polyynes mixture purified in ciclohexane (c-hexane), and phase-transfered in acetonitrile (MeCN) deriving from water and glycerol (GLY) (10% by volume) solution.

It can be seen, probably as a result of the various purification and concentration steps, that the peaks associated with the long chains have comparable intensities in the two cases, although the final solution is more concentrated. This means that much of the longer chains were lost during the various steps. However, to be absolutely certain that all the glycerol in the solution was completely removed, it was necessary to perform all the previous steps to avoid possible column clogging in the HPLC. The same procedures were done with a water-only solution so that both had undergone the same processes. In this way, the possible losses or degradations of the polyynes mixtures are similar, making the data comparable. At this point 15 μl of each solution was injected into the HPLC, and through the UV-Vis spectra of the separated polyynes, the concentration and percentage change between the two cases were calculated. Table 4.2 shows the values of the concentrations of HC_8H and $HC_{10}H$. Due to the high dilution of the starting solution and the low injection volume, information regarding the longer chains could not be obtained.

Polyynes	Concentration [mol/l]	Concentration (GLY) [mol/l]	Change %
HC_8H	1.36e-06	3.77e-06	+ 278%
$HC_{10}H$	6.45e-08	1.85e-07	+ 286%

Table 4.2: Value of concentrations and percentage change for separated polyynes for solution derived from water, and water and glycerol (GLY).

Increasing the injection volume or skipping the phase transfer step was not considered, as there is a risk of occlusion of the HPLC column. One could further concentrate the solution after the phase transfer step, but as shown in Figure 4.11, the UV-Vis signal of the long chains is much lower than in the previous steps, probably because of the low stability of the longer chains to all these various processes, and therefore the final information on the concentration of the longer chains could be biased. In contrast, as described above, we have no information on the longer chains, but we do have comparable data for the HC_8H and $HC_{10}H$. The increase in production of the shorter chains is remarkable, nearly 300% for both lengths. This significant increase can be explained both by the increase in viscosity within the limit value and the fact that a carbon source was added within the solvent itself.

Given these major increases in production, further investigation was sought into how production could be further increased again by exploiting glycerol. The idea is to synergistically exploit the effect of increased viscosity, the introduction of a carbon source into the solvent, and the stabilizing action of silver nanoparticles during the PLAL step. Indeed, the AgNPs in glycerol synthesized as described in Section 3.1.3 were used, and two aqueous solutions of AgNPs in glycerol were produced: one at 10% and one at 20% by volume. From previous analyses, it was inferred that a 10% concentration by volume of glycerol was optimal for polyynes production. In this case, ablations with twice the concentration were tried to see if the presence of AgNPs had any influence. 1 ml of each solution was ablated for 30 minutes, and UV-Vis spectra were then performed by diluting the solutions 5 times to avoid peak saturation. Figure 4.12 shows a comparison of polyynes mixtures from these two solutions and water only. The spectrum of polyynes derived from water alone was diluted twice because, given the low concentration of the chains, a higher dilution would not allow visualization of the peaks.
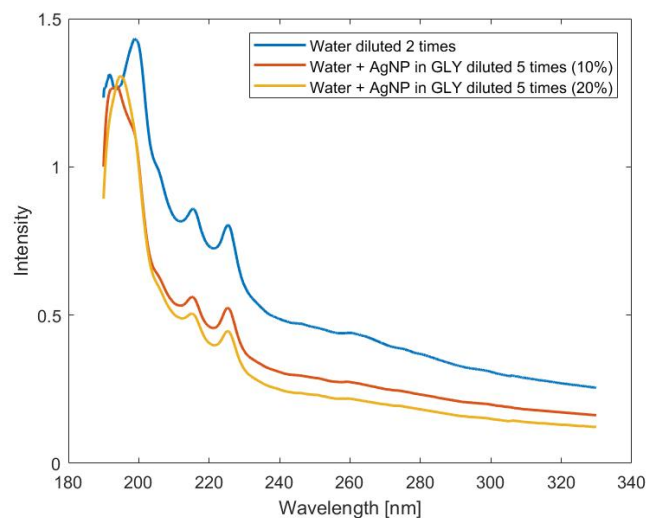
Figure 4.12: UV-Vis spectra of polyynes mixture deriving from water, water and glycerol (GLY) containing AgNPs (10% by volume), and water and glycerol (GLY) containing AgNPs (20% by volume) solutions.

Despite the high dilution, the peaks of the short chains are clearly visible, and, as was the case with the glycerol solutions, a concentration of 10% by volume provides better results. To further appreciate the increase and compare the case in the absence and with AgNPs, spectra at 5 times dilutions for both cases are shown in Figure 4.13.
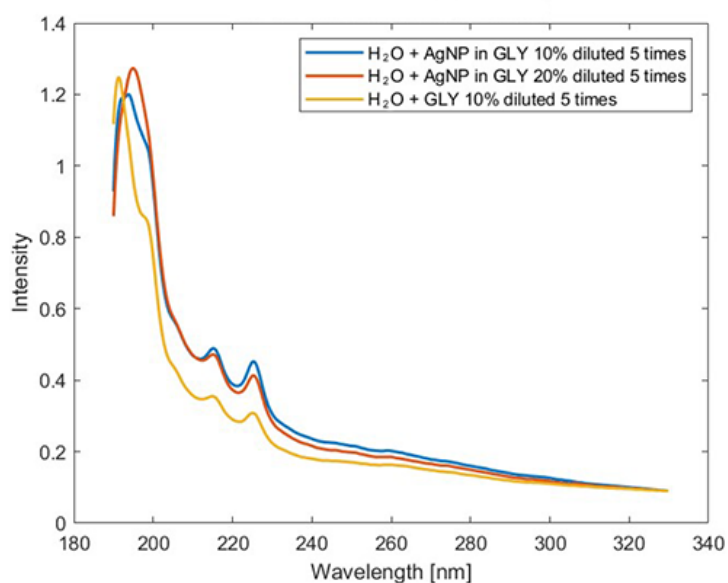
Figure 4.13: UV-Vis spectra of polyynes mixture deriving from water and glycerol (GLY), water and glycerol (GLY) containing AgNPs (10% by volume), and water and glycerol (GLY) containing AgNPs (20% by volume) solutions.

As can be seen, the addition of AgNPs further stabilize the polyynes, making the signal more intense for short chains, *i.e.*, HC$_8$H. There is also an increase for the longer chains, but it is less pronounced than for the shorter ones. In particular, if in the case of the aqueous glycerol solution, for the HC$_8$H and HC$_{10}$H, almost a 300% increase in production had been obtained, it is even higher in this case for the shorter chains. Indeed, in the same way, as also described above for the estimated assessment of concentrations, the peaks are about twice as high, and thus an increase of about 450% can be estimated compared to the water-only case. As discussed in Section 1.5, AgNPs have a stabilizing effect on polyynes, and the combination of proper viscosity and the nanoparticles themselves further improves the production yield compared to using water alone. One possible reason why AgNPs stabilize some chain lengths more than others may lie in the different selectivity of the silver atoms of the nanoparticles to interact with the end groups of the polyynes depending on their length. Particularly, as anticipated in Sections 1.4.1 some silver atoms might replace the hydrogen terminations promoting the stability of the polyynes, but presumably, the probability for which this happens may be influenced by the length of the polyyne itself, and rather than a substitution, an interaction is plausible. In this case, HPLC could not be used because the complexes of polyynes and AgNPs would clog the chromatographic column.

Given these important improvements in production yield, it was decided to try the same strategy on viscosity increase, no longer with aqueous solution, but exploiting organic solvents. This is because compared to water, organic solvents generally have better yield in polyyne production with PLAL. A solution between acetone and glycerol was tried. However, the final solution was not homogeneous given the poor solubility of glycerol in acetone. Hence, it was decided to opt for the use of an alcohol since, like water, it provides good solubility. Specifically, isopropyl alcohol (IPA) was used and two solutions were made at 10% and 20% by volume, respectively, with glycerol. 1 ml of each solution was ablated for 15 minutes, and then UV-Vis spectra were performed. Using the same parameters and conditions, a reference solution of IPA alone was also ablated. Figure 4.14 shows and compares the spectra, all diluted 10 times. Despite the high dilution, around 220 nm there is the peak saturation, while for shorter wavelengths there is solvent cutoff.
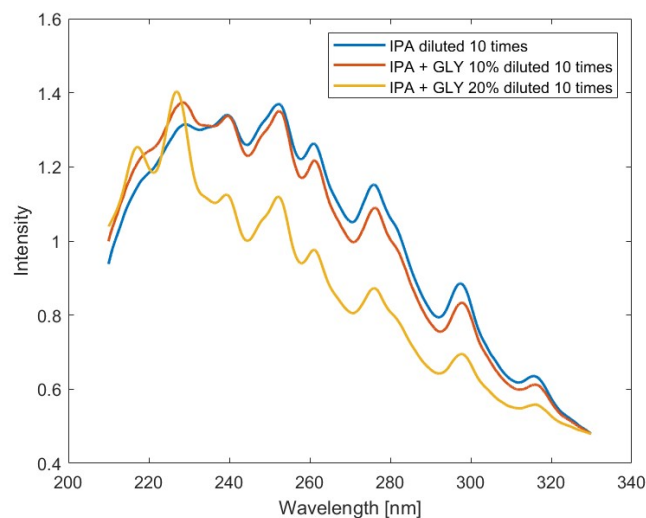
Figure 4.14: UV-Vis spectra of polyynes mixture deriving from IPA, IPA and glycerol (GLY) (10% by volume), and IPA and glycerol (GLY) (20% by volume) solutions.

As can be seen, all peaks associated with polyynes obtained from the glycerol-containing solutions are smaller in magnitude than in the case of IPA alone. This could be further confirmation of the existence of a range of optimal viscosity values to maximize polyynes production. Indeed, if water has a viscosity of about 1 mPa*s at a temperature of 20°C, IPA has a viscosity of 2.2 mPa*s at 20°C [121]. Therefore, when the aqueous glycerol solutions were made, the viscosity was in the range of 1.31 to 1.76 mPa*s at 20°C [122, 123], and as observed, there was a significant improvement in production yield. In the case of IPA, the starting viscosity was already high, and therefore the use of glycerol only increased the viscosity further, no longer achieving yield improvement. Similar to the case of aqueous solutions, the high viscosity in this case also worsened the production yield probably because the radicals and polyynes formed during the ablation process remained confined to a circumscribed portion of the solution and subsequently degraded by the laser passage.

Having performed this last experiment that further supports the thesis of the importance and existence of an optimal viscosity range for solutions to be ablated, it was decided to use polymer solutions as a way to increase viscosity. As with the last experiment, it was used an organic solvent, since it offered better yields than water at the outset. At the same time operating in this way also allowed us to analyze the effect of the presence of carbon atoms within the solution and the effect of other functional groups or atoms, such as OH groups. If for aqueous solutions we had the double contribution between carbon source added to the solution and viscosity increase, using an organic solvent, the aim is to observe only the effect of viscosity, since carbon atoms are already present

within the solvent itself. For these reasons, acetonitrile (MeCN) was chosen as the organic solvent for twofold reasons: first because as noted in Section 4.1 it offers excellent starting performance even for long chains, and second because it has a viscosity of 0.35 mPa*s at 20°C [124], thus far from the optimal range identified earlier.

In the first experiment with MeCN, poly(methyl methacrylate) (PMMA) was chosen. The choice has multiple reasons: the first lies in the good compatibility and solubility between this polymer and MeCN; the second is to use a high molecular weight polymer, 350000 MW, such that small amounts were sufficient to increase viscosity; and the third is the presence of oxygen atoms in the polymer; the fourth reason because PMMA is not compatible with water and there was a desire to try to exploit this fact to try to separate, after ablations, the polymer from the solution. To search for the optimal concentration, three different solutions were made with PMMA concentrations of 0.125 wt%, 1.25 wt%, and 2.5 wt%, respectively. Each solution was ablated for 15 minutes with a volume of 2 ml and was compared with a solution of MeCN alone, used as a reference. Right after each ablation, UV-Vis spectra were performed by diluting the solution 10 times to avoid peak saturation. Figure 4.15 shows the various spectra and they are compared.
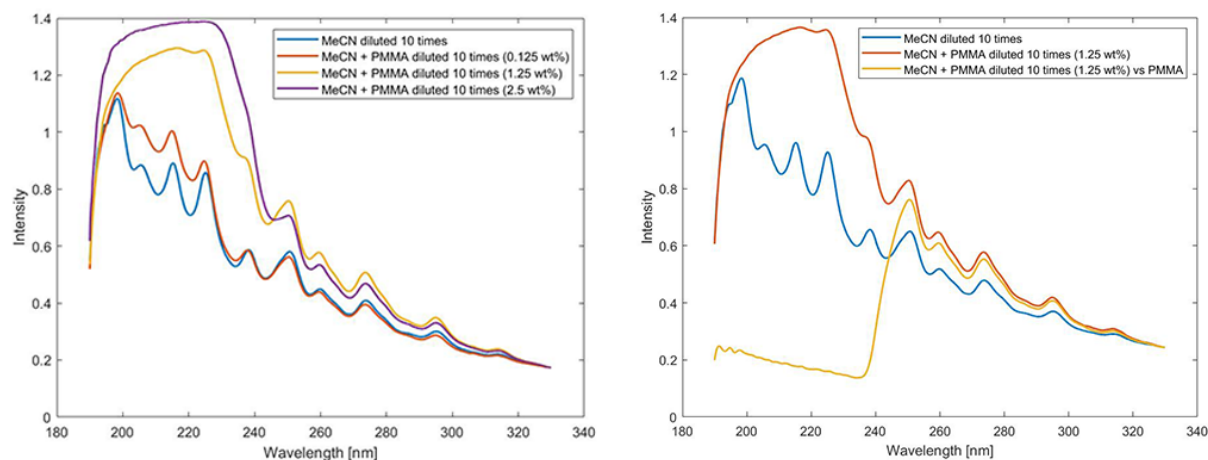
Figure 4.15: UV-Vis spectra of polyynes mixture deriving from MeCN, MeCN and PMMA (0.125 wt%), MeCN and PMMA (1.25 wt%), and MeCN and PMMA (2.5 wt%) solutions. A comparison of various polymer concentrations is shown on the left. A comparison of polyynes derived from MeCN and the 1.25wt% solution is shown on the right.

Analyzing by increasing order of concentration, in Figure 4.15 on the left, it can be seen that for the lowest value, there is little change except in the region between 200 and 220 nm where there are more intense signals. However, this difference is due to the absorption of PMMA, which even though present in such a small amount, has a strong cutoff. By in-

creasing the concentration, the PMMA cutoff is no longer avoidable, and for wavelengths below about 240 nm, the signal is always saturated. However, when analyzing the longer wavelengths of the cutoff, significant increases can be seen. Especially for the signals at around 300 nm and 320 nm, associated with $HC_{14}H$ and $HC_{16}H$, the larger magnitude of the signals can be observed. Furthermore, it is observed that for the higher concentration value, there is a worsening of the peak intensity with respect to lower concentration spectrum. Once again, the justification may lie in the fact that too high a concentration, may have increased the viscosity too much, and thus making the process less efficient. Therefore, also in this case, the concentration value in the medium, turns out to be the best. In Figure 4.15 on the right, on the other hand, the aim was to analyze whether the increase in peak intensity was due to PMMA adsorption or was actually associated with an increase in production. As analyzed in Section 4.1, the possibility of by-products in this region of the spectrum is ruled out because they tend to absorb for shorter wavelengths. Thus, it is observed that even when operating a subtraction with the PMMA solution (yellow line in the right graph in Figure 4.15), the signals for wavelengths between 250 and 320 nm are of greater magnitude than in the case of MeCN alone. Therefore, by observing these spectra, it can be stated how increasing viscosity through the use of a low-concentration polymer solution can be a winning strategy to increase the production yield for long chains.

As anticipated earlier, one of the choices for which PMMA was used lies in its incompatibility with water. For this very reason, to try to obtain information regarding short chains as well, PMMA was tried to be removed from the ablated solution by the addition of water. Specifically, 0.09 ml of water was subsequently added to 1.2 ml of ablated solution. Immediately after addition, precipitation of the polymer at the bottom of the vial was noticed. In addition, to further decrease the solubility of the polymer in the solution, it was placed in the refrigerator. However, after a UV-Vis spectrum, the solution still showed the observed cutoff due to the presence of PMMA. For this reason, water was gradually added until the precipitation of PMMA was no longer observed. A total of 1.2 ml more water was subsequently added. After that, a UV-Vis spectrum was performed again and compared with the ablated solution with PMMA without the addition of water. Figure 4.16 shows the two spectra for comparison.
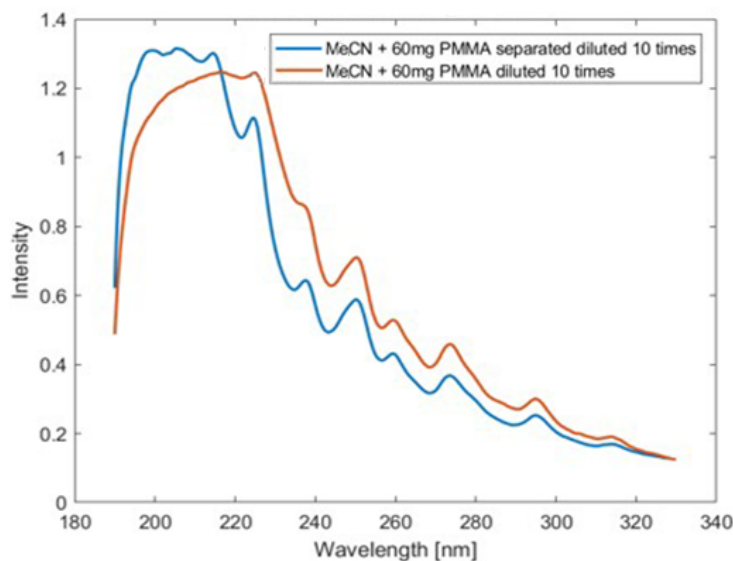
Figure 4.16: UV-Vis spectra of polyynes mixture deriving from MeCN and PMMA (1.25 wt%) solution before and after the adding of water.

It can be seen that the solution spectrum following the separation of PMMA with water is generally less intense. This is because the starting solution is more dilute than not having added water. Despite the addition of water that allowed the PMMA to precipitate, the peaks between 190 and 220 nm are still saturated. One possible justification might lie in the fact that not all of the PMMA was removed in this manner. However, PMMA is completely insoluble in water, and given a final solution of about 50:50 by volume between water and MeCN, the residual concentration in the solution should be insignificant and should not lead to saturation of the peaks. Furthermore, as shown previously in Figure 4.15 on the left, for a concentration of 0.125 wt%, there was no saturation of the peaks. Hence, a more plausible solution, is that as in the case of AgNPs that preferentially bond to short chains, PMMA or fragments of it, also create stable complexes preferentially with the shorter chains.

Given the partial effectiveness of separation by water, to further investigate the study it was decided to do a purification in cyclohexane. Specifically, 2 ml of MeCN 1.25 wt% PMMA and 2 ml of MeCN were ablated for 15 min, respectively. After that, through a separating funnel, the solutions were purified in about 10 ml of cyclohexane. Finally, a phase transfer from cyclohexane to MeCN was performed through rotavapor, and the final solutions were concentrated back to 2 ml. This process was performed for both solutions so that the results could be compared by HPLC analysis. The choice of cyclohexane was crucial, given the insolubility of PMMA in it [125]. This had a dual effect of removing the byproducts and PMMA from the starting solution. To prevent possible traces, albeit

minute, of PMMA from still being present in the solution, risking clogging the chromatographic column, 5 μl was injected into the HPLC. Table 4.3 shows the concentration values obtained as a result of HPLC analysis.

Polyynes	Concentration [mol/l]	Concentration (PMMA) [mol/l]	Change %
HC$_8$H	8.65e-06	7.70e-06	- 10,91%
HC$_{10}$H	4.85e-06	4.43e-06	- 8,72%
HC$_{12}$H	2.25e-06	2.19e-06	- 2,68%
HC$_{14}$H	1.14e-06	1.20e-06	+ 5,08%
HC$_{16}$H	4.06e-07	4.66e-06	+ 14,83%

Table 4.3: Value of concentrations and percentage change for separated polyynes derived from MeCN, and 1.25wt% PMMA MeCN solutions (PMMA).

As can be seen, there is an increase in concentration only for the longer chains, while there is a decrease in concentration for the shorter chains. Potential explanations for this behavior may be multiple. As a matter of fact, from the UV-Vis spectra (Figures 4.15), given the intense cut-off of PMMA, there is no information related to the shorter chains, and the only information related to them is from the HPLC analysis. One possible justification for the concentration of the short chains being lower than in the case without PMMA is that the short chains tend to interact more with PMMA. If this were the case, during the cyclohexane purification process, all the chains that formed a complex with PMMA would have been removed along with the PMMA present in the solution, ultimately resulting in a lower concentration. Conversely, the longer chains could interact less with the polymer and therefore the final concentration value is less altered. This justification is also in line with previous results, where greater activity of the short chains was observed with the AgNPs present in the solution. However, in this case, it cannot be ruled out that there is no enhancement of short chain production at all. For longer chains, on the other hand, there is an improvement of up to almost 15% for HC$_{16}$H. The reasons for this increase can be accounted for by the increased viscosity of the solution, which optimizes the chain accretion process over the termination process.

In summary, several possible strategies to improve and optimize the production yield and the length of obtainable chains, such as using low temperatures and increasing viscosity, have been analyzed and explored in this Chapter.

5 —— Optimization of Nanofibers Production

In this Section, experimental data related to the optimization of electrospinning parameters for the production of polymer nanofibers embedding polyynes are discussed. By varying the composition of the solutions and the electrospinning parameters, the geometries of the nanofibers were modified, attempting to improve their stability over time of the embedded polyynes. Finally, in the last Section, the causes of degradation are more thoroughly investigated. The main techniques used for characterization are SEM and SERS.

5.1. Effect of AgNP and Polyynes on Size of Nanofibers

In this Section, it was studied how the composition of the solution could influence the diameters of the nanofibers. Specifically, nanofibers obtained from aqueous solutions of 10wt% of PVA were compared with other nanofibers deriving from solution having AgNPs, polyynes, and MeCN in them. Furthermore, by keeping the type and concentration of a solution constant, the electrospinning process parameters were changed, and the obtained effects on diameter were observed.

Before proceeding to the discussion of the data, it is good to delve into how the various solutions were prepared. The first solution that was prepared was a 10wt% aqueous solution of PVA. To speed up the polymer dissolution process, the solution was stirred and heated around 80-90°C, and it was always kept in closed containers to avoid changes in composition. Finally, before electrospinning, the solution was allowed to cool down to room temperature. This solution is the one that was used as a reference for subsequent nanofiber diameter measurements. For nanofibers containing AgNPs, aqueous colloidal solutions obtained by the Lee-Meisel method described in Section 3.1.3 were used. Depending on the type of solution, an amount of PVA, such that at final volume a concentration of 10wt%, was added. The AgNPs and PVA solution was stirred and heated around 80°C to dissolve the polymer, after which it was allowed to cool to room

temperature. At this point, depending on the type of solution to be obtained, mixtures of polyynes obtained by PLAL in different solvents were added. As explained in previous chapters, PVA was chosen as the polymer because it is water-soluble, and thus allows the use of AgNPs colloidal aqueous solutions, and because its most intense Raman peak is outside our region of interest, *i.e.,* the ECC region between 1800 and 2300 cm^{-1}.

The first reference solution is 10wt% aqueous solution of PVA. To evaluate the fiber diameters, a few fibers were electrospun on top of a Silicon substrate, for the reasons described in Section 3.2.6. The electrospinning parameters used were: a flow rate of 0.3 ml/h, a voltage of 17 kV, and a distance between the nozzle and collector of 20 cm. Regarding the environmental parameters, spinning was performed in an environment with 23.2°C and 47% humidity. The choice of these parameters is justified by previous studies and numerous tests on samples observed under an optical microscope to verify the absence of defects in the fibers. An SEM image is shown in Figure 5.1, and Table 5.1 shows the mean, minor, and maximum diameter values observed. The measurements of these diameters were obtained by analyzing numerous images using the Matlab program given in Appendix A.
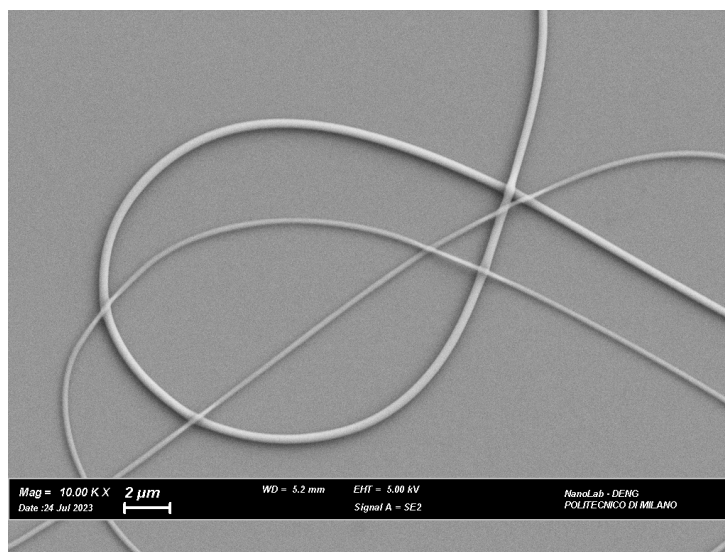
Figure 5.1: SEM image of nanofibers obtained from an aqueous solution of 10wt% PVA.

Diameter	Dimension [nm]
Overall Mean value	350.2
1st **Distribution Mean Value**	261.8 ± 42.3
2st **Distribution Mean Value**	429.6 ± 46.5

Table 5.1: Nanofibers were obtained from an aqueous solution of PVA 10wt%. Overall mean value, and distriburions mean value of diameters found among the analyzed images. Values obtained using the Matlab program in Appendix A.

A bimodal distribution of fibers sizes can be seen from both Figure 5.1 and Table 5.1, as also observed in previous studies [103]. Thus, nanofibers having average diameters around 260 and 430 nm. Although water is not among the preferred solvents for electrospinning, as discussed in Section 2.1, homogeneous fibers without major defects were obtained with these process parameters.

The first effect to be observed is related to the addition of AgNPs. Indeed, a 10wt% solution of PVA was obtained using the AgNPs aqueous colloidal solution. Specifically, the AgNPs used were produced by the Lee-Meisel method described in Section 3.1.3 and were concentrated about 40-fold by centrifugation. The electrospinning parameters used remained the same as in the case of the PVA aqueous solution seen previously, while the environmental conditions at which it was operated were 23.7°C and 47% humidity. An SEM image is shown in Figure 5.2, where AgNPs can be observed within the fibers (small white dots). This last aspect is of paramount importance because the actual insertion of AgNPs inside the fibers could be seen. Table 5.2 shows the average diameter value obtained by analysis of numerous images using the program in Appendix A.
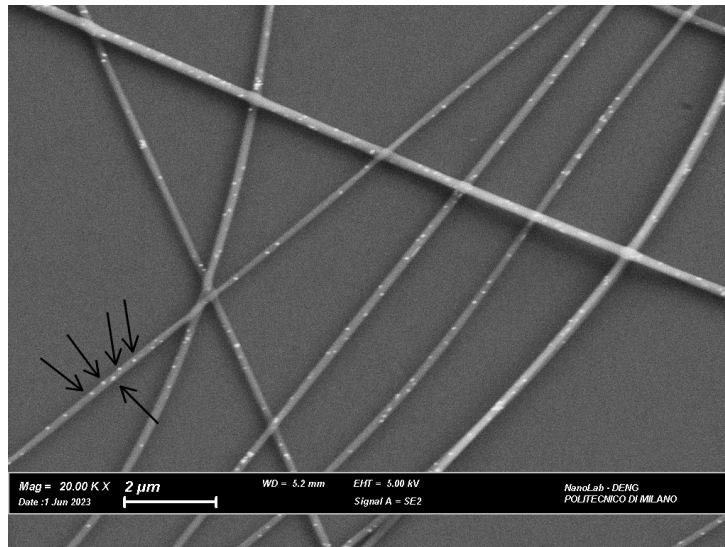
Figure 5.2: SEM image of nanofibers obtained from AgNPs aqueous colloidal solution of 10wt% PVA. Black arrows highlight some AgNPs embedded into the nanofibers.

Diameter	Dimension [nm]
Mean value	213.6 ± 34.7

Table 5.2: Mean value of the diameter of nanofibers obtained from AgNPs aqueous colloidal solution of PVA 10wt%. Value obtained using the Matlab program in Appendix A.

The first important difference observed is the absence of a bimodal distribution in fiber diameters. When compared to the previous case, there would seem to be a similarity in size here concerning the first bimodal distribution, although in the second case, the nanofibers appear to have smaller diameters. This aspect could be justified by the fact that AgNPs affect the conductivity of the solution, a parameter of crucial importance during spinning, explored in more detail in Section 2.1.2. Hence, it would seem that, under the same electrospinning conditions, the addition of AgNPs in the solutions to be electrospun would allow nanofibers with single-mode distribution to be obtained and promote nanofibers with smaller diameters.

Having investigated the role of nanoparticles in the architecture and size of nanofibers, the aim now was to study what the role of polyynes was. To produce the solution to be electrospinned, polyynes obtained by a 30 minutes ablation in 2 mL of water, AgNPs colloidal aqueous solution, and PVA were used. Specifically, the AgNPs were concentrated such that at final volume they were 40 times more concentrated than the initial volume. After that, PVA at 10wt%, relative to the final mass, was allowed to dissolve in the

concentrated AgNPs solution by the use of a magnetic stirrer and heater. Upon complete dissolution of the polymer, the solution was allowed to cool down to room temperature. This is important since if the polyynes had been added to a hot solution, they could have degraded. Finally, the same volume amount of the AgNPs as the polyynes mixture was added, and the final solution was stirred to make it homogeneous. This solution was electrospinned using three different combinations of process parameters. This is because, as discussed in Section 5.2, depending on the diameter value, the time stability was also to be analyzed. The first nanofibers were obtained using the same parameters as the two previous cases, thus: a flow rate of 0.3 ml/h, a voltage of 17 kV, and a distance between the nozzle and collector of 20 cm. The other two configurations instead were: flow rate of 0.1 ml/h, voltage of 17 kV, and the distance between nozzle and collector of 20 cm; flow rate of 0.3 ml/h, voltage of 13 kV, and the distance between nozzle and collector of 20 cm. From here on in the discussion, the fibers will be referred to as Version 1H, Version 2H, and Version 3H fibers, respectively, at the parameters by which they were obtained above. The choice of parameters in Version 2, and Version 3 are such that the effect on the final fiber geometry and architecture is intended to be analyzed by first varying only the flow rate from the reference case, and then varying only the voltage. All three Versions were obtained with the same environmental parameters of 21.4°C and 51% humidity. Table 5.3 shows SEM images and the average values of various diameters for each Version.
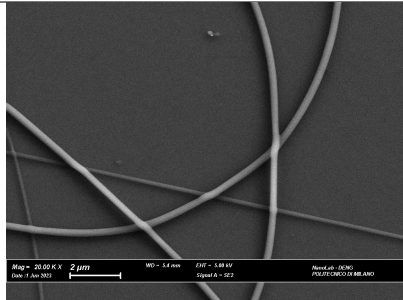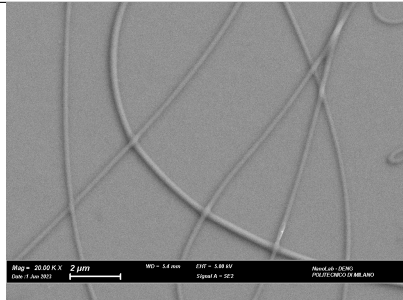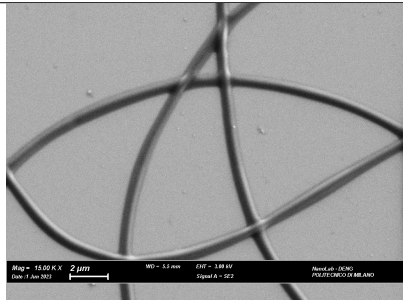
Version	Diameter	Dimension [nm]	SEM Image
Version 1H	**Overall Mean value**	196.5	
	1st **Distribution**	176.8 ± 16.3	
	2st **Distribution**	284.2 ± 32.3	
Version 2H	**Mean Value**	267.9 ± 60.4	
Version 3H	**Mean Value**	672.5 ± 98.6	

Table 5.3: Values for the geometries of the nanofibers obtained from a 50% by volume AgNPs colloidal aqueous concentrated solution, 50% by volume polyynes mixture obtained via PLAL from water and PVA 10wt%. The values were calculated using the program in Appendix A. Version 1H: flow rate of 0.3 ml/h, voltage of 17 kV; Version 2H: flow rate of 0.1 ml/h, voltage of 17 kV; Version 3H: flow rate of 0.3 ml/h, voltage of 13 kV; for all three versions the distance between nozzle and collector was 20 cm.

The first thing that can be noticed is that only Version 1H shows a bimodal distribution of diameters. This means that for the same process parameters, the introduction of polyynes into the solution further changes the type of geometry and architecture of the nanofibers. In particular, the situation again becomes similar to the first discussed case of the 10wt% aqueous PVA solution, despite the presence of AgNPs. However, the average values of the diameters of the distributions between the two cases, are markedly different. Indeed, in Version 1H these turn out to be smaller. This could be justified by the presence of the AgNPs, which, as shown above, cause a reduction in the mean

diameter. Therefore, in summary, comparing Version 1H with the two cases seen just above, there are: the average diameters of the distributions are smaller than the case in which AgNPs are not present; the average value of the diameter of the fibers obtained from the solution without the polyynes, is in the middle compared to the average values of the distributions of Version 1H. The reason for this behavior is not entirely clear, but it could be associated with the interaction between polyynes and AgNPs. These could form complexes with the nanoparticles and change the conductivity, viscosity, and surface tension of the solution. However, it is difficult to be able to say precisely which cause governs the process. The second thing that can be noted is that the bimodal distribution is not homogeneous. This can be said by looking at the overall mean value, which was obtained by analyzing numerous images of the same Version 1H and represents the mean value of the diameter regardless of the type of distribution. The overall mean value is about 196 nm and is closer to the value of the first distribution. This means that overall the probability of finding nanofibers belonging to the first modal distribution is higher. In contrast, the results of Versions 2H and 3H appear to agree with the changes made to the process parameters. In the case of Version 2H, having decreased the flow rate but kept the voltage constant, what is observed is a decrease in the average diameter. As explained in Section 2.1.1, this causes less solution to be simultaneously stretched, resulting in a smaller diameter. In the case of Version 3H, the voltage value was decreased, keeping the flow rate constant. In this case, the expected result is opposite to that of Version 2H, and an enlargement of the mean diameter was also experimentally observed. This, in agreement with theory (Section 2.1.1), is given by the fact that the fiber in the gap between syringe and collector, was less stretched, resulting in a coarser fiber. Finally, a single-mode diameter distribution is observed for both. These important differences in the values of the diameters as the process parameters change will be exploited for obtaining membranes to be used for SERS and evaluating stability time-dependent trends, discussed in Section 5.2.

Given the improvements in production yield and length of polyynes produced via PLAL from solutions of water and glycerol (Section 5.2), it was decided to study the trend of diameters by changing the type of polyynes mixture. This allows to produce nanofibers containing more polyynes. Indeed, 2 ml of a 10% by volume aqueous solution of glycerol was ablated for 30 min and was then used for the solution to be electrospun. The solution preparation procedure is equal to that of Versions 1H, 2H, and 3H, except for the origin of polyynes. In this case, an attempt was made to use the process parameters used for electrospinning equal to the three previous Versions, but due to the different starting solutions, some combinations were not possible. Specifically, for a voltage of 17 kV and a flow rate of 0.3 ml/h (parameters used in Version 1H), spinning was not homogeneous in

this case and numerous beads were observed under the optical microscope. Similarly happened for parameters equal to the flow rate of 0.1 ml/h and voltage of 17 kV (parameters used in Version 2H). After several attempts, the three combinations used that resulted in homogeneous fibers are defined below: Version 1G: flow rate of 0.05 ml/h and voltage of 17 kV; Version 2G: flow rate of 0.1 ml/h and voltage of 13 kV; Version 3G: flow rate of 0.3 ml/h and voltage of 13 kV; for all three cases the distance between nozzle and collector was 20 cm. There could be many reasons why the parameters had to be changed, such as the high boiling point of glycerol, a possible interaction between glycerol and polyynes or between glycerol and AgNPs, which altered the properties of the solution (Section 2.1), compared to the previous three Versions. The environmental parameters were the same during the three cases equal to 21°C and humidity of 56%. Table 5.4 shows examples of SEM images of the three Versions 1G, 2G, and 3G, and the corresponding values of the average diameters obtained with the program in Appendix A. As can be seen, all three cases resulted in a single-mode distribution of diameters.
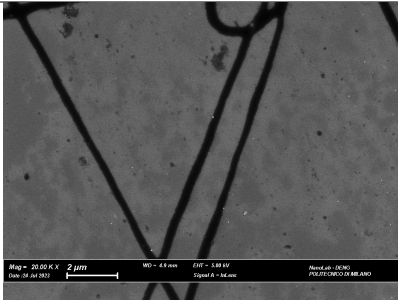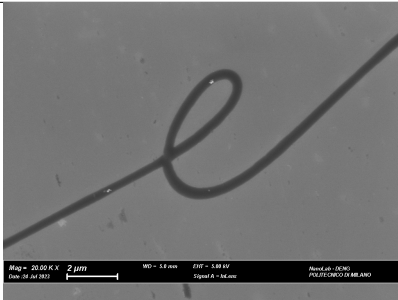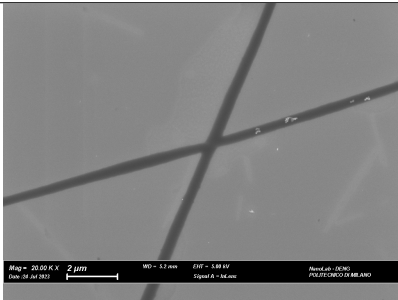
Version	Diameter	Dimension [nm]	SEM Image
Version 1G	**Mean Value**	326 ± 80.3	
Version 2G	**Mean Value**	370.6 ± 49.2	
Version 3G	**Mean Value**	431.4 ± 43.4	

Table 5.4: Values for the geometries of the nanofibers obtained from a 50% by volume AgNPs colloidal aqueous concentrated solution, 50% by volume polyynes mixture obtained via PLAL from 10% by volume aqueous solution of glycerol and PVA 10wt%. The values were calculated using the program in Appendix A. Version 1G: flow rate of 0.05 ml/h, voltage of 17 kV; Version 2G: flow rate of 0.1 ml/h, voltage of 13 kV; Version 3G: flow rate of 0.3 ml/h, voltage of 13 kV; for all three versions the distance between nozzle and collector was 20 cm.

During the various electrospinning trials, the use of high voltages was found to be ineffective, because, through an inspection with an optical microscope, fibers with defects were often noted. Indeed, the Version 1G fibers, where the voltage was set to 17 kV, were shown to have greater variability in diameter than the other two cases. In general, however, the trend in diameters respected the expected result theoretically described in Section 2.1.

Then, solutions that also contained MeCN were investigated. This is because the yield

of polyynes production by PLAL in MeCN is high, as discussed in Section 4, and, therefore, it is possible to further increase the concentration of polyynes inserted within the nanofibers. However, PVA is found to be poorly compatible with MeCN, and for this reason, aqueous solutions of MeCN are necessary to ensure proper solubility of PVA. The solution used as a reference is a solution of 40% by-volume of MeCN, 60% by-volume of water, and 10 wt% of PVA. The choice of this solution comes from previous studies on optimizing the solubility of PVA in the presence of MeCN by trying to maximize its content [126]. Specifically, PVA was dissolved inside water by means of a heater and stirrer and, upon dissolution, allowed to cool down to room temperature. After that, MeCN was added and stirred until the solution was homogenized. The electrospinning parameters used were: 1M version: flow rate of 0.3 ml/h and voltage of 13 kV; 2M version: flow rate of 0.1 ml/h and voltage of 17 kV. The choice of these parameters was dictated by the fact that similar parameters to the various previous Versions were tried to be used, although in this case there is MeCN. For both cases, the environmental parameters were 25.1°C and humidity at 45%. Table 5.5 shows the two Versions 1M and 2M and the values of the diameters measured using the program in Appendix A.
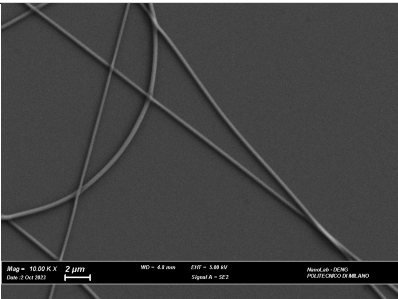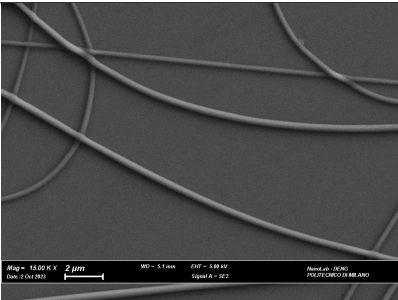
Version	Diameter	Dimension [nm]	SEM Image
Version 1M	Overall Mean value	348.9	
	1st Distribution	289.2 ± 55.8	
	2st Distribution	381.9 ± 37	
Version 2M	Overall Mean value	357.7	
	1st Distribution	299.7 ± 22.3	
	2st Distribution	424.7 ± 31	

Table 5.5: Values for the geometries of the nanofibers obtained from a 60% by-volume water, 40% by-volume MeCN solution, and PVA 10wt%. The values were calculated using the program in Appendix A. Version 1M: flow rate of 0.3 ml/h, voltage of 13 kV; Version 2M: flow rate of 0.1 ml/h, voltage of 17 kV; for all three versions the distance between nozzle and collector was 20 cm.

It can be seen that for both Versions, there are bimodal distributions of the diameters and that the values of the diameters are similar for both versions. Indeed, compared to previous cases where variations in process parameters greatly alter the fiber geometry, in this case, the results are comparable. In both cases, the fibers are homogeneous and free of defects. At this stage, it was decided to replace water with the concentrated aqueous colloidal AgNP solution and study the effect the latter has with MeCN. Specifically, a solution of 40% by-volume MeCN, 60% by-volume AgNP colloidal aqueous solution, and 10wt% PVA was made. The PVA was first dissolved in the AgNPs by heater and stirrer, and finally, the MeCN was added. The electrospinning parameters are identical to the Versions 1M and 2M so that the results can be compared. The environmental parameters are 24.9°C and humidity of 47%. Table 5.6 shows SEM images and evaluations of nanofiber diameters.
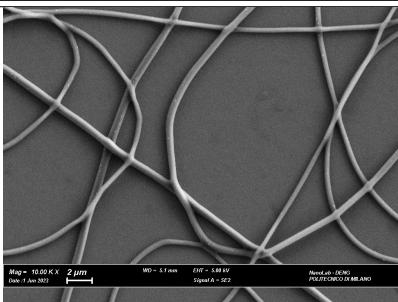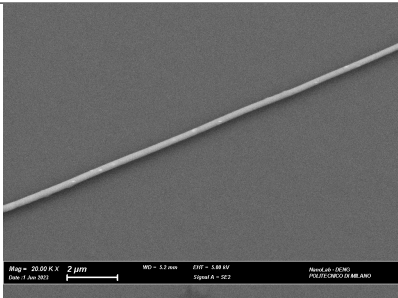
Version	Diameter	Dimension [nm]	SEM Image
Version 1N	Mean Value	277.1 ± 64.3	
Version 2N	Mean Value	294.8 ± 45.2	

Table 5.6: Values for the geometries of the nanofibers obtained from a 60% by-volume AgNPs colloidal aqueous concentrated solution, 40% by-volume MeCN solution, and PVA 10wt%. The values were calculated using the program in Appendix A. Version 1N: flow rate of 0.3 ml/h, voltage of 13 kV; Version 2N: flow rate of 0.1 ml/h, voltage of 17 kV; for all three versions the distance between nozzle and collector was 20 cm.

Significant differences can be observed by comparing Versions 1M and 2M with 1N and 2N. The addition of AgNPs means that under the same conditions and process parameters, the diameter distributions are mono-modal, and the average diameter has decreased for both versions. However, comparing the Versions 1N and 2N the diameters are similar

despite the variations on process parameters.

Finally, the effect of polyynes derived from the MeCN solution obtained by PLAL was analyzed. The electrospinned solutions were obtained similarly to the 1N and 2N Versions, except that the 40% by-volume of MeCN is replaced with a PLAL mixtures of polyynes in MeCN. The process parameters for electrospinning were the same as the previous cases of MeCN-containing solutions, plus an additional combination was analyzed. Process parameters are defined below: Version 1A: flow rate of 0.3 ml/h and voltage of 13 kV; Version 2A: flow rate of 0.1 ml/h and voltage of 17 kV; Version 3A: flow rate of 0.1 ml/h and voltage of 13 kV. The environmental parameters were 26.1°C and humidity at 41%. Table 5.7 shows some SEM images and the values of the diameters calculated with the program in Appendix A.

Version	Diameter	Dimension [nm]	SEM Image
Version 1A	**Overall Mean value**	318.5	
	1st **Distribution**	165.4 ± 23	
	2st **Distribution**	471.6 ± 31.8	
Version 2A	**Overall Mean value**	283.2	
	1st **Distribution**	253.8 ± 26.1	
	2st **Distribution**	315.1 ± 44	
Version 3A	**Mean Value**	276.9 ± 178.3	

Table 5.7: Values for the geometries of the nanofibers obtained from a 60% by-volume Ag-NPs colloidal aqueous concentrated solution, 40% by-volume polyynes mixture obtained via PLAL from MeCN solution, and PVA 10wt%. The values were calculated using the program in Appendix A. Version 1A: flow rate of 0.3 ml/h, voltage of 13 kV; Version 2A: flow rate of 0.1 ml/h, voltage of 17 kV; Version 3A: flow rate of 0.1 ml/h, voltage of 13 kV; for all three versions the distance between nozzle and collector was 20 cm.

The first thing that can be noticed is that comparing Versions 1N and 2N with 1A and 2A, thus with the same process parameters, there is a change in the distributions of the diameters. Indeed, in the case of fibers containing polyynes, there is again a bimodal distribution, as in Versions 1M and 2M, and the average value of the diameters is lower, probably due to the presence of AgNPs. In Version 3A the intention was to spin by exploiting a low flow rate and voltage, resulting in a single-mode distribution of diameters. However, the fiber diameter does not turn out to be homogeneous and constant, and nanofibers with irregular diameters varying along the cross-section were obtained.

In summary, comparing the various results under the same conditions, it can be said that the introduction of AgNp alone results in a decrease in the average diameter of the nanofibers and they occur with the single-mode distribution. The combination of polyynes mixture and AgNPs causes results that depend on the operating conditions and the type of solution. Both monomodal and bimodal distributions can be obtained, and the diameter value, compared with reference cases, is decreased, probably attributable to AgNPs.

5.2. Analysis of Nanocomposites Embedding Polyynes Produced from Water and MeCN Solutions

In this Section, the idea is to study how the geometry and architecture of nanofibers affect stability over time. Through the study discussed in the previous Section, several membranes were obtained with nanofibers containing polyynes derived from different solutions. These were then analyzed by SERS and the evolution of the signals over time was observed.

The first study concerns membranes obtained from solutions 50% by-volume from AgNP colloidal concentrated aqueous solution and 50% by-volume of polyynes mixture obtained by PLAL from aqueous solution. For the fabrication of the membranes, the same electrospinning parameters as for the Versions 2H and 3H were used. The choice is justified by the fact that in this way the obtained mebranes both have a single-mode distribution and the difference between the average diameters is considerable. Indeed, the 3H Version has average values more than twice as high as the 2H Version (Table 5.3). The nanofibers were electrospun on top of a substrate made of aluminum foil stuck on a glass substrate. In addition, for membranes to be used for SERS, the deposition times were 1 hour for each sample. This step is critical to obtain a layer thick enough to allow SERS measurement. An example of an obtained sample is shown in Figure 5.3, and the good and homogeneous deposition can be seen.

Figure 5.3: PVA nanofibers with concentrated AgNPs and PLAL water polyynes mixture electrospun for 1h.

As soon as electrospinning was finished, several SERS measurements were taken at different positions of the sample to check its actual homogeneity. Figure 5.4 shows two examples of SERS spectra of the Version 2H sample and two examples of the Version 3H sample.
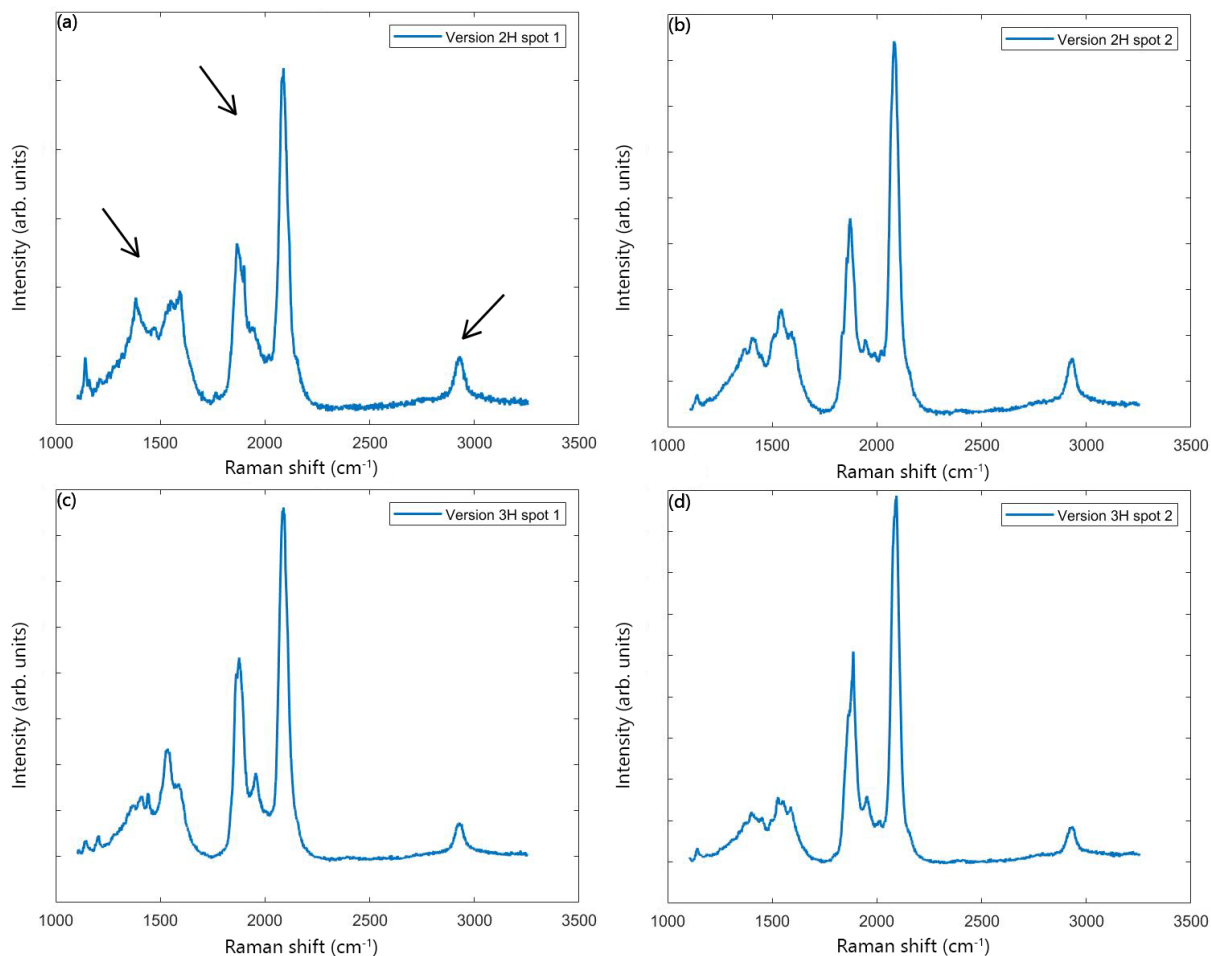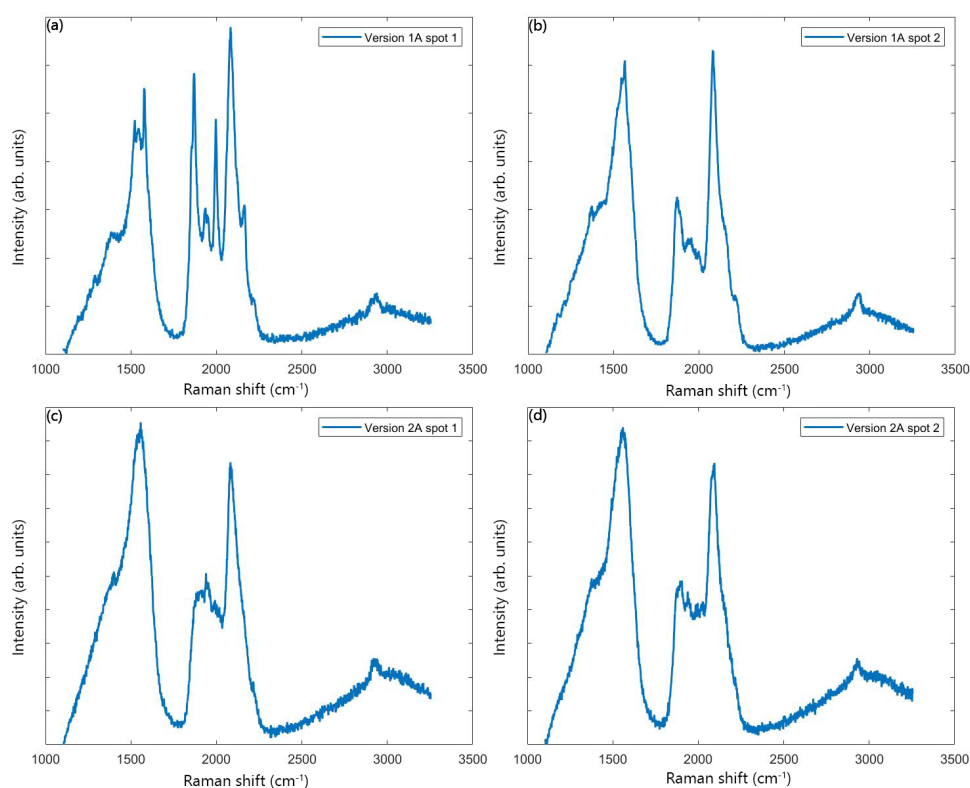
Figure 5.4: SERS spectra of PVA nanofibers with concentrated AgNPs and PLAL water polyynes mixture. (a) Version 2H first analysis spot and black arrows highlight main discussed peaks; (b) Version 2H second analysis spot; (c) Version 3H first analysis spot; (d) Version 3H second analysis spot. The parameters used for measurement were: laser power of 0.533 mW, 3 accumulations for 10 seconds.

As can be observed in all four cases, the spectra are very similar: this is important because it means that for both Versions the final result is homogeneous and as soon as the electrospinning is completed, although they have different process parameters, the results are comparable. As discussed in Section 3.1.2, the peak in the region around 3000 cm^{-1} is associated with the stretching of CH bonds attributable to PVA and for all cases has a similar intensity and magnitude [127]. This means a homogeneous concentration of polymer within the fibers. The region around 2000 cm^{-1} attributable to the SERS signal of polyynes and the region around 1500 cm^{-1} attributable to the numerous interactions of AgNPs are very similar in both shape and magnitude in all cases [56, 58]. Having obtained

confirmation on the homogeneity of the samples and similarity as initial conditions, it was decided to perform several analysis over time. Then, SERS spectra were made all using the same parameters, namely: laser power of 0.533 mW, 3 accumulations each 10 seconds long. Figure 5.5 shows the various spectra of Version 2H as a function of time since electrospinning.
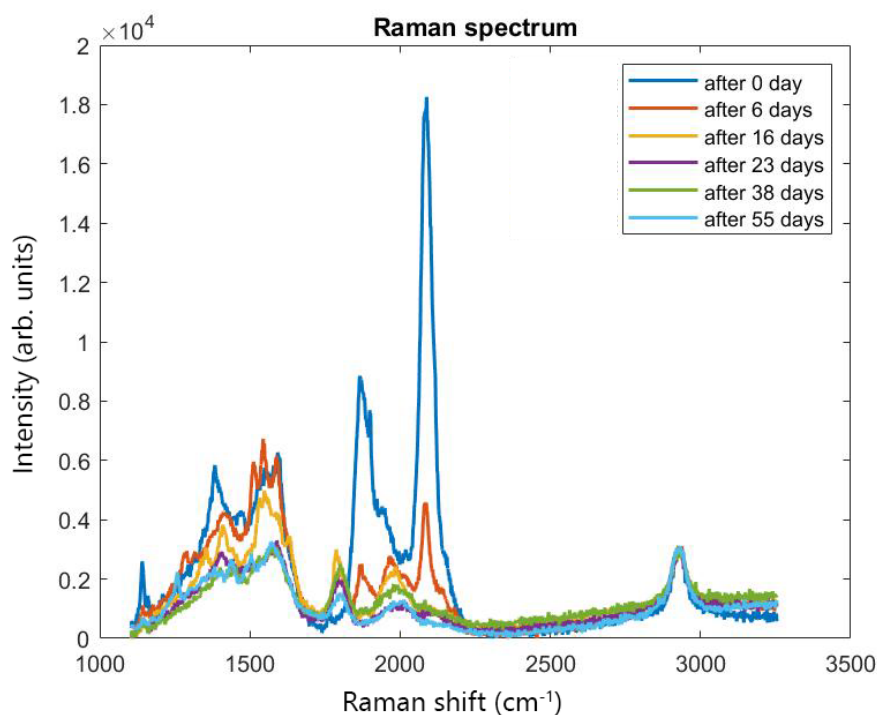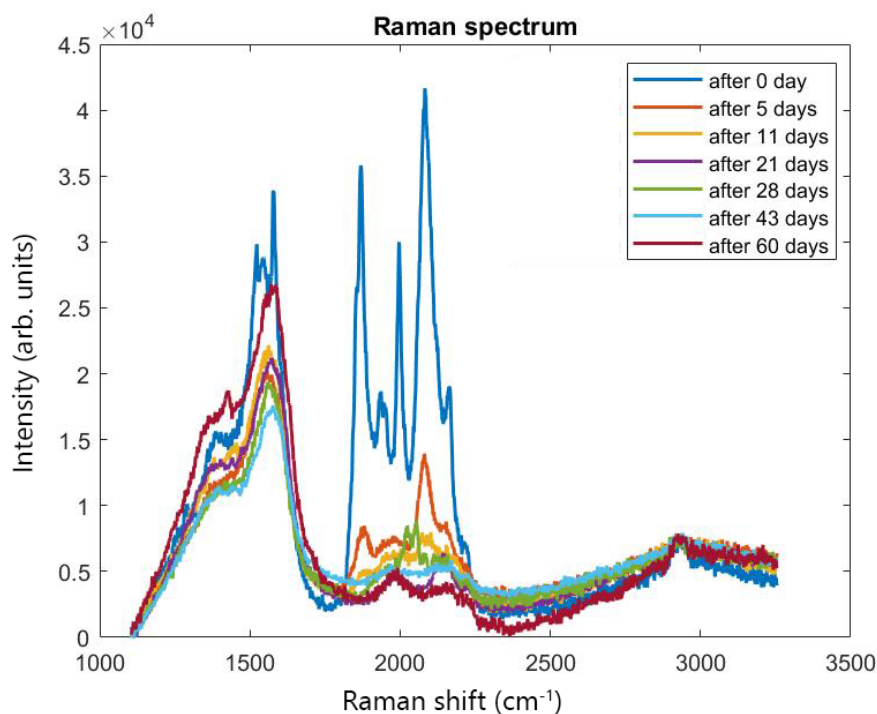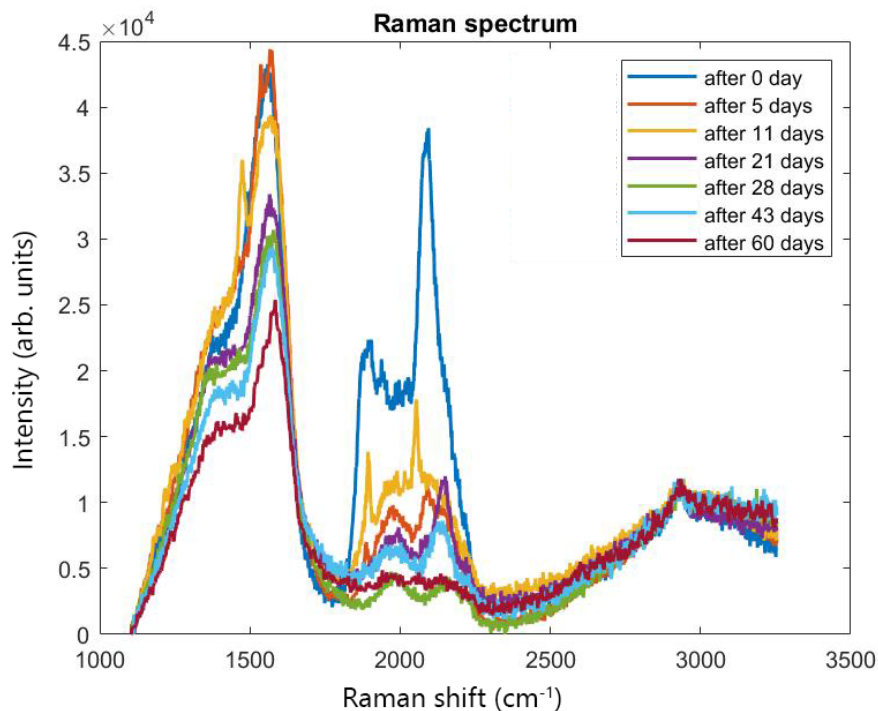

Figure 5.5: SERS spectra of PVA electrospun nanofibers containing concentrated AgNPs and PLAL water polyynes mixture (Version 2H) measured at different times. The spectra are displayed on the same y-axis and normalized on the polymer peak. The parameters used for measurement were: laser power of 0.533 mW, 3 accumulations for 10 seconds.

Spectra were collected up to 55 days after spinning, and what can be observed is a clear decrease in both the peaks attributable to polyynes, *i.e.,* around 2000 cm^{-1}, and the AgNP interaction region in the area around 1500 cm^{-1}. The decrease in peak magnitude is probably associated with the degradation of the polyynes. However, the signal is still visible after 55 days. Another aspect that can be observed is that the signal of the polyynes passed about 23 days, it would seem to stabilize and then remain comparable at subsequent measurements. What is observed is an initial rapid decrease in the SERS signal after the first few days after deposition, and then to have a weak but fairly constant signal over time. Two hypotheses have been proposed to explain this behavior: the first states that, given the high instability of polyynes, they degrade very rapidly, thus causing a

rapid decrease in the SERS signal. Then, as the days progress, by decreasing the quantity, the degradation rate would also decrease, thus causing the display of weaker, but more homogeneous signals over time. The second hypothesis, on the other hand, would state that the polyynes, being embedded within the nanofibers, are relatively stable in the short term, but it would be the interaction with oxygen and other weathering that would trigger the degradation [40, 68]. The latter aspect was investigated more by doing tests with polymer films containing solutions with concentrated AgNPs and 20-day-old polyynes. The choice is justified by the fact that there is a sudden decay in the SERS signals associated with the polyynes in the first few days while doing so was intended to obtain weaker, but more constant signals over time. Operating in this way resulted in graphs with less variation in intensity, which helped more in the investigation of the stability of the polyynes over time. What was observed was that the SERS signal remained constant for about 8 days and then began to decrease. A possible justification for this could lie in the permeation of oxygen and/or other gases within the polymer film. This means that even nanofibers are not a perfect barrier against weathering, and that the decrease in SERS signals is caused by the combined effect between the natural degradation of polyynes and contact with atmospheric agents after passing through the polymer. Figure 5.6 shows the SERS spectra of Version 3H and a comparison with the spectra for Version 2H is desired.
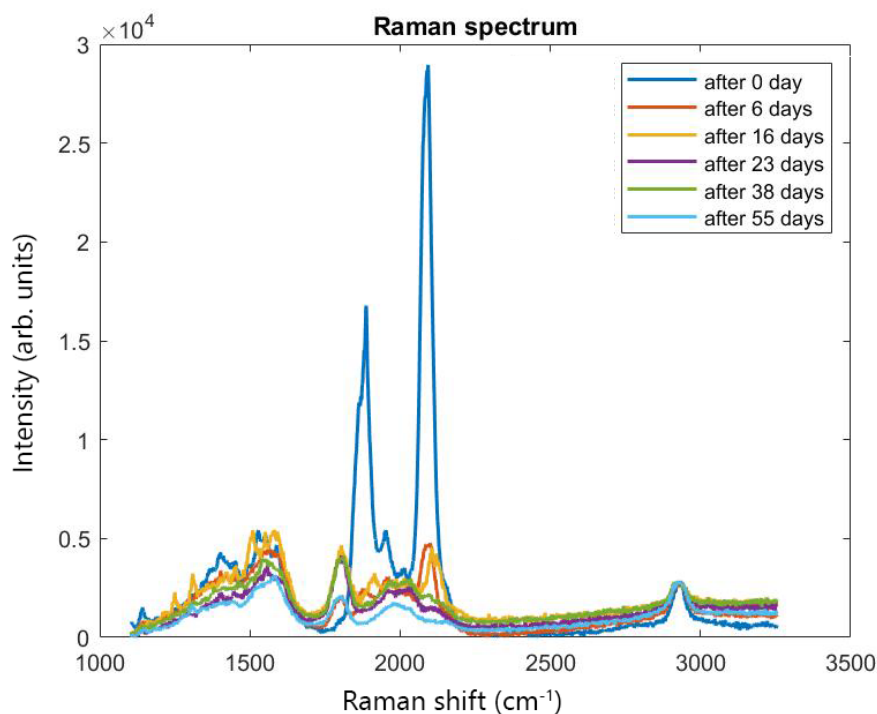
Figure 5.6: SERS spectra of PVA electrospun nanofibers containing concentrated AgNPs and PLAL water polyynes mixture (Version 3H) measured at different time. The spectra are displayed on the same y-axis and normalized on the polymer peak. The parameters used for measurement were: laser power of 0.533 mW, 3 accumulations for 10 seconds.

Compared with the previous case, very similar behaviors are observed on the trend of SERS signals as a function of time. The only appreciable difference would seem to be that the signals related to polyynes stabilize over time after about 16 days, and not 23 as in Version 2H, and their intensity value is slightly higher. These aspects could be associated with the different diameters of the fibers, whereas in Version 3H they are larger. Probably, larger diameters may have a smaller surface area-to-volume ratio and thus fewer exposed polyynes. This could therefore protect the polyynes embedded in the nanofibers more. The possible justifications regarding the behavior of SERS signals, are similar to those discussed for the previous case. In summary, for 2H and 3H Versions, it was observed that SERS signals attributable to polyynes tend to decrease over time regardless of nanofiber size. However, for larger nanofibers (Version 3H), the intensity of SERS signals from polyynes tends to stabilize faster and maintains slightly higher intensity values. This could be associated with greater stability of the polyynes within the nanofibers.

Then, the same study was performed for PVA electrospun nanofibers derived from 60% by volume solutions of concentrated AgNP and 40% of polyynes mixture obtained by PLAL in MeCN (Versions A). For the electrospinning parameters chosen for making the samples,

Versions 1A and 2A were decided upon, since as discussed in the previous Section, the parameters of Version 3A did not provide homogeneous nanofibers. Again, two samples were obtained where the nanofibers were deposited on top of a substrate consisting of aluminum foil stuck on a glass substrate. After electrospinning was finished, several SERS spectra were performed at different positions of the samples to verify the actual correct fabrication and homogeneity of the samples. Two examples for both versions are shown in Figure 5.7, and there is a good similarity between all spectra. Specifically, the ratios between the different peaks are all comparable.

Figure 5.7: SERS spectra of PVA nanofibers with concentrated AgNPs and PLAL water polyynes mixture. (a) Version 1A first analysis spot; (b) Version 1A second analysis spot; (c) Version 2A first analysis spot; (d) Version 2A second analysis spot. The parameters used for measurement were: laser power of 0.533 mW, 3 accumulations for 10 seconds.

In this case, the samples are sufficiently comparable, although, in some areas of Version 1A, the SERS had more peaks than in the other spots and Version 2A. However, given the chaotic nature of the interaction of AgNPs with polyynes, it is possible that different spots show different SERS. At this point, SERS data were collected for each Version as a function of time, and those for Version 1A are shown in Figure 5.8

Figure 5.8: SERS spectra of PVA electrospun nanofibers containing concentrated AgNPs and PLAL MeCN polyynes mixture (Version 1A) measured at different times. The spectra are displayed on the same y-axis and normalized on the polymer peak. The parameters used for measurement were: laser power of 0.533 mW, 3 accumulations for 10 seconds.

Similar to the previous cases of the 2H and 3H Versions, there is a strong reduction in signal intensity compared with the starting condition, caused by the degradation of polyynes. In addition, the signal attributable to polyynes does not seem to stabilize after a given period, but seems to decrease steadily. In any case, the signal is still visible after 60 days. Notable is the presence of a background around 3000 cm^{-1}, probably associated with the presence of moisture on the membrane surface. A similar effect will be discussed in Section 5.3. Figure 5.9 shows the time-dependent SERS spectra of Version 2A.
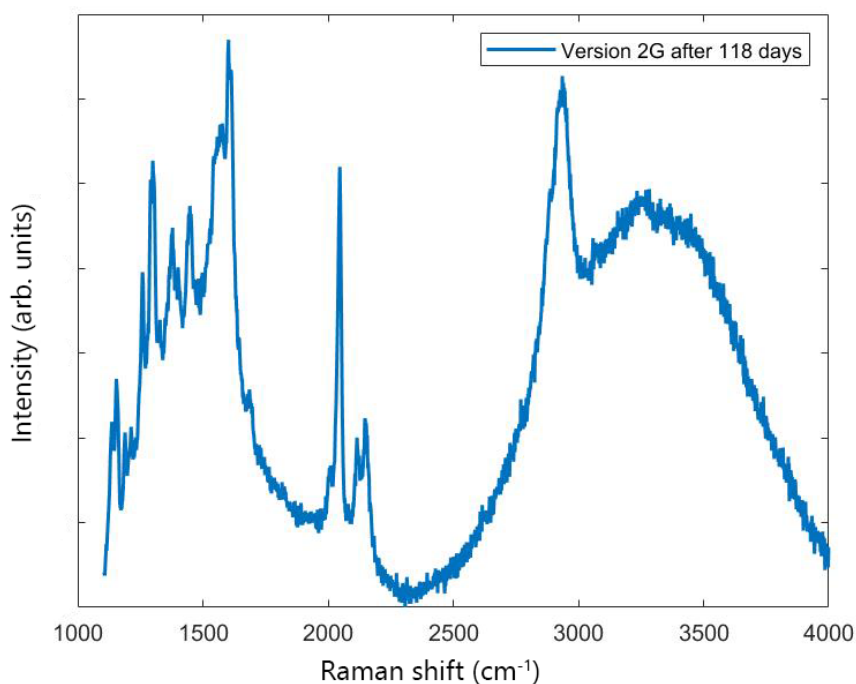
Figure 5.9: SERS spectra of PVA electrospun nanofibers containing concentrated AgNPs and PLAL MeCN polyynes mixture (Version 2A) measured at different times. The spectra are displayed on the same y-axis and normalized on the polymer peak. The parameters used for measurement were: laser power of 0.533 mW, 3 accumulations for 10 seconds.

Comparing the SERS spectra of Versions 1A and 2A, it can be seen that for the second case the region attributable to polyynes, decreases over time with a lower rate. This could be justified by the fact that the diameters of the nanofibers are larger in the case of Version 2A, thus increasing the shielding effect toward the external environment for the polyynes. However, it would appear to be only a momentary effect, since the 60-day spectra are of comparable intensity. The fact that the degradation of polyynes occurs at two different rates could be justified by the different oxygen permeability times within the nanofibers. Since the two Versions consist of the same polymer, *i.e.,* PVA, they will have very similar oxygen permeability coefficients. However, having different geometries, the times required to have the interaction between atmospheric gases and polyynes would be different. This would justify the trends that are observed.

In summary, it appears that samples exhibiting a bimodal distribution of nanofiber diameters have a constant degradation over time of a longer duration. Reference is made to the fact that, in contrast to the 2H and 3H versions, the time required for the SERS signal to reach a fairly constant value over time was obtained after about 43 days and not after 16 or 23 days. However, the H and A versions have different origins, and the

presence of MeCN in the starting solution must also be taken into account, namely the different diameters. However, since the solvents evaporate during the electrospinning process, the nanofibers should have a very similar composition. Therefore, the explanation attributable to the type of distribution would seem the most convincing for the description of this phenomenon. It should not be forgotten, however, that the polyynes obtained from PLAL in MeCN may also exhibit cyano-terminations. Therefore, this aspect could also play a role in the rate of degradation of polyynes itself. Also of relevance is the value of the diameter of the nanofibers themselves. It would seem that larger values or distributions, delay the attainment of the steady-state magnitude value of the SERS signal of the polyynes. One possible explanation for this retarding effect is the different weathering permeability time due to the different geometries.

5.3.   Effect of Glycerol on Stability of Nanocomposites

In this Section, a similar study to the one presented in Section 5.2 is to be carried out, but exploiting the solution of PVA 10wt%, 50% by-volume of concentrated AgNPs, and 50% by-volume of polyynes obtained by PLAL from an aqueous glycerol solution. As discussed in Section 5.1, the choice of electrospinning parameters for this solution always resulted in single-mode distributions of the diameters. The parameters used for the membranes correspond to those in Versions 1G and 2G of Section 5.1. Both samples were obtained by electrospinning for 1h, and Figure 5.10 shows SERS spectra obtained immediately after finishing deposition at different spots.
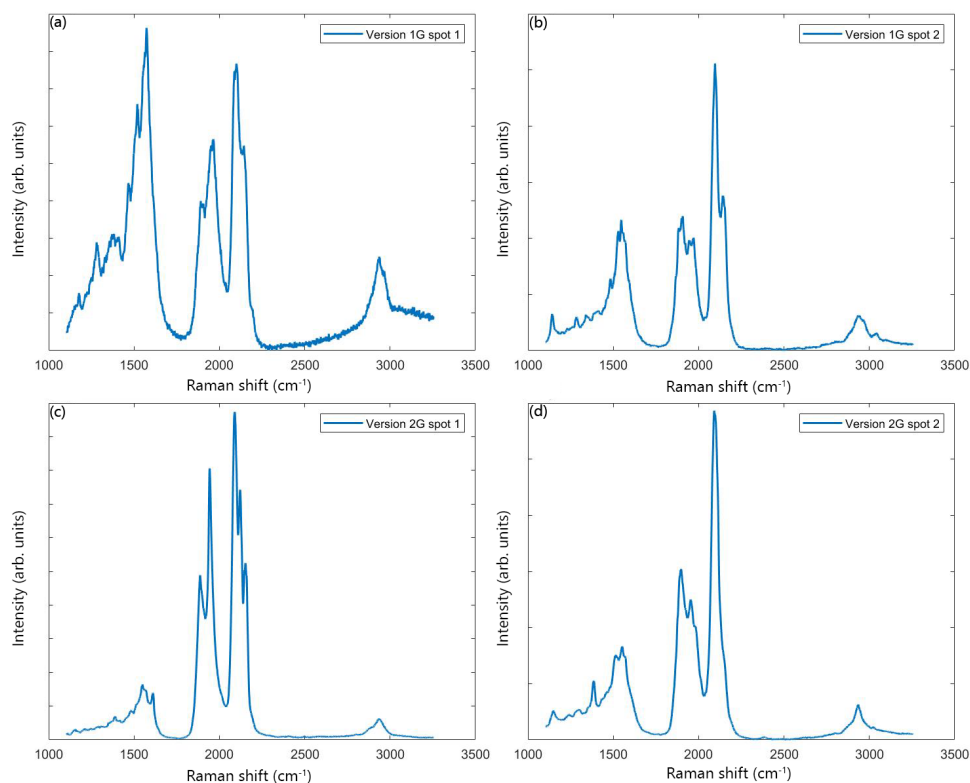
Figure 5.10: SERS spectra of PVA nanofibers with concentrated AgNPs and PLAL water and glycerol polyynes mixture. (a) Version 1G first analysis spot; (b) Version 1G second analysis spot; (c) Version 2G first analysis spot; (d) Version 2G second analysis spot. The parameters used for measurement were: laser power of 0.533 mW, 3 accumulations for 10 seconds.

It can be seen that the spectra obtained for Version 1G differ from each other, as opposed to Version 2G spectra, which are more similar. This means that the Version 1G parameters resulted in an inhomogeneous sample. This aspect ended with the membrane detaching from the support after about a dozen days, thus rendering the sample unusable. For this reason, SERS spectra will be shown only of Version 2G, which proved to be homogeneous and it was firmly attached to the substrate. The reasons for the instability of Version 1G can probably be traced to suboptimal parameters for electrospinning. Figure 5.11 shows the SERS spectra of the 2G version up to 48 days after deposition.
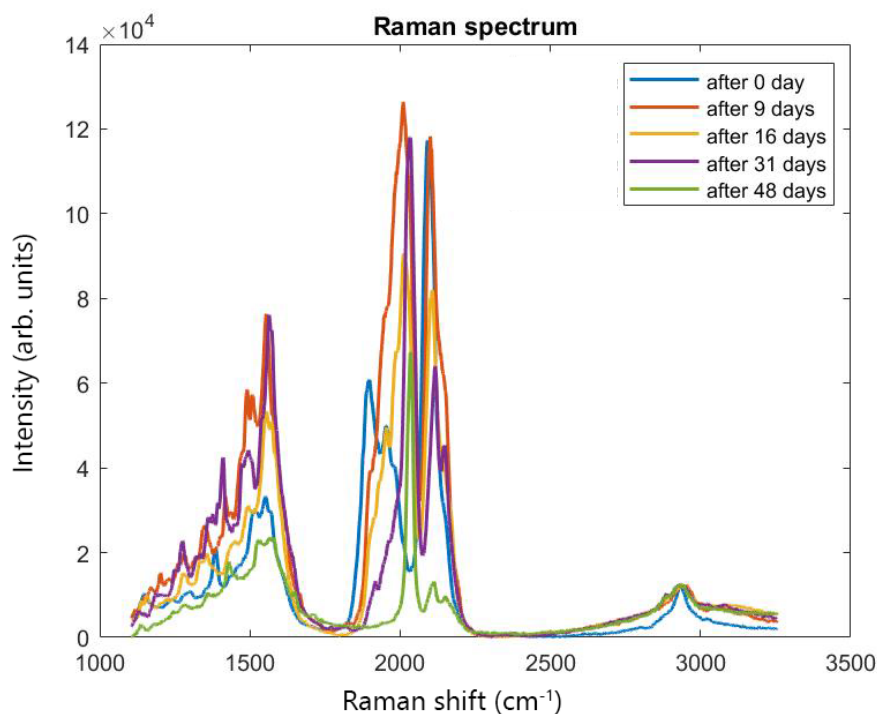
Figure 5.11: SERS spectra of PVA electrospun nanofibers containing concentrated AgNPs and polyynes produced with ablation in a water/glycerol mixture (Version 2G) measured at different times. The spectra are displayed on the same y-axis and normalized on the polymer peak. The parameters used for measurement were: laser power of 0.533 mW, 3 accumulations for 10 seconds.

It can be seen that the signal remains very constant over time and only begins to decrease in the 48-day spectrum. As in the previous cases, the position of polyyne-associated peaks varies across measurements and, as explained above, the reason is the chaotic interaction with AgNPs. In particular, the signal attributable to polyynes seems stable and similar compared to the various spectra, while there are variations in the areas around 1500 cm^{-1} and 3000 cm^{-1}. The zone attributable to AgNPs seems to have no definite trend over time, this is probably due to the chaotic nature of the interaction between AgNPs and polyynes and probably also to possible zones where the concentration distribution of AgNPs is not uniform. One thing that is noticeable right from the 9-day spectrum is the broadening of the peak around 3000 cm^{-1}. What is thought is that after deposition, moisture begins to be deposited on the surface. thus causing the broadening of the peak due to the signal related to OH stretching (see Figure 5.12) and fluorescence. This aspect can be appreciated if one looks at Figure 5.12 showing the SERS spectrum after 118 days.

Figure 5.12: SERS spectrum of PVA electrospun nanofibers containing concentrated Ag-NPs and PLAL water polyynes mixture (Version 2G) measured after 118 days. The parameters used for measurement were: laser power of 0.533 mW, 3 accumulations for 10 seconds.

One can observe the large band around 3200 cm^{-1} attributable to OH stretching. Probably some moisture was absorbed on the membrane surface due to direct contact with the atmosphere. Although to a lesser extent, a similar effect had also been noted in the discussion of the data in Section 5.2. In this case, since 118 days have passed, the amount of water is greater, and therefore the band in the Raman spectrum is greater. In addition, the wide peak width is due to the simultaneous contribution from fluorescence, OH stretching, and CH stretching of PVA. The second important aspect is that although 118 days have passed, the SERS attributable to polyynes is still clearly visible and intense. This is an important confirmation that the use of Version 2G solutions, improves the stability of polyynes over time. The reason why there is this improvement in stability compared to the cases seen previously in Section 5.2, could lie in a stabilizing action of glycerol on the polymer, or a stabilizing action of glycerol on the polyynes. Of the two, the most plausible justification is that glycerol stabilizes the nanofiber polymer. Specifically, it would assume a plasticizing effect on PVA by changing its solubility parameters to atmospheric gases [128]. This would justify the trends in SERS signals that have been observed.

Finally, all spectra of all Versions (referring to Section 5.2 and this Section) were obtained by keeping the same SERS parameter at all times. For this reason, a comparison of stability from the various Versions of this Section and the previous one can be evaluated. Comparing the spectra, it is noticeable how Version 2G provided SERS signals of the polyynes, *i.e.,* the region around 2000 cm $^{-1}$, whose intensity and magnitude remain more stable over time. In particular, the signal after 118 days is visible, whereas for Versions H and A tend to flatten out in less time. For all Versions except the H Versions, with time, there is the appearance of a band around 3200 cm^{-1}, which can be attributed to an absorption of water on the membrane surface. This justification was made through the analysis of Figure 5.12, since for a very long time, the Versions A show no more intense signal than the SERS of the polyynes at the same Raman parameter setup.

5.4.   Study on SERS Signal of Nanofibers Embedding Size-Separated Polyynes

In this Section, the aim was to investigate the SERS signal of polyynes separated by both termination and length embedded within PVA electrospun nanofibers. The analysis on SERS spectra seek to show whether, as with normal Raman, there is signal downshift as the length of polyynes increases, even for SERS signals (see Section 1.4.1). In addition, the time trend as a function of the type of polyynes embedded in the nanofibers was observed. To make these composites, it was necessary to use HPLC to separate the polyynes to be inserted into the nanofibers (see Section 3.2.5). Given the dilution of the solution coming out of the HPLC, it was decided to concentrate the solution to be injected, to be sure to obtain a good concentration at the end of the separation. It was also decided to use polyynes derived from MeCN since the yield in this solvent is high (see Section 4.1). Specifically, the steps that were taken were the following: five 2-mL ablations were performed in MeCN for 15 min each; after that, the 10 mL mixture was concentrated by rotavapor to a final volume of 1.5 mL; finally, through the syringe filter, the solution was filtered to remove the larger-sized impurities. HC_8H, $HC_{10}H$, $HC_{12}H$, $HC_{14}H$, $HC_{16}H$ and $HC_{18}H$ chains were then collected and separated. To compare the data, all samples were electrospinned with the same parameters and, having done the study in Section 5.2, it was decided to use the same parameters as in Version 2A; namely, the flow rate of 0.1 ml/h, voltage of 17 kV, distance between nozzle and collector of 20 cm, and the electrospinning time was 1h for each sample. The nanofibers for all samples were deposited on an aluminum substrate and placed on top of a glass substrate. The starting solution consisted of 10wt% PVA was initially dissolved in 60% by volume of AgNP concentrated

solution and 40% by volume of separated polyynes solution. The only difference between the solutions was the type of polyynes separated. As done for the previous Versions discussed in Sections 5.2 and 5.3, SERS spectra were made in multiple spots to check the homogeneity of the membranes, and for all cases, good and homogeneous deposition was observed. Figure 5.13 shows SERS spectra for each sample, all obtained immediately after completing deposition and with all the same Raman-related parameters.
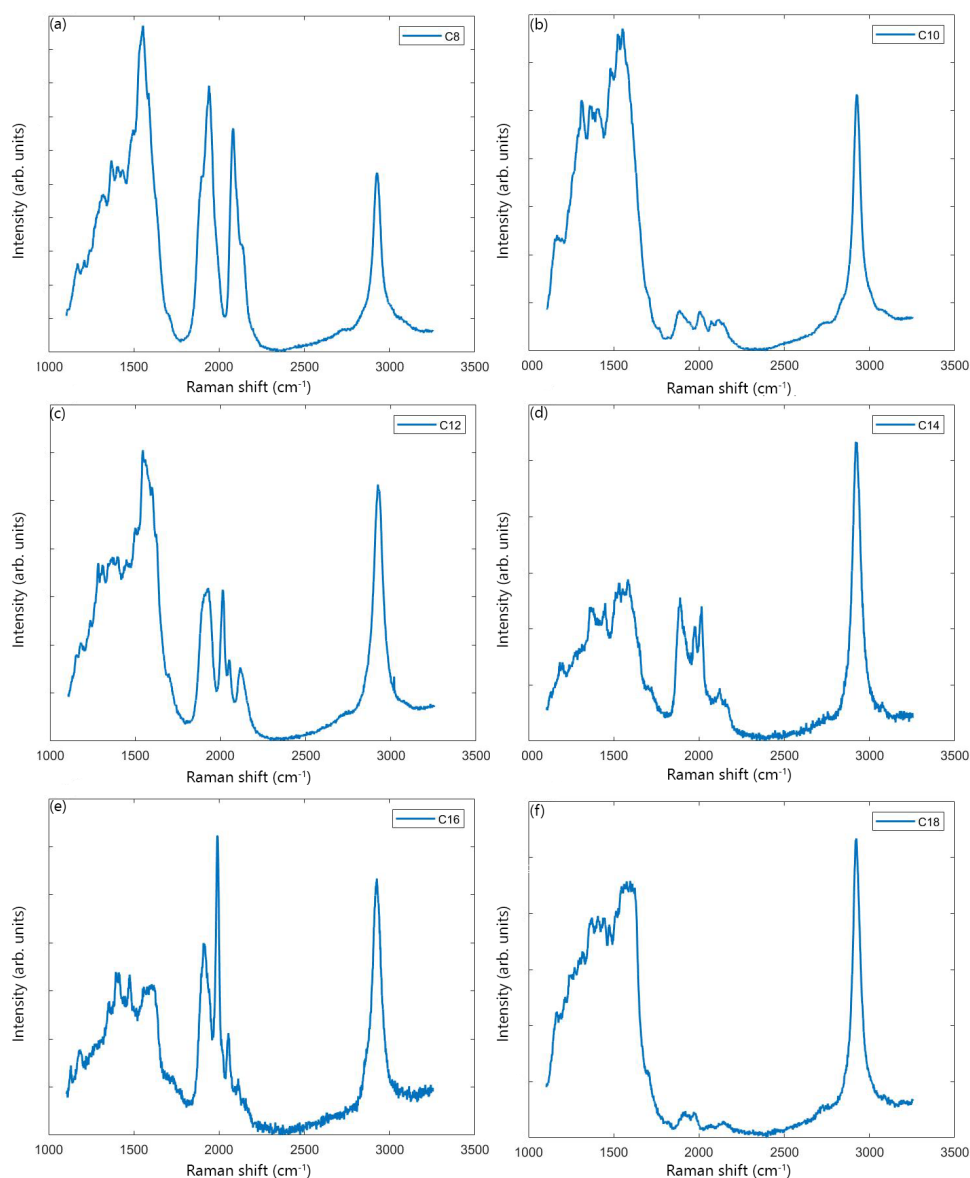
Figure 5.13: SERS spectra of PVA nanofibers with concentrated AgNPs and PLAL size-separated polyynes mixtures. Rispectively, the embedded polyynes are: (a) HC_8H; (b) $HC_{10}H$; (c) $HC_{12}H$; (d) $HC_{14}H$; (e) $HC_{16}H$; (f) $HC_{18}H$. The parameters used for measurement were: laser power of 0.533 mW, 3 accumulations for 10 seconds.
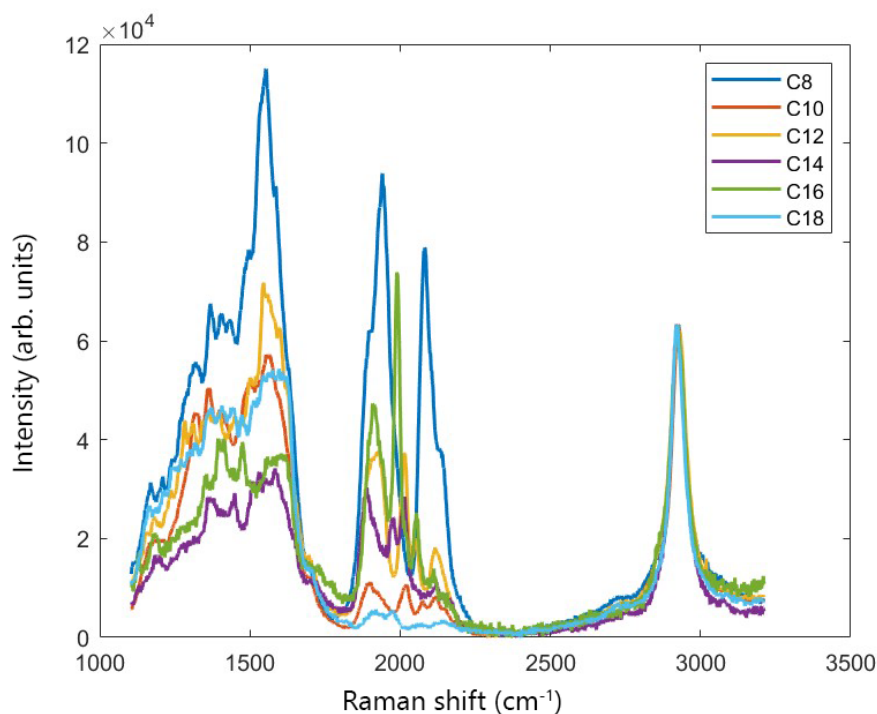
Figure 5.14: SERS spectra of PVA nanofibers with concentrated AgNPs and PLAL size-separated polyynes mixtures. The spectra are displayed on the same y-axis and normalized on the polymer peak. The parameters used for measurement were: laser power of 0.533 mW, 3 accumulations for 10 seconds.

What can be observed is that the SERS signal attributable to polyynes, changes depending on the type of size-separated polyynes embedded within the nanofibers. The position of the signals is for all cases placed in the same area around 2000 cm^{-1} and the length-dependent shift of the peaks is not observed as in normal Raman, as shown in Figure 5.14 (see Section 1.4.1). This is given because of the interaction of AgNPs with polyynes, which can form complexes or bind with them, making the nature of the SERS signal chaotic. More interesting observations can be made regarding the intensity and magnitude of the SERS peaks of the polyynes and the zone attributable to AgNPs and SERS of possible sp^2-byproducts, $i.e.,$ around 1500 cm^{-1}. It would appear that a pattern is obtained depending on the length that varies by two carbon atoms in two. In particular, HC$_8$H shows an intense SERS signal, while HC$_{10}$H is weaker, and then has a more intense signal again with HC$_{12}$H and so on. This behavior is interesting and it is difficult to justify, partly because it is good to take into account that the Raman cross section increases as the length of the polyynes increases, and it is not clear what function is shaping this. Besides the fact that in part the signal depends on the concentration of the polyynes. However, this is not the case here, because, taking HC$_8$H, HC$_{10}$H, and HC$_{12}$H as examples, the

concentration of the $HC_{12}H$ is lower than the $HC_{10}H$ (see Section 4.1 where concentration trends are shown), but there is not the same behavior with the SERS signal. To explain this effect, the only justification is that AgNPs have different interactions with polyynes depending on their length. AgNPs could form complexes, or silver atoms could replace some hydrogen terminations, or in general bind differently with polyynes depending on their length [62]. Then, stability as a function of polyynes length was studied. Figure 5.15 shows the various SERS spectra of all samples. The spectra for HC_8H, $HC_{10}H$, and $HC_{12}H$ were obtained up to 91 days after deposition occurred, while $HC_{14}H$, $HC_{16}H$, and $HC_{18}H$ up to 42 days. For all samples, except those containing long chains, there is a decrease in SERS signal over time. While the membranes containing $HC_{16}H$ and $HC_{18}H$, seem to show more stable signals over time, albeit of different magnitude. In addition, compared to the observations made regarding Figure 5.13, with time it would appear that only sample $HC_{16}H$ shows a time-stable and intense SERS signal, while the other samples, for long periods, tend to have low intense signals. So, except for this sample, the others have a behavior similar to that observed in Section 5.2 for Versions A. As anticipated, one possible explanation for this behavior could be a particular chain length-dependent interaction between AgNPs and the polyynes themselves. Another important observation is that for the one containing $HC_{10}H$, the SERS signal is stable over time, if not even greater in some cases. This particular aspect is not entirely clear, since for all samples and even for the many Versions also analyzed in previous Sections, it never happened. Thus, this aspect can probably be associated with a manufacturing defect in the specimen, where agglomerates probably formed between AgNP and polyynes within the membrane. Finally, the last noteworthy aspect is that the signal caused by AgNPs, after a high initial value, tends to remain constant over time for all samples.
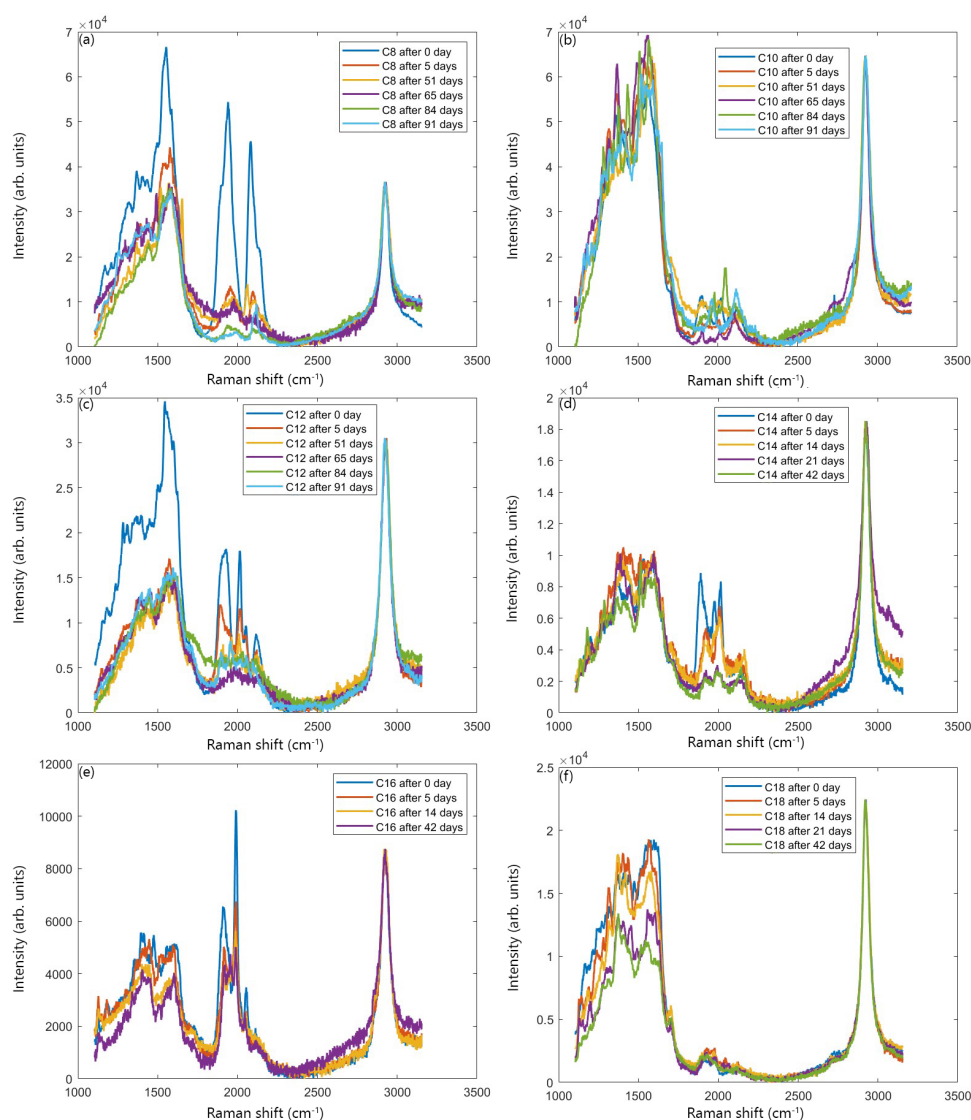
Figure 5.15: SERS spectra of PVA electrospun nanofibers containing concentrated AgNPs and PLAL size-terminated polyynes measured at different times.(a) HC_8H; (b) $HC_{10}H$; (c) $HC_{12}H$; (d) $HC_{14}H$; (e) $HC_{16}H$; (f) $HC_{18}H$. The spectra are displayed on the same y-axis and normalized on the polymer peak. The parameters used for measurement were: laser power of 0.533 mW, 3 accumulations for 10 seconds.

In summary, there would seem to be a correlation between the preferential binding between AgNPs and polyynes, dictated by the length of the latter. This aspect is appreciable when no time has elapsed since the fabrication of the specimens. Indeed, as time passes, the SERS signal of the polyynes from the various specimens tends to homogenize, probably due to the degradation of the polyynes into sp^2 compounds. If this is the case, this would support the previous hypothesis, since, given the loss of the initial configuration, the preferential binding contribution between AgNPs and the length of the polyynes would

no longer occur. The only exception observed was for the specimen containing $HC_{16}H$, where the signal remained constant and intense even in the long run.

6 —— Conclusions and future developments

The main goals of this thesis work were related to the investigation of new strategies aimed at improving production yields of polyynes produced by PLAL and the study of the effects that nanofiber geometry and morphology have on stability over time of the embedded polyynes. Nanofibers containing polyynes selected for both length and termination were produced, and studies related to SERS signal and stability over time were conducted.

The use of low temperatures during the ablation process improved the production of the longest chains, specifically, $HC_{14}H$ and $HC_{16}C$ by about 6% and 9.6%, respectively, in MeCN solutions. The other strategy discussed to increase the production and length of the chains produced is to increase the viscosity of the solution to be ablated. Indeed, by using glycerol in aqueous solutions, approximately 300% higher yields were obtained. Moreover, by combining the increase in viscosity and the stabilizing effect of AgNPs, the yields improved further, estimating 450%. These increases are also partly attributed to the addition of a carbon source within a solution that lacked one. The use of PMMA in MeCN solution to increase viscosity is also reported. Here the yield was also improved for long chains, achieving up to about 15% more for $HC_{16}H$. Regarding the study of polymer matrix nano-composites, numerous samples were produced by electrospinning. An initial study focused on observing what changes AgNP and polyynes make to the geometry and morphology of the nanofibers. Furthermore, with the same solution composition, the effects of electrospinning process parameters on the diameter of nanofibers were investigated. The experimental results were in agreement with the various theoretical parameters described in Section 2.1,, and in some cases, bimodal distributions of fiber diameters were demonstrated. Then studies were conducted using SERS to evaluate the stability over time as a function of nanofiber diameter and as a function of composition. It was observed that the use of plasticizers, glycerol, in this case, could be a winning strategy to increase the stability over time of the nanocomposites. Finally, a study was performed on the stability of size-selected polyynes embedded within nanofibers and a

study on possible causes attributable to the degradation of polyynes. In the first case, a possible interaction of AgNPs dependent on the length of the polyynes was observed. In the second case, the possible degradation of polyynes due to the combined effect between their intrinsic degradation and contact with the atmosphere was investigated.

For possible future studies, the idea of increasing viscosity could be thought of extending to more solutions and using new compounds to try to further improve the yield and length of polyynes. Related to stability through the creation of composite materials, the gelling effect of certain solutions could be thought of as a way to obtain gels containing polyynes immediately after ablation. One example would be to use an aqueous solution of isinglass and AgNP, with a high enough concentration of isinglass to induce gelling. Then, one could, through thermocouples or a heater, adjust the temperature of the solution during ablation, making sure that the temperature is high enough to ensure the liquid phase of the solution, but not too much to change its volume due to evaporation. After that, when ablation is finished, it will be sufficient to place the sample back in the refrigerator to promote gelation. Having introduced AgNPs, it should, in theory, be possible to perform SERS analyses of the gelatin. However, high concentrations of isinglass could degrade under the effect of the laser and, therefore, it is good to conduct a thorough study of the correct concentration. Another aspect is that in this way, ablation by-products would also be incorporated into the gelatin, which, however, is also the case for polyyne mixtures incorporated into fibers obtained by electrospinning. However, with gelation, the many steps required to make the composite could be avoided, and the timelines, between polyyne production and incorporation within a matrix, would be reduced. Finally, one could extend the same idea in forming gels to other types of solutions, based on organic solvents, thus further increasing the production yield of polyynes.

Bibliography

[1] Th Henning and F. Salama. Carbon in the universe. *Science*, 282(5397):2204–2210, 1998.

[2] Andreas Hirsch. The era of carbon allotropes. *Nature Materials*, 9(11):868–871, 2010.

[3] Julio Atkins, Peter; de Paula. Physical Chemistry. *Journal of the Franklin Institute*, 272(4), oct 1961.

[4] Lionel Salem. Intermolecular orbital theory of the interaction between conjugated systems. I. General theory. *Journal of the American Chemical Society*, 90(3):543–552, jan 1968.

[5] C. S. Casari, M. Tommasini, R. R. Tykwinski, and A. Milani. Carbon-atom wires: 1-D systems with tunable properties. *Nanoscale*, 8(8):4414–4435, 2016.

[6] Donald R. Askeland. Dispersion Strengthening by Phase Transformation and Heat Treatment. *The Science and Engineering of Materials*, 1991.

[7] Salisu Nasir, Mohd Zobir Hussein, Zulkarnain Zainal, and Nor Azah Yusof. Carbon-based nanomaterials/allotropes: A glimpse of their synthesis, properties and some applications. *Materials*, 11(2):1–24, 2018.

[8] A. K. Geim. Graphene: Status and prospects. *Science*, 324(5934):1530–1534, 2009.

[9] A. L. Ivanovskii. Graphynes and graphdyines. *Progress in Solid State Chemistry*, 41(1-2):1–19, 2013.

[10] Meng Hu, Quan Huang, Zhisheng Zhao, Bo Xu, Dongli Yu, and Julong He. Superhard and high-strength yne-diamond semimetals. *Diamond and Related Materials*, 46:15–20, 2014.

[11] Carl Glaser. Beitrage zur Kenntnifs des Acetenylbenzols. *Ber. Dtsch. Chem. Ges.*, 2:422–424, 1869.

[12] Adolf Baeyer. Ueber Polyacetylenverbindungen. *Berichte der deutschen chemischen Gesellschaft*, 18(2):2269–2281, jul 1885.

[13] John D. Bu'Lock. Acetylenic compounds as natural products. *Quarterly Reviews, Chemical Society*, 10(4):371, 1956.

[14] Annabelle L. K. Shi Shun and Rik R. Tykwinski. Synthesis of Naturally Occurring Polyynes. *Angewandte Chemie International Edition*, 45(7):1034–1057, feb 2006.

[15] Yu P. Kudryavtsev. *The Discovery of Carbyne*, pages 1–6. Springer Netherlands, Dordrecht, 1999.

[16] H. W. Kroto, J. R. Heath, S. C. O'Brien, R. F. Curl, and R. E. Smalley. C60: Buckminsterfullerene. *Nature*, 318(6042):162–163, nov 1985.

[17] Sumio Iijima. Helical microtubules of graphitic carbon. *Nature*, 354(6348):56–58, nov 1991.

[18] Mingjie Liu, Vasilii I Artyukhov, Hoonkyung Lee, Fangbo Xu, and Boris I Yakobson. Carbyne from First Principles: Chain of C Atoms, a Nanorod or a Nanorope. *ACS Nano*, 7(11):10075–10082, nov 2013.

[19] S. Tongay, R. T. Senger, S. Dag, and S. Ciraci. Ab-initio electron transport calculations of carbon based string structures. *Physical Review Letters*, 93(13):2–5, 2004.

[20] Shujiang Yang and Miklos Kertesz. Bond length alternation and energy band gap of polyyne. *Journal of Physical Chemistry A*, 110(31):9771–9774, 2006.

[21] Alberto Milani, Matteo Tommasini, Mirella Del Zoppo, Chiara Castiglioni, and Giuseppe Zerbi. Carbon nanowires: Phonon and π-electron confinement. *Physical Review B - Condensed Matter and Materials Physics*, 74(15):1–4, 2006.

[22] A. Karpfen. Ab initio studies on polymers. I. the linear infinite polyyne. *Journal of Physics C: Solid State Physics*, 12(16):3227–3237, 1979.

[23] Alberto Milani, Matteo Tommasini, Daniele Fazzi, Chiara Castiglioni, Mirella Del Zoppo, and Giuseppe Zerbi. First-principles calculation of the Peierls distortion in an infinite linear carbon chain: The contribution of Raman spectroscopy. *Journal of Raman Spectroscopy*, 39(2):164–168, 2008.

[24] Alberto Milani, Matteo Tommasini, and Giuseppe Zerbi. Carbynes phonons: A tight binding force field. *Journal of Chemical Physics*, 128(6), 2008.

[25] Alberto Milani, Matteo Tommasini, Valeria Russo, Andrea Li Bassi, Andrea Lucotti, Franco Cataldo, and Carlo S. Casari. Raman spectroscopy as a tool to investigate the structure and electronic properties of carbon-atom wires. *Beilstein Journal of Nanotechnology*, 6(1):480–491, 2015.

[26] Shujiang Yang and Miklos Kertesz. Linear Cn clusters: Are they acetylenic or cumulenic? *Journal of Physical Chemistry A*, 112(1):146–151, 2008.

[27] Chien-Pin Chou, Wun-Fan Li, Henryk A. Witek, and Marcin Andrzejak. *Vibrational Spectroscopy of Linear Carbon Chains*, pages 375–415. World Scientific, 2011.

[28] Yu P. Kudryavtsev, S. E. Evsyukov, M. B. Guseva, V. G. Babaev, and V. V. Khvostov. Carbyne - the third allotropic form of carbon. *Russian Chemical Bulletin*, 42(3):399–413, 1993.

[29] Yu P. Kudryavtsev, R. B. Heimann, and S. E. Evsyukov. Carbynes: Advances in the field of linear carbon chain compounds. *Journal of Materials Science*, 31(21):5557–5571, 1996.

[30] Peter Siemsen, Robert C. Livingston, and François Diederich. Acetylenic coupling: A powerful tool in molecular construction. *Angewandte Chemie - International Edition*, 39(15):2632–2657, 2000.

[31] Martyn Jevric and Mogens Brøndsted Nielsen. Synthetic strategies for oligoynes. *Asian Journal of Organic Chemistry*, 4(4):286–295, 2015.

[32] Yueze Gao and Rik R. Tykwinski. Advances in Polyynes to Model Carbyne. *Accounts of Chemical Research*, 55(24):3616–3630, 2022.

[33] Lei Shi, Philip Rohringer, Kazu Suenaga, Yoshiko Niimi, Jani Kotakoski, Jannik C. Meyer, Herwig Peterlik, Marius Wanko, Seymur Cahangirov, Angel Rubio, Zachary J. Lapin, Lukas Novotny, Paola Ayala, and Thomas Pichler. Confined linear carbon chains as a route to bulk carbyne. *Nature Materials*, 15(6):634–639, 2016.

[34] Wesley A. Chalifoux, Michael J. Ferguson, Robert McDonald, Frederic Melin, Luis Echegoyen, and Rik R. Tykwinski. Adamantyl-endcapped polyynes. *Journal of Physical Organic Chemistry*, 25(1):69–76, 2012.

[35] H. Ushida, N. Takada, and K. Sasaki. Diagnostics of liquid-phase laser ablation plasmas by spectroscopic methods. *Journal of Physics: Conference Series*, 59(1):563–566, 2007.

[36] P Milani and S Iannotta. *Cluster beam synthesis of nanostructured materials.* 1999.

[37] Franco Cataldo. Simple generation and detection of polyynes in an arc discharge between graphite electrodes submerged in various solvents. *Carbon*, 41(13):2671–2674, 2003.

[38] Sonia Peggiani, Andrea Senis, Anna Facibeni, Alberto Milani, Patrick Serafini, Gianmarco Cerrato, Andrea Lucotti, Matteo Tommasini, Daniele Fazzi, Chiara Castiglioni, Valeria Russo, Andrea Li Bassi, and Carlo S. Casari. Size-selected polyynes synthesised by submerged arc discharge in water. *Chemical Physics Letters*, 740(October 2019), 2020.

[39] Graham K. Hubler. Pulsed Laser Deposition. *MRS Bulletin*, 17(2):26–29, 1992.

[40] Sonia Peggiani, Pietro Marabotti, Riccardo Alberto Lotti, Anna Facibeni, Patrick Serafini, Alberto Milani, Valeria Russo, Andrea Li Bassi, and Carlo Spartaco Casari. Solvent-dependent termination, size and stability in polyynes synthesized: Via laser ablation in liquids. *Physical Chemistry Chemical Physics*, 22(45):26312–26321, 2020.

[41] Franco Cataldo. Polyynes and cyanopolyynes synthesis from the submerged electric arc: About the role played by the electrodes and solvents in polyynes formation. *Tetrahedron*, 60(19):4265–4274, 2004.

[42] Rajesh Kumar, Rajesh Kumar Singh, Pawan Kumar Dubey, Ram Manohar Yadav, Dinesh Pratap Singh, R. S. Tiwari, and O. N. Srivastava. Highly zone-dependent synthesis of different carbon nanostructures using plasma-enhanced arc discharge technique. *Journal of Nanoparticle Research*, 17(1), 2015.

[43] Giuseppe Compagnini, Valentina Mita, Rosario Sergio Cataliotti, Luisa D'Urso, and Orazio Puglisi. Short polyyne chains produced by pulsed laser ablation of graphite in water. *Carbon*, 45(12):2456–2458, 2007.

[44] Vincenzo Amendola and Moreno Meneghetti. Laser ablation synthesis in solution and size manipulation of noble metal nanoparticles. *Physical Chemistry Chemical Physics*, 11(20):3805–3821, 2009.

[45] Vincenzo Amendola and Moreno Meneghetti. What controls the composition and the structure of nanomaterials generated by laser ablation in liquid solution? *Physical Chemistry Chemical Physics*, 15(9):3027–3046, 2013.

[46] Patrick Lorazo, Laurent J. Lewis, and Michel Meunier. Short-pulse laser ablation of solids: From phase explosion to fragmentation. *Physical Review Letters*, 91(22):1–4, 2003.

[47] A. De Giacomo, M. Dell'Aglio, O. De Pascale, and M. Capitelli. From single pulse to double pulse ns-Laser Induced Breakdown Spectroscopy under water: Elemental analysis of aqueous solutions and submerged solid samples. *Spectrochimica Acta - Part B Atomic Spectroscopy*, 62(8):721–738, 2007.

[48] Takeshi Tsuji, Yasuyuki Tsuboi, Noboru Kitamura, and Masaharu Tsuji. Microsecond-resolved imaging of laser ablation at solid-liquid interface: Investigation of formation process of nano-size metal colloids. *Applied Surface Science*, 229(1-4):365–371, 2004.

[49] Fumitaka Mafune, Jun-ya Kohno, Yoshihiro Takeda, and Tamotsu Kondow. Formation of Gold Nanoparticles by Laser Ablation in Aqueous Solution of Surfactant. pages 5114–5120, 2001.

[50] P. Marabotti, S. Peggiani, A. Facibeni, P. Serafini, A. Milani, V. Russo, A. Li Bassi, and C. S. Casari. In situ surface-enhanced Raman spectroscopy to investigate polyyne formation during pulsed laser ablation in liquid. *Carbon*, 189:219–229, 2022.

[51] Hanran Li, Yangliu Wu, Yifan Zhang, Tianxiang Zhu, Takahiro Maruyama, and Yi Liu. Submerged carbon arc in deionized water : A green route for scalable preparation of gas containing polyynes. *Chemical Physics*, 535(April):110804, 2020.

[52] Paul Rostron, Safa Gaber, and Dina Gaber. Raman Spectroscopy , Review. (September), 2016.

[53] Tania Dey. Microplastic pollutant detection by Surface Enhanced Raman Spectroscopy (SERS): a mini-review. *Nanotechnology for Environmental Engineering*, 8(1):41–48, 2023.

[54] Lisa G. Neven and Mac Morford. Effects of Irradiation on Phenoloxidase Levels in Codling Moth (Lepidoptera: Tortricidae) Larvae. *Journal of Economic Entomology*, 91(2):534–538, 1998.

[55] Chira Castiglioni, Matteo Tommasini, and Giuseppe Zerbi. Raman spectroscopy of polyconjugated molecules and materials: Confinement effect in one and two dimensions. *Philosophical Transactions of the Royal Society A: Mathematical, Physical and Engineering Sciences*, 362(1824):2425–2459, 2004.

[56] A. Lucotti, M. Tommasini, M. Del Zoppo, C. Castiglioni, G. Zerbi, F. Cataldo, C. S. Casari, A. Li Bassi, V. Russo, M. Bogana, and C. E. Bottani. Raman and SERS investigation of isolated sp carbon chains. *Chemical Physics Letters*, 417(1-3):78–82, 2006.

[57] Andrea Lucotti, Matteo Tommasini, Daniele Fazzi, Mirella Del Zoppo, Wesley A. Chalifoux, Michael J. Ferguson, Giuseppe Zerbi, and Rik R. Tykwinski. Evidence for solution-state nonlinearity of sp-carbon chains based on IR and raman spectroscopy: Violation of mutual exclusion. *Journal of the American Chemical Society*, 131(12):4239–4244, 2009.

[58] Hiroshi Tabata, Minoru Fujii, Shinji Hayashi, Tatsuya Doi, and Tomonari Wakabayashi. Raman and surface-enhanced Raman scattering of a series of size-separated polyynes. *Carbon*, 44(15):3168–3176, 2006.

[59] Giuseppe Compagnini, Giacomo Patanè, Luisa D'Urso, Orazio Puglisi, Rosario Sergio Cataliotti, and Bruno Pignataro. On the interaction of carbon nanowires with noble metals through a study of their surface-enhanced Raman spectra. *Journal of Physical Chemistry C*, 112(51):20301–20306, 2008.

[60] Roberto Pilot, Raffaella Signorini, Christian Durante, Laura Orian, Manjari Bhamidipati, and Laura Fabris. A review on surface-enhanced Raman scattering. *Biosensors*, 9(2), 2019.

[61] A. Lucotti, C. S. Casari, M. Tommasini, A. Li Bassi, D. Fazzi, V. Russo, M. Del Zoppo, C. Castiglioni, F. Cataldo, C. E. Bottani, and G. Zerbi. sp Carbon chain interaction with silver nanoparticles probed by Surface Enhanced Raman Scattering. *Chemical Physics Letters*, 478(1-3):45–50, 2009.

[62] C. S. Casari, V. Russo, A. Li Bassi, C. E. Bottani, F. Cataldo, A. Lucotti, M. Tommasini, M. Del Zoppo, C. Castiglioni, and G. Zerbi. Stabilization of linear carbon structures in a solid Ag nanoparticle assembly. *Applied Physics Letters*, 90(1), 2007.

[63] Werner Mäntele and Erhan Deniz. UV–VIS absorption spectroscopy: Lambert-Beer reloaded. *Spectrochimica Acta - Part A: Molecular and Biomolecular Spectroscopy*, 173:965–968, 2017.

[64] Ryutaro Matsutani, Fumiyoshi Ozaki, Riyo Yamamoto, Tomoe Sanada, Yutaka Okada, and Kazuo Kojima. Preparation of polyynes up to C22H2 by liquid-phase laser ablation and their immobilization into SiO2 gel. *Carbon*, 47(7):1659–1663, 2009.

[65] Kohei Inoue, Ryutaro Matsutani, Tomoe Sanada, and Kazuo Kojima. Preparation of long-chain polyynes of C24H2 and C26H2 by liquid-phase laser ablation in decalin. *Carbon*, 48(14):4209–4211, 2010.

[66] C. S. Casari and A. Milani. Carbyne: From the elusive allotrope to stable carbon atom wires. *MRS Communications*, 8(2):207–219, 2018.

[67] Franco Cataldo. Polyynes production in a solvent-submerged electric arc between graphite electrodes. III. Chemical reactivity and stability toward air, ozone, and light. *Fullerenes Nanotubes and Carbon Nanostructures*, 12(3):633–646, 2004.

[68] Franco Cataldo. Stability of polyynes in air and their degradation by ozonolysis. *Polymer Degradation and Stability*, 91(2):317–323, 2006.

[69] C. S. Casari, A. Li Bassi, L. Ravagnan, F. Siviero, C. Lenardi, P. Piseri, G. Bongiorno, C. E. Bottani, and P. Milani. Chemical and thermal stability of carbyne-like structures in cluster-assembled carbon films. *Physical Review B - Condensed Matter and Materials Physics*, 69(7), 2004.

[70] Franco Cataldo. Storage stability of polyynes and cyanopolyynes in solution and the effect of ammonia or hydrochloric acid. *Fullerenes Nanotubes and Carbon Nanostructures*, 15(3):155–166, 2007.

[71] Franco Cataldo, Ornella Ursini, Alberto Milani, and Carlo S. Casari. One-pot synthesis and characterization of polyynes end-capped by biphenyl groups (α,ω-biphenylpolyynes). *Carbon*, 126:232–240, 2018.

[72] Franco Cataldo, Luca Ravagnan, Eugenio Cinquanta, Ivano Eligio Castelli, Nicola Manini, Giovanni Onida, and Paolo Milani. Synthesis, characterization, and modeling of naphthyl-terminated sp carbon chains: Dinaphthylpolyynes. *Journal of Physical Chemistry B*, 114(46):14834–14841, 2010.

[73] Rik R. Tykwinski, Wesley Chalifoux, Sara Eisler, Andrea Lucotti, Matteo Tommasini, Daniele Fazzi, Mirella Del Zoppo, and Giuseppe Zerbi. Toward carbyne: Synthesis and stability of really long polyynes. *Pure and Applied Chemistry*, 82(4):891–904, 2010.

[74] Shu Okada, Minoru Fujii, and Shinji Hayashi. Immobilization of polyynes adsorbed on Ag nanoparticle aggregates into poly(vinyl alcohol) films. *Carbon*, 49(14):4704–4709, 2011.

[75] Kang An, Guotong Wei, Gongmin Qi, Leimei Sheng, Liming Yu, Wei Ren, and Xinluo Zhao. Stability improvement of C8H2 and C10H2 embedded in poly(vinyl alcohol) films with adsorption on gold nanoparticles. *Chemical Physics Letters*, 637:71–76, 2015.

[76] C. S. Casari, V. Russo, A. Li Bassi, C. E. Bottani, F. Cataldo, A. Lucotti, M. Tom-

masini, M. Del Zoppo, C. Castiglioni, and G. Zerbi. Stabilization of linear carbon structures in a solid Ag nanoparticle assembly. *Applied Physics Letters*, 90(1), 2007.

[77] Ay??e G??l ??ener, Ali Saffet Altay, and Filiz Altay. Effect of voltage on morphology of electrospun nanofibers. *ELECO 2011 - 7th International Conference on Electrical and Electronics Engineering*, pages 324–328, 2011.

[78] Karen I Winey and Richard A Vaia. Polymer Nanocomposites. *MRS Bulletin*, 32(4):314–322, apr 2007.

[79] Soad Z. Al Sheheri, Zahra M. Al-Amshany, Qana A. Al Sulami, Nada Y. Tashkandi, Mahmoud A. Hussein, and Reda M. El-Shishtawy. The preparation of carbon nanofillers and their role on the performance of variable polymer nanocomposites. *Designed Monomers and Polymers*, 22(1):8–53, 2019.

[80] O. Breuer and Uttandaraman Sundararaj. Big returns from small fibers: A review of polymer/carbon nanotube composites. *Polymer Composites*, 25(6):630–645, 2004.

[81] Jayesh Doshi and Darrell H. Reneker. Electrospinning process and applications of electrospun fibers. *Conference Record - IAS Annual Meeting (IEEE Industry Applications Society)*, 3:1698–1703, 1993.

[82] Binoy Bera. Literature Review on Electrospinning Process (A Fascinating Fiber Fabrication Technique). *Imperial Journal of Interdisciplinary Research (IJIR*, 2(8):972–984, 2016.

[83] Andreas Greiner and Joachim H. Wendorff. Electrospinning: A fascinating method for the preparation of ultrathin fibers. *Angewandte Chemie - International Edition*, 46(30):5670–5703, 2007.

[84] Ramazan Asmatulu. Highly Hydrophilic Electrospun Polyacrylonitrile/ Polyvinypyrrolidone Nanofibers Incorporated with Gentamicin as Filter Medium for Dam Water and Wastewater Treatment. *Journal of Membrane and Separation Technology*, 5(2):38–56, 2016.

[85] Jayesh Doshi and Darrell H. Reneker. Electrospinning process and applications of electrospun fibers. *Journal of Electrostatics*, 35(2-3):151–160, 1995.

[86] Audrey Frenot and Ioannis S. Chronakis. Polymer nanofibers assembled by electro-spinning. *Current Opinion in Colloid and Interface Science*, 8(1):64–75, 2003.

[87] Darrell H Reneker and Iksoo Chun. Nanometre diameter fibres of polymer, produced by electrospinning. *Nanotechnology*, 7(3):216–223, sep 1996.

[88] Abdullah Khalil, Boor Singh Lalia, Raed Hashaikeh, and Marwan Khraisheh. Electrospun metallic nanowires: Synthesis, characterization, and applications. *Journal of Applied Physics*, 114(17), 2013.

[89] Tamer Uyar and Flemming Besenbacher. Electrospinning of uniform polystyrene fibers: The effect of solvent conductivity. *Polymer*, 49(24):5336–5343, 2008.

[90] Jamal A. Abbas, Ibtisam A. Said, Manaf A. Mohamed, Suhad A. Yasin, Zeravan A. Ali, and Idrees H. Ahmed. Electrospinning of polyethylene terephthalate (PET) nanofibers: Optimization study using taguchi design of experiment. *IOP Conference Series: Materials Science and Engineering*, 454(1), 2018.

[91] A. Koski, K. Yim, and S. Shivkumar. Effect of molecular weight on fibrous PVA produced by electrospinning. *Materials Letters*, 58(3-4):493–497, 2004.

[92] Yu-Qin Wan, Ji-Huan He, Jian-Yong Yu, and Yue Wu. Electrospinning of high-molecule PEO solution. *Journal of Applied Polymer Science*, 103(6):3840–3843, mar 2007.

[93] Rosane M.D. Soares, Nataly M. Siqueira, Molamma P. Prabhakaram, and Seeram Ramakrishna. Electrospinning and electrospray of bio-based and natural polymers for biomaterials development. *Materials Science and Engineering C*, 92(November 2017):969–982, 2018.

[94] C. J. Luo, M. Nangrejo, and M. Edirisinghe. A novel method of selecting solvents for polymer electrospinning. *Polymer*, 51(7):1654–1662, 2010.

[95] Chunxue Zhang, Xiaoyan Yuan, Lili Wu, Yue Han, and Jing Sheng. Study on morphology of electrospun poly(vinyl alcohol) mats. *European Polymer Journal*, 41(3):423–432, 2005.

[96] Xiao Yan Yuan, Yuan Yuan Zhang, Cunhai Dong, and Jing Sheng. Morphology of ultrafine polysulfone fibers prepared by electrospinning. *Polymer International*, 53(11):1704–1710, 2004.

[97] Ayşe Gül Şener, Ali Saffet Altay, and Filiz Altay. Effect of voltage on morphology of electrospun nanofibers. In *2011 7th International Conference on Electrical and Electronics Engineering (ELECO)*, pages I–324–I–328, 2011.

[98] Adnan Haider, Sajjad Haider, and Inn Kyu Kang. A comprehensive review summarizing the effect of electrospinning parameters and potential applications of nanofibers in biomedical and biotechnology. *Arabian Journal of Chemistry*, 11(8):1165–1188, 2018.

[99] Darrell H. Reneker, Alexander L. Yarin, Hao Fong, and Sureeporn Koombhongse. Bending instability of electrically charged liquid jets of polymer solutions in electrospinning. *Journal of Applied Physics*, 87(9 I):4531–4547, 2000.

[100] Zhenyu Li and Ce Wang. Effects of Working Parameters on Electrospinning. *SpringerBriefs in Materials*, pages 15–28, 2013.

[101] Paul D. Dalton, Doris Klee, and Martin Möller. Electrospinning with dual collection rings. *Polymer*, 46(3):611–614, 2005.

[102] Su A. Park, Koeun Park, Hyeon Yoon, Joon Gon Son, Teijin Min, and Geun Hyung Kim. Apparatus for preparing electrospun nanofibers: Designing an electrospinning process for nanofiber fabrication. *Polymer International*, 56(11):1361–1366, 2007.

[103] J M Deitzel, J Kleinmeyer, D Harris, and N C Beck Tan. The effect of processing variables on the morphology of electrospun. *Polymer*, 42:261–272, 2001.

[104] K. H. Lee, H. Y. Kim, H. J. Bang, Y. H. Jung, and S. G. Lee. The change of bead morphology formed on electrospun polystyrene fibers. *Polymer*, 44(14):4029–4034, 2003.

[105] Chang Seok Ki, Doo Hyun Baek, Kyung Don Gang, Ki Hoon Lee, In Chul Um, and Young Hwan Park. Characterization of gelatin nanofiber prepared from gelatin-formic acid solution. *Polymer*, 46(14):5094–5102, 2005.

[106] Chidchanok Mit-uppatham, Manit Nithitanakul, and Pitt Supaphol. Ultrafine Electrospun Polyamide-6 Fibers: Effect of Solution Conditions on Morphology and Average Fiber Diameter. *Macromolecular Chemistry and Physics*, 205(17):2327–2338, nov 2004.

[107] Qingbiao Yang, L. I. Zhenyu, Youliang Hong, Yiyang Zhao, Shilun Qiu, C. E. Wang, and Yen Wei. Influence of solvents on the formation of ultrathin uniform poly(vinyl pyrrolidone) nanofibers with electrospinning. *Journal of Polymer Science, Part B: Polymer Physics*, 42(20):3721–3726, 2004.

[108] Chitral J. Angammana and Shesha H. Jayaram. Analysis of the effects of solution conductivity on electrospinning process and fiber morphology. *IEEE Transactions on Industry Applications*, 47(3):1109–1117, 2011.

[109] H Fong, I Chun, and D.H Reneker. Beaded nanofibers formed during electrospinning. *Polymer*, 40(16):4585–4592, jul 1999.

[110] S. De Vrieze, T. Van Camp, A. Nelvig, B. Hagström, P. Westbroek, and K. De

Clerck. The effect of temperature and humidity on electrospinning. *Journal of Materials Science*, 44(5):1357–1362, 2009.

[111] P. C. Lee and D. Meisel. Adsorption and surface-enhanced Raman of dyes on silver and gold sols. *Journal of Physical Chemistry*, 86(17):3391–3395, 1982.

[112] Anjana Sarkar, Sudhir Kapoor, and Tulsi Mukherjee. Synthesis and characterisation of silver nanoparticles in viscous solvents and its transfer into non-polar solvents. *Research on Chemical Intermediates*, 36(4):411–421, 2010.

[113] K. J. Thomas, M. Sheeba, V. P.N. Nampoori, C. P.G. Vallabhan, and P. Radhakrishnan. Raman spectra of polymethyl methacrylate optical fibres excited by a 532 nm diode pumped solid state laser. *Journal of Optics A: Pure and Applied Optics*, 10(5), 2008.

[114] Yu Wan, Zhirui Guo, Xiaoli Jiang, Kun Fang, Xiang Lu, Yu Zhang, and Ning Gu. Quasi-spherical silver nanoparticles: Aqueous synthesis and size control by the seed-mediated Lee-Meisel method. *Journal of Colloid and Interface Science*, 394(1):263–268, 2013.

[115] Marco Benoliel. Investigation of naphthalene and its hydrogenated derivatives in the formation process of polyynes by Pulsed Laser Ablation in Liquid. 2021.

[116] Ryutaro Matsutani, Takuya Kakimoto, Hiromasa Tanaka, and Kazuo Kojima. Preparation of polyynes by liquid-phase laser ablation using different irradiation target materials and solvents. *Carbon*, 49(1):77–81, 2011.

[117] Kohei Inoue, Ryutaro Matsutani, Tomoe Sanada, and Kazuo Kojima. Preparation of long-chain polyynes of C24H2 and C26H2 by liquid-phase laser ablation in decalin. *Carbon*, 48(14):4209–4211, 2010.

[118] Aaron C. LaForge, Debadarshini Mishra, Lauren M. Gorman, Sergio Díaz-Tendero, Fernando Martín, and Nora Berrah. Time-resolved imaging of an elusive molecular reaction: hydrogen roaming in acetonitrile. XXX(Xx):1–9, 2023.

[119] Luling Wang and Sanford A. Asher. Refractive-index matching avoids local field corrections and scattering bias in solid-state Na 2SO 4 ultraviolet Raman cross-section measurements. *Applied Spectroscopy*, 66(2):157–162, 2012.

[120] Koichi Takamura, Herbert Fischer, and Norman R. Morrow. Physical properties of aqueous glycerol solutions. *Journal of Petroleum Science and Engineering*, 98-99:50–60, nov 2012.

[121] Thames River Chemical. Safety Data Sheet. *Material Safety Data Sheet*, 4(2):8–10, 2012.

[122] J. B. Segur and Helen E. Oderstar. Viscosity of Glycerol and Its Aqueous Solutions. *Industrial and Engineering Chemistry*, 43(9):2117–2120, 1951.

[123] Abel G.M. Ferreira, Ana P.V. Egas, Isabel M.A. Fonseca, Ana C. Costa, Danielly C. Abreu, and Lélio Q. Lobo. The viscosity of glycerol. *Journal of Chemical Thermodynamics*, 113(June 2016):162–182, 2017.

[124] Product Number. Acetonitrile. (1907), 2023.

[125] Ying Ma, Xinyu Cao, Xinjian Feng, Yongmei Ma, and Hong Zou. Fabrication of super-hydrophobic film from PMMA with intrinsic water contact angle below 90°. *Polymer*, 48(26):7455–7460, 2007.

[126] Tesi Di, Laurea Magistrale, Ingegneria Dei, and Materiali E Delle. Investigation of polyynes in polymeric electrospun nanofibers. 2021.

[127] I. Yu Prosanov and A. A. Matvienko. Study of PVA thermal destruction by means of IR and Raman spectroscopy. *Physics of the Solid State*, 52(10):2203–2206, 2010.

[128] R. Sothornvit and J. M. Krochta. Plasticizer effect on oxygen permeability of β-lactoglobulin films. *Journal of Agricultural and Food Chemistry*, 48(12):6298–6302, 2000.

A —— Appendix A

Below is the Matlab code used in this thesis work for dimensional evaluation of SEM images.

```matlab
% CODE V.ENG
% Clear previous and close all
clc; clear all; close all;
clearvars;
imtool close all;
% Be sure that workspace is opened
workspace;

% Style setting
format bank;
format compact;
carattere_scritte = 11;

% Starting message for user in Command Window
fprintf('The program is calculating the dimensions...\n');

%------------------------------------------------------------
% NB!!! Put the photo in the same workbook to avoid mistakes
baseFileName = 'test.png';
folder = fileparts(which(baseFileName));
fullFileName = fullfile(folder, baseFileName);
originalImage = imread(fullFileName);
scalaImage = imread(fullFileName);
%------------------------------------------------------------

% Image cropping and scale evaluation
originalImage = originalImage(1:650, :);
```

```matlab
28  scalaImage = scalaImage(692:713, 155:430);
29
30  % The image used for the scale is shown
31  subplot(3, 2, 5);
32  imshow(scalaImage);
33  title('Scale used in the image', 'FontSize',
        carattere_scritte);
34
35  % Grayscale image conversion if it wasn't already
36  [rows, columns, numberOfColorChannels] = size(scalaImage);
37  if numberOfColorChannels > 1
38      avviso_2 = sprintf('Your image has %d color channels.\nDo
            you want to convert it to grayscale?',
          numberOfColorChannels);
39      tasto = questdlg(avviso_2, 'Continue', 'Convert and
          continue', 'Cancel', 'Convert and continue');
40      if strcmp(tasto, 'Cancel')
41          fprintf(1, 'The program has ended.\n');
42          return;
43      end
44
45      scalaImage = rgb2gray(scalaImage);
46  end
47
48  % The scale is made binary
49  Th_Value_scala = 0.65; % Value between 0 and 1.
50  immagine_binaria_scala = im2bw(scalaImage, Th_Value_scala);
            % There are other willing ways to make the image
        binary
51
52  % With this command we fill the "holes" of our image with
53  % input
54  immagine_binaria_scala = imfill(immagine_binaria_scala, '
        holes');
55
56  % Label the image
57  labeledImage_scala = bwlabel(immagine_binaria_scala);
```

```matlab
58  % Make measurements of bounding box
59  props = regionprops(labeledImage_scala, 'BoundingBox');
60
61  % Calculation of pixel scale
62  width = props.BoundingBox(3);
63
64  % The scale is shown with the box defining the size
65  subplot(3, 2, 6);
66  imshow(scalaImage);
67  title('Image with reference scale outline', 'FontSize',
        carattere_scritte);
68  axis('on', 'image');
69  contorni_scala = bwboundaries(immagine_binaria_scala);
70  numero_di_contorni_scala = size(contorni_scala, 1);
71
72  hold on;
73  for k = 1 : numero_di_contorni_scala
74      thisBoundary = contorni_scala{k};
75      x = thisBoundary(:,2);
76      y = thisBoundary(:,1);
77      plot(x, y, 'r-', 'LineWidth', 2);
78  end
79  hold off;
80
81  % Checking whether the scale has been recognized correctly
82  domanda = sprintf('Was the scale recognized correctly?');
83  controllo = questdlg(domanda, 'Do you want to continue?', '
        Yes', 'No', 'Yes');
84  if strcmpi(controllo, 'No')
85      fprintf(1, 'The program is ended.\n');
86      return;
87  end
88
89  %-----------------------------------------------------------
90  % Data entry
91  scelta_campione = sprintf('Do you want to calculate the size
        of nanoparticles?');
```

```matlab
 92  risposta_2 = questdlg(scelta_campione, 'There are
        nanoparticles in the picture', 'Yes', 'No', 'Yes');
 93  if strcmpi(risposta_2, 'Yes')
 94
 95      % Grayscale image conversion if it wasn't already
 96      [rows, columns, numberOfColorChannels] = size(
            originalImage);
 97      if numberOfColorChannels > 1
 98          avviso_2 = sprintf('Your image has %d color channels
                .\nDo you want to convert it to grayscale?',
                numberOfColorChannels);
 99          tasto = questdlg(avviso_2, 'Continue', 'Convert and
                continue', 'Cancel', 'Convert and continue');
100          if strcmp(tasto, 'Cancel')
101              fprintf(1, 'The program is ended.\n');
102              return;
103          end
104
105          originalImage = rgb2gray(originalImage);
106      end
107      %-------------------------------------------------------
108      % Data entry
109      prompt = {'Enter reference length [nm]:'};
110      dlgtitle = 'Input';
111      dims = [1 35];
112      definput = {'1'};
113      answer = inputdlg(prompt,dlgtitle,dims,definput);
114      dati = str2double(answer);
115
116
117      % See how the image is converted. If it is converted
            poorly,
118      % help the program by improving the contrast between
            background and objects to be
119      % measure. If in case images and titles are confusing,
120      % change WindowState from normal to maximized.
121      subplot(3, 2, 1);
```

```matlab
122        imshow(originalImage);
123        hFig1 = gcf;
124        hFig1.Units = 'normalized';
125        hFig1.WindowState = 'normal';
126        hFig1.NumberTitle = 'on';
127        hFig1.Name = 'Analisi immagine';
128        drawnow;
129        frase = sprintf('Image for analysis');
130        title(frase, 'FontSize', carattere_scritte);
131        axis('on', 'image');
132
133        %--------------------------------------------------------
134        % This method is chosen because often the difference
             between the grays to be
135        % measured is small. Photos are recommended with high
             contrast between background (black)
136        % and object to be measured (as white as possible). By
             doing tests we
137        % recommend changing the threshold value to 0.4 for
             images of
138        % nanoparticles. For certain images try playing around
             with the
139        % value to find the best one.
140
141        Th_Value = 0.25; % Value between 0 and 1.
142        immagine_binaria = im2bw(originalImage, Th_Value);
             % One way to threshold to binary
143
144        % With this command we fill the "holes" of our image with
145        % input
146        immagine_binaria = imfill(immagine_binaria, 'holes');
147
148        % Image converted to binary BW.
149        subplot(3, 2, 2);
150        imshow(immagine_binaria);
151        title('Binary Image', 'FontSize', carattere_scritte);
152
```

```matlab
153     %----------------------------------------------------------
154     % A number is associated with each pixel so as to
           identify the object
155     % and separate it from other objects. The pixels that
           make up the same object
156     % will be labeled with the same number and will then be
           displayed as a
157     % grayscale image depending on the label associated with
           each
158     % object
159
160     [immagine_labeled, numero_di_oggetti] = bwlabel(
           immagine_binaria);
161
162     % Now to visualize the objects better, we assign each
           object a
163     % different color and we plot its
164     immagine_oggetti_colorati = label2rgb (immagine_labeled,
           'hsv', 'k', 'shuffle');
165
166     subplot(3, 2, 3);
167     imshow(immagine_oggetti_colorati);
168     axis image; % Make sure image is not artificially
           stretched because of screen's aspect ratio.
169     frase = sprintf('Image with recognized colored objects.')
           ;
170     title(frase, 'FontSize', carattere_scritte);
171
172     %=========================================================
173     % CALCULATION OF DIMENSIONS
174     caratteristiche = regionprops(immagine_labeled,
           originalImage, 'all');
175     numero_di_oggetti = numel(caratteristiche);
176     %=========================================================
177
178     %----------------------------------------------------------
179     % An image is now created that highlights the outlines of
```

```matlab
                    each object
180     % identified, so that its operation can be checked.
181     subplot(3, 2, 4);
182     imshow(originalImage);
183     title('Image with object outlines', 'FontSize',
            carattere_scritte);
184     axis('on', 'image');
185     contorni = bwboundaries(immagine_binaria);
186     numero_di_contorni = size(contorni, 1);
187
188     hold on;
189     for k = 1 : numero_di_contorni
190         thisBoundary = contorni{k};
191         x = thisBoundary(:,2);
192         y = thisBoundary(:,1);
193         plot(x, y, 'r-', 'LineWidth', 2);
194     end
195     hold off;
196
197     %-----------------------------------------------------------
198     % The results of the characteristics of the objects
           detected in the photo
199     % are printed in the command window
200     textFontSize = 11;
201     fprintf(1,'Object #     Mean Intensity   Area
           Perimeter   Center    Diameter     Diameter [nm]\n');
202
203     %The area is calculated outside the for loop otherwise
           the subplot function
204     %after gives problems
205     diametro_metro = [caratteristiche.EquivDiameter]* dati
           (1,1) / width;
206
207     for k = 1 : numero_di_oggetti
208
209         diametro        = caratteristiche(k).EquivDiameter;
210         intesita_media = caratteristiche(k).MeanIntensity;
```

```
211        area              = caratteristiche(k).Area;

212        perimetro         = caratteristiche(k).Perimeter;

213        centro            = caratteristiche(k).Centroid;
214
215
216        fprintf(1,'#%2d %17.1f %11.1f %8.1f %8.1f %8.1f %8.1f
              %8.1f\n', k, intesita_media, area, perimetro,
              centro, diametro, diametro_metro(k));
217        text(centro(1), centro(2), num2str(k), 'FontSize',
              textFontSize, 'FontWeight', 'Bold', '
              HorizontalAlignment', 'center', 'VerticalAlignment
              ', 'middle');
218    end
219
220    %-----------------------------------------------------
221    % Now we assign numbers to the objects that are detected
222    centri_oggetti = vertcat(caratteristiche.Centroid);

223    centroidsX = centri_oggetti(:, 1);
224    centroidsY = centri_oggetti(:, 2);
225
226    subplot(3, 2, 3);
227    for k = 1 : numero_di_oggetti
228
229        text(centroidsX(k), centroidsY(k), num2str(k), '
              FontSize', textFontSize, 'FontWeight', 'Bold', '
              HorizontalAlignment', 'center', 'VerticalAlignment
              ', 'middle');
230    end
231
232    %-----------------------------------------------------
233    % Now the centers found above the original image are
              drawn. Here
234    % we can select the fact that it finds objects larger
```

```matlab
                  than a certain
235    % threshold and mark them in red.
236
237    area_oggetti = [caratteristiche.Area];
238    subplot(3, 2, 1);
239    hold on;
240    for k = 1 : numero_di_oggetti
241
242        oggetto_piccolo = area_oggetti(k) < 2200;
243        if oggetto_piccolo
244            % Plot dimes with a red +.
245            plot(centroidsX(k), centroidsY(k), 'bx', '
                    MarkerSize', 15, 'LineWidth', 2);
246        else
247            % Plot nickels with a blue x.
248            plot(centroidsX(k), centroidsY(k), 'r+', '
                    MarkerSize', 15, 'LineWidth', 2);
249        end
250    end
251
252    %---------------------------------------------------------
253    % Notice that the program has ended
254    avviso = sprintf('The program has finished. \nHere you
           find the images, the results are in the Command Window
           .');
255
256    %---------------------------------------------------------
257    % Now we create a new window where individual objects are
            separated, so we can observe how they were identified
258    avviso = sprintf('Do you want to get the individual
           images of the objects?');
259    risposta = questdlg(avviso, 'Do you want to separate them
           ?', 'Yes', 'No', 'Yes');
260
261    if strcmpi(risposta, 'Yes')
262
263        hFig2 = figure;
```

```matlab
264            hFig2.Units = 'normalized';
265            hFig2.WindowState = 'normal';
266            hFig2.NumberTitle = 'on';
267            hFig2.Name = 'Separate object images';
268
269            for k = 1 : numero_di_oggetti
270
271                contorni_immagine = caratteristiche(k).
                      BoundingBox;
272                singole_immagini = imcrop(originalImage,
                      contorni_immagine);
273                subplot(4, 5, k);
274                imshow(singole_immagini);
275                frase = sprintf('Object #%d \nDiameter = %.1f nm\
                      nArea = %d pixels', ...
276                    k, diametro_metro(k), caratteristiche(k).Area
                        );
277                title(frase, 'FontSize', textFontSize);
278
279            end
280
281        end
282
283 else
284
285     % Grayscale image conversion if it wasn't already
286     [rows, columns, numberOfColorChannels] = size(
              originalImage);
287     if numberOfColorChannels > 1
288         avviso_2 = sprintf('Your image has %d color channels
                  .\nDo you want to convert it to grayscale?',
                  numberOfColorChannels);
289         tasto = questdlg(avviso_2, 'Continue', 'Convert and
                  continue', 'Cancel', 'Convert and continue');
290         if strcmp(tasto, 'Cancel')
291             fprintf(1, 'The program is ended.\n');
292             return;
```

```
293        end
294
295        originalImage = rgb2gray(originalImage);
296     end
297    %--------------------------------------------------------
298    % Data entry
299     prompt = {'Enter reference length [nm]:'};
300     dlgtitle = 'Input';
301     dims = [1 35];
302     definput = {'1'};
303     answer = inputdlg(prompt,dlgtitle,dims,definput);
304     dati = str2double(answer);
305
306
307     % See how the image is converted. If it is converted
              poorly,
308     % help the program by improving the contrast between
              background and objects to be
309     % measure. If in case images and titles are confusing,
310     % change WindowState from normal to maximized.
311     subplot(3, 2, 1);
312     imshow(originalImage);
313     hFig1 = gcf;
314     hFig1.Units = 'normalized';
315     hFig1.WindowState = 'normal';
316     hFig1.NumberTitle = 'on';
317     hFig1.Name = 'Analisi immagine';
318     drawnow;
319     frase = sprintf('Image for analysis');
320     title(frase, 'FontSize', carattere_scritte);
321     axis('on', 'image');
322
323     % This method is chosen because often the difference
              between the grays to be
324     % measured is small. Photos are recommended with high
              contrast between background (black)
325     % and object to be measured (as white as possible). By
```

```matlab
            doing tests we
    %recommend changing the threshold value from 0.8 and up
        for fibers.
    %For certain fiber pictures try playing with the value a
        bit to find the best one.

    Th_Value = 0.45; % Value between 0 and 1.
    immagine_binaria = im2bw(originalImage, Th_Value);
        % One way to threshold to binary

    % With this command we fill the "holes" of our image with
    % input
    immagine_binaria = imfill(immagine_binaria, 'holes');

    % Immagine convertita in binario BW.
    subplot(3, 2, 2);
    imshow(immagine_binaria);
    title('Binary image', 'FontSize', carattere_scritte);

    % Label the image
    [labeledImage, numero_di_oggetti] = bwlabel(
        immagine_binaria);

    % Ora per visualizzare meglio gli oggetti, assegnamo a
        ciascun oggetto un
    % colore differente e ne facciamo il plot
    immagine_oggetti_colorati = label2rgb (labeledImage, 'hsv
        ', 'k', 'shuffle');

    subplot(3, 2, 3);
    imshow(immagine_oggetti_colorati);
    axis image; % Make sure image is not artificially
        stretched because of screen's aspect ratio.
    frase = sprintf('Image with recognized colored objects.')
        ;
    title(frase, 'FontSize', carattere_scritte);
```

```matlab
354    % Make measurements of bounding box
355    caratteristiche = regionprops(labeledImage, originalImage
          , 'all');
356    numero_di_oggetti = numel(caratteristiche);
357    % An image is now created that highlights the outlines of
          each object
358    % identified, so that its operation can be checked.
359    subplot(3, 2, 4);
360    imshow(originalImage);
361    title('Image with object outlines', 'FontSize',
          carattere_scritte);
362    axis('on', 'image');
363    contorni = bwboundaries(immagine_binaria);
364    numero_di_contorni = size(contorni, 1);
365
366    hold on;
367    for k = 1 : numero_di_contorni
368        thisBoundary = contorni{k};
369        x = thisBoundary(:,2);
370        y = thisBoundary(:,1);
371        plot(x, y, 'r-', 'LineWidth', 2);
372    end
373    hold off;
374
375
376    %============================================================
377    % CALCULATION OF DIMENSIONS
378     caratteristiche = regionprops(labeledImage,
          originalImage, 'all');
379     numero_di_oggetti = numel(caratteristiche);
380     %============================================================
381
382     % The results of the characteristics of the objects
          detected in the photo
383     % are printed in the command window
384     textFontSize = 11;
385     fprintf(1,'Object #     Axis1       Axis2       Diameter1
```

```matlab
                      Diameter2\n');
386
387      diametro_metro_1 = [caratteristiche.MajorAxisLength]*
            dati(1,1) / width;
388      diametro_metro_2 = [caratteristiche.MinorAxisLength]*
            dati(1,1) / width;
389
390     for k = 1 : numero_di_oggetti
391
392         asse_1 = caratteristiche(k).MajorAxisLength;
393         asse_2 = caratteristiche(k).MinorAxisLength;
394         centro = caratteristiche(k).Centroid;
395
396         fprintf(1,'#%2d %15.1f %11.1f %11.1f %13.1f\n', k,
                asse_1, asse_2, diametro_metro_1(k),
                diametro_metro_2(k));
397         text(centro(1), centro(2), num2str(k), 'FontSize',
                textFontSize, 'FontWeight', 'Bold', '
                HorizontalAlignment', 'center', 'VerticalAlignment
                ', 'middle');
398 end
399
400     % Now we assign numbers to the objects that are detected
401     centri_oggetti = vertcat(caratteristiche.Centroid);
402     centroidsX = centri_oggetti(:, 1);
403     centroidsY = centri_oggetti(:, 2);
404
405     subplot(3, 2, 4);
406     for k = 1 : numero_di_oggetti
407
408         text(centroidsX(k), centroidsY(k), num2str(k), '
                FontSize', textFontSize, 'FontWeight', 'Bold', '
                HorizontalAlignment', 'center', 'VerticalAlignment
                ', 'middle');
409     end
410 end
```

The following are two example cases of using the program. In Figure A.1 the program analyzes the size of AgNPs. As described in the code, it is important to use high-contrast images and to modify the appropriate values within the code to achieve proper evaluation of the size of the objects in the image. AgNPs are only a few nanometers in size, and their identification in the image is quite simple because there are no problems with possible shadows.
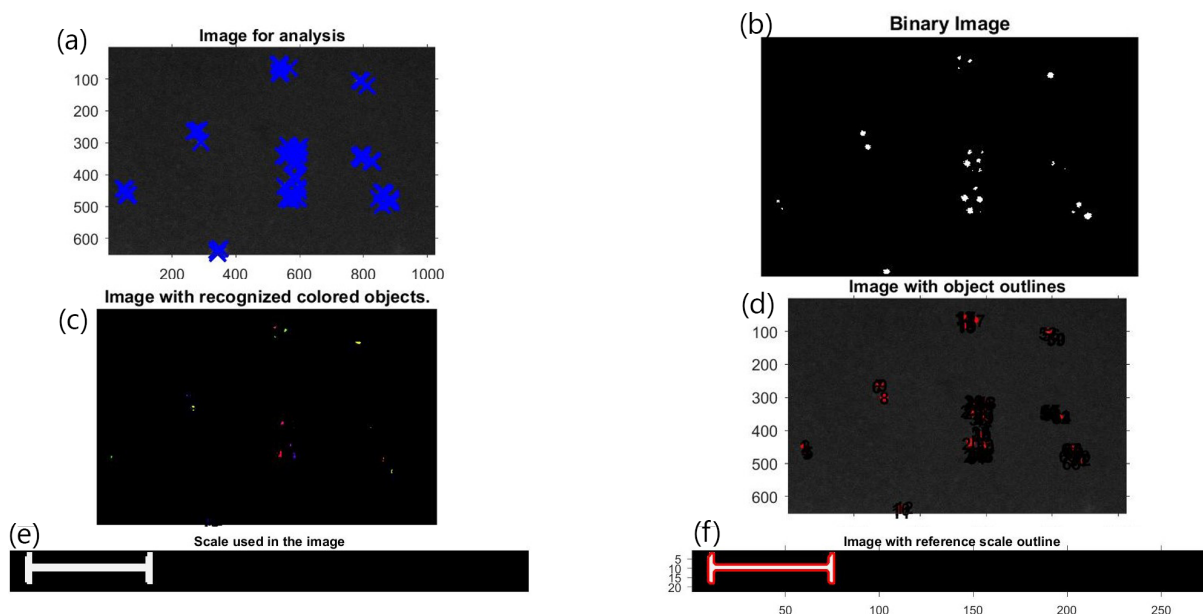
Figure A.1: Matlab program output (Appendix A). (a) Image whose AgNPs dimensions are to be identified and evaluated. Each recognized object is marked with a blue cross; (b), It is the binary image of the original image; (c) Image with colored detected objects; (d) Image with identified outlines of objects colored red; (e) It is the scale of the image; (f) Image scale with red-colored individuated outlines.

Figure A.2 shows the output of the Matlab program. As can be seen, compared to the use of the nanoparticle program seen just above, in this case, more objects are identified in the image than the actual number. This stems from the fact that identifying the contours of nanofibers is more complex since they generate a much more prominent shadow on the substrate than nanoparticles. For this reason, the sensitivity of the program to grayscale detection to correctly make the identification of objects in the image must be modified. In this way nanofibers are correctly detected in the images, however, it is possible that a pixel or groups of pixels within the image, have the same identification parameter, which is used for nanofibers. Therefore, these will also be identified as objects by the program. However, this does not pose a problem, since the size that the program will calculate, will be relative to the size of a single pixel or a few. As can be seen at the bottom of Figure

A.2, excluding the first two objects, *i.e.*, the nanofibers, the other objects all have the same size equal to the pixel or group of pixels and therefore it is easy to skim over the correct values.
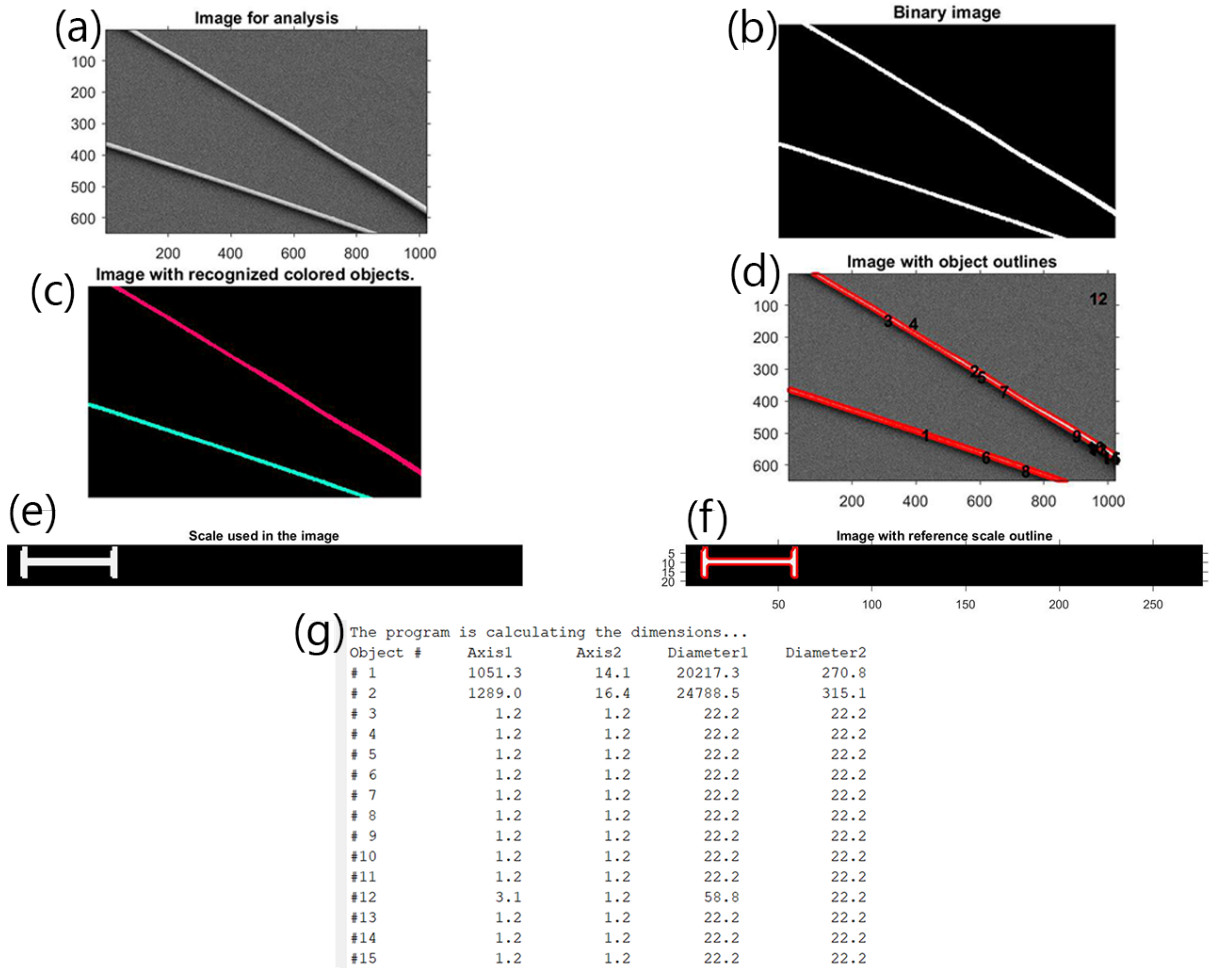
Figure A.2: Matlab program output (Appendix A).(a) Image whose nanofibers' dimensions are to be identified and evaluated; (b) It is the binary image of the original image; (c) Image with colored detected objects; (d) Image with identified outlines of objects colored red; (e) It is the scale of the image; (f) Image scale with red-colored individuated outlines; (g) Numerical output.

List of Figures

List of Tables